Optimisation of a stiffness-graded fracture fixation plate
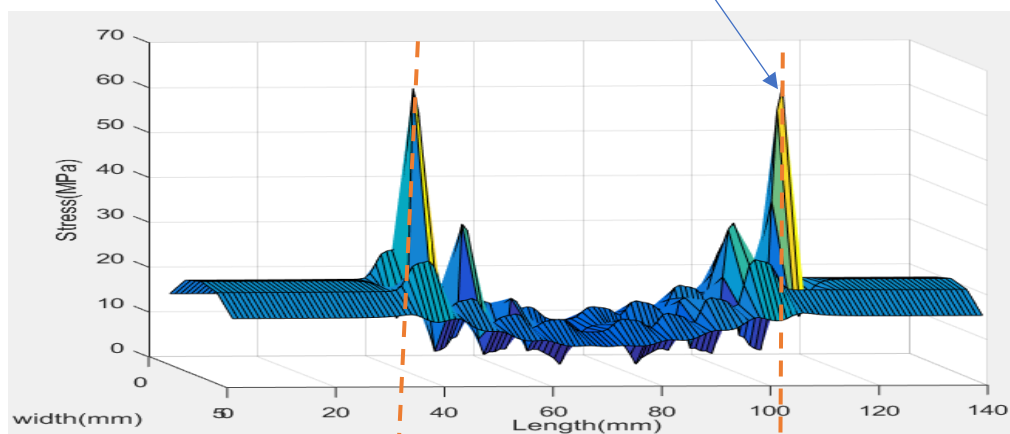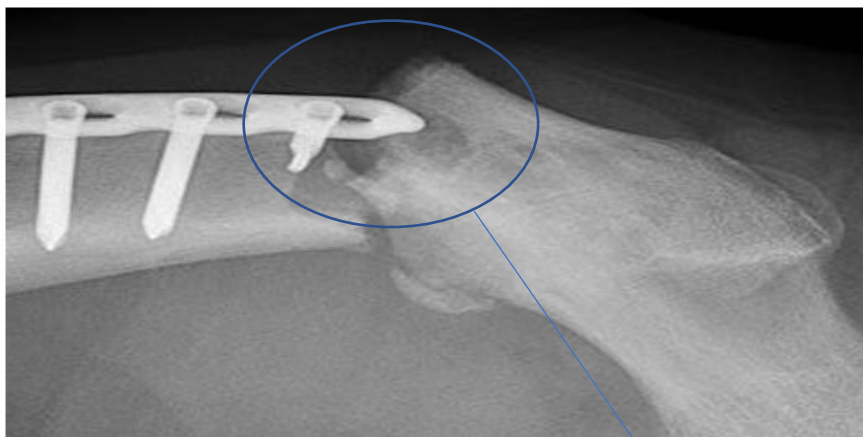
Subject: Master Thesis report

Program: Mechanical Engineering (Track: Biomechanical Design)

Supervisors: Prof. Dr. Ir. Harrie Weinans and Dr. Vahid Arbabi

Date: 05/08/2018

University: Delft University of Technology (TUDelft)

Abstract:

It has been observed that fractured bones which are stabilized with a titanium fracture fixation plate, once healed, often refracture at an edge of the plate. This is believed to be caused by stress concentrations in the bone that take place at the location of the edges of the plate. Various implant parameters are known to affect these concentrations of stress, but we further hypothesized that the material of the plate has the most significant influence in reducing these concentrations, here referred to as 'peak stresses'. Moreover, it was reasoned, based on relevant literature, that minimizing the peak stresses was not the only criteria that should be considered for the design of an optimal implant, the effect of the Interfragmentary strain on the healing outcome in the early stages after implantation is also crucial for the success of the implant. Otherwise the bone will never heal in the first place.

Thus, by assuming that different regions of the plate have a different influence in the peak stresses, it was suggested that a stiffness graded plate could minimize the peak stresses while still allowing for an acceptable interfragmentary strain at the early stages of healing, through an optimization. In order to prove or disprove all the hypotheses mentioned above, a Finite Element model of a fracture fixation construct was developed. For the selection of many of the modelling assumptions, a literature study was carried out. For the selection of the contact properties to be used, a graphical comparison study was done. For choosing an appropriate mesh, a mesh study was implemented.

Using this Finite Element model, it was possible firstly to show that while the material properties of the plate do in fact appear to be very influential in reducing the peak stresses, the thickness seems to be even more influential. For the latter a parametric study was carried out using the Taguchi method. Secondly, it was shown that different regions of the fracture fixation plate do have a different influence in the peak stresses of the bone. The outer most sections of the plate seem to always be the most influential. Lastly, optimisations were carried out in three different ways and although they all reduced the peak stresses, the method thought to be the simplest, yielded the most useful results. This consisted of dividing the plate only into three sections and assigning one material to the outer sections and another to the inner section.

Contents

1   Introduction:

1.1   Background:

Why is the fracture fixation needed?

When a bone fractures, a hematoma occurs which undergoes tissue differentiation in a series of stages. First comes inflammation, then the formation of a callus at the periosteal and endosteal surfaces of the cortical bone at a distance from the fracture, which then grows towards the fracture gap with increasing diameter through endochondral and intramembranous ossification, as shown in the figure below. Such bone healing is often referred to as 'secondary healing'. This callus stabilizes the fracture to a level at which the final bridging of the gap can occur through bone remodelling (often referred to as 'direct' or 'primary' bone healing). This is characterized by bone formation without the

need for any intermediate callus, instead, bone remodelling (osteoclast cells resorb bone while osteoblast cells form new bone in a constant cycle) occurs directly (Frost, 1989)(Claes and Heigele, 1999).
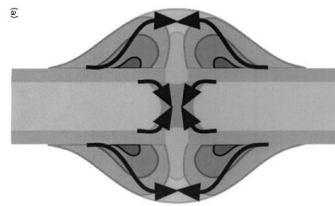

Figure 1: Figure taken from (Claes and Heigele, 1999) showing the process of fracture healing.

If the bone is left to heal on its own, it can be intuitively deduced that the large natural loads imposed by a patient's body will cause high levels of interfragmentary movement (IFM). As explained above, and further demonstrated by another study of Lutz Claes (Claes *et al.*, 2009), if the structure is not stable enough, direct bone healing will not take place. Thus, some form of fixation is needed to ensure the bone heals appropriately. The most common forms are external fixation, plate fixation and intramedullary nails (Steiner *et al.*, 2014).

What is a Fracture fixation plate and why use it instead of other types of fixation mechanisms?

A fracture fixation plate is a plate that fixes the two broken bone ends together by being attached to them. The most common form of attachment are screws as shown below.
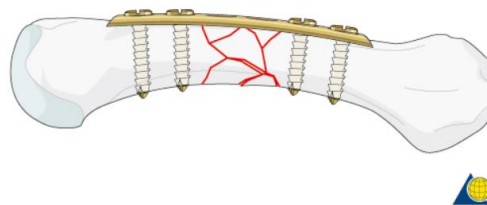
Figure 2:Fracture fixation plate attached to a bone with a comminuted fracture. Image taken from (DePuy Synthes, 2004).

It has been found that both the direction and magnitude of the stiffness offered by the fixation device is related to the stimulated healing. Small and moderate axial dynamization has been demonstrated to enhance healing both through Finite Element Modelling and through experiments (Aro and Chao, 1993)(Claes *et al.*, 1995)(Steiner *et al.*, 2014). Translational shear movement however, has been shown to result in delayed as well as incomplete fracture healing (Augat *et al.*, 2003). The advantages of axial motion over shear motion are made much more obvious in the study conducted by Malte Steiner et al. (Steiner *et al.*, 2014) where the two interfragmentary motion directions are thoroughly compared.

External as well as plate fixation cause mostly an IFM in the axial compressive direction due to a relatively low bending stiffness (Mason, 2009). Intramedullary nails on the other hand, cause large shear IFM as a consequence of the relative movement between the nail and the bone fragments (Wehner *et al.*, 2011)(Ateshian and Mow, 2005). Considering also the previous statements, it can be deduced that intramedullary nailing is not generally the preferred fixation method.

Figure 3: Intramedullary nail. Image taken from (Hodgson, 2009).

External fixation is the only fixation technique that allows a person to modify stability intraoperatively and post operatively (Ateshian and Mow, 2005). However, the stability it can provide is limited by the large necessary gap between the plate and the bone. Hence, a larger stability can be achieved using internal plate fixation devices. Lastly, external fixation appears to be much more uncomfortable and less aesthetically pleasing for a patient than internal plate fixation.

Figure 4: Image of external fixation device. Taken from (Hodgson, 2009).

What are the problems that arise from fracture fixation with a plate?

Unfortunately, the stability offered by conventional internal fixation plates in the axial direction is usually too low. Even though it was stated that a relatively low axial stiffness combined with a high shear stiffness would be ideal (Steiner *et al.*, 2014), if the axial stiffness is too low, the bone wont heal well either. Thus, the target is to be able to control the axial stiffness accurately such that it is not too low and not too high. Moreover, bone resorption underneath rigid plates was detected (Uhthoff and Dubuc, 1971) and is now very well accepted as a fact thanks to further experiments such as that carried out by A.J. Tonino et al. (Tonino, 1976). This phenomenon is often referred to as 'stress shielding' because the bone effectively feels less stress due to it being 'shielded' by the rigid plate. The cause for this lack of stress experienced by the bone is however not only due to a difference in young's modulus between the parts, as is shown in the results section of this report.

How have these problems been solved so far?

Many innovative designs have been created to solve the above problems. For tackling the 'stress shielding' problem, the use of titanium, whose modulus of elasticity is half as large as that of stainless steel, has been very beneficial (Claes, 2011). On the other hand, controlling the stability of the fracture fixation plate to achieve the desired healing type at the fracture gap has proven to be more difficult. A suitable solution to increase the level of stability offered by fracture fixation plates was developed: Locked Compression Plates (LCP).

Much like external fixation devices, these plates allow for a gap between the bone and the plate by forcing the screws to be locked inside the plate. In this manner, the axial stiffness of the construct is no longer dependent on the shear strength of the bone, but rather on the bending strength of the screws (Cronier *et al.*, 2010). A very simplified study about the concept of locking plates (Cronier *et al.*, 2010) shows this quite nicely by loading a piece of wood axially both with the conventional method as well as with the LCP system. This comparison is shown below.
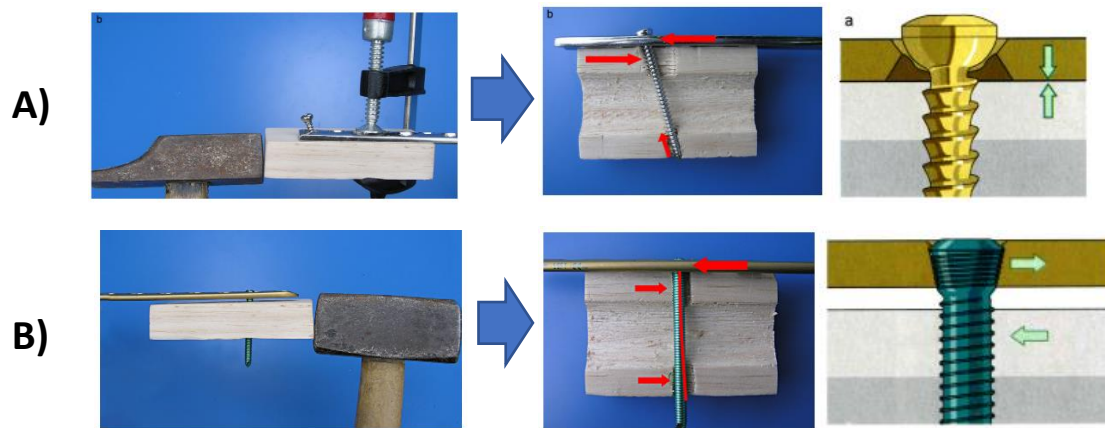
Figure 5: A) Conventional fracture fixation plate vs B) Locked Compression Plate (LCP). Images taken from (Cronier et al., 2010). Notice than in B directions do not match as they should, these are directly copied from the referenced article.

However, this system does not solve the problem entirely. As explained above, the ideal Fracture Fixation plate should allow for a certain amount of Interfragmentary motion in order to stimulate optimal healing. Moreover, this motion should be as homogeneous as possible throughout the contact surface area of the bone fragments. Locked Compression Plates can be tailored to allow for the right amount of IFM, but this motion won't be evenly distributed, the motion will be higher on the side of the bone opposite to the plate. This is nicely illustrated by the images on the review by Claes (Claes, 2011) as shown below. However, by optimising various parameters such as the number of screws, length of plate, thickness of the plate etc. the healing outcome can be greatly improved.
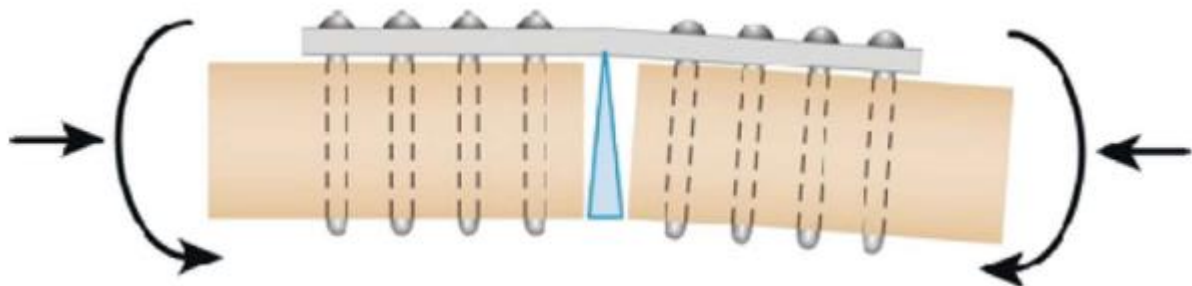

Figure 6: Illustration of how the interfragmentary strain (blue section) is distributed throughout the fracture interface.

Why is there still a need for further research, what problems does this report address?

The above mentioned problem is best solved through patient-specific optimizations, a methodology for such a process is discussed by Joshua C. Arnone et al. (Arnone, 2013). The proposed objective function is the factor of safety, such that the maximum Von Mises Stress seen in the plate is minimized relative to the yield strength, but the proposed methodology can be tailored for other purposes. The reason why the optimizations should be patient-specific (or at least specific to a group of people who share similar enough features) is that the bones of patients are usually quite different between different groups (Nelson *et al.*, 2004).

However, the problem that this study is concerned with is another one, which to our knowledge has not yet been discussed in the literature. The issues discussed so far have been about the starting phase of the healing process, when the implant is fixed to the fractured bone. Eventually, if things work as desired, the bone heals and there is no longer a fracture gap. In many patients, this is followed by removal of the fracture fixation plate (Sommer *et al.*, 2003) to ensure the bone is no longer 'shielded' by the stiffer implant. However, in some patients, such as children with Osteogenesis Imperfecta (OI)

(Albert *et al.*, 2017), the plate is not removed. A surgeon at the Utrecht Medical Centre (UMC) reported that he does not remove these plates in Children with OI because the surgery could be very dangerous given their condition. However, there are other reasons for not removing the plate.

What was also observed by the surgeon is that the bones of these children, after healing has concluded, eventually break at the edges of the plate. This phenomenon is shown below. This is the problem that this report deals with, namely, attempting to answer the following questions: (1) How can we prevent long bones that have been implanted with a fracture fixation plate and have healed properly, from breaking at an edge of the plate?, (2) How can we do the latter while still allowing the bone to heal properly and ensuring that the implant will not fail?
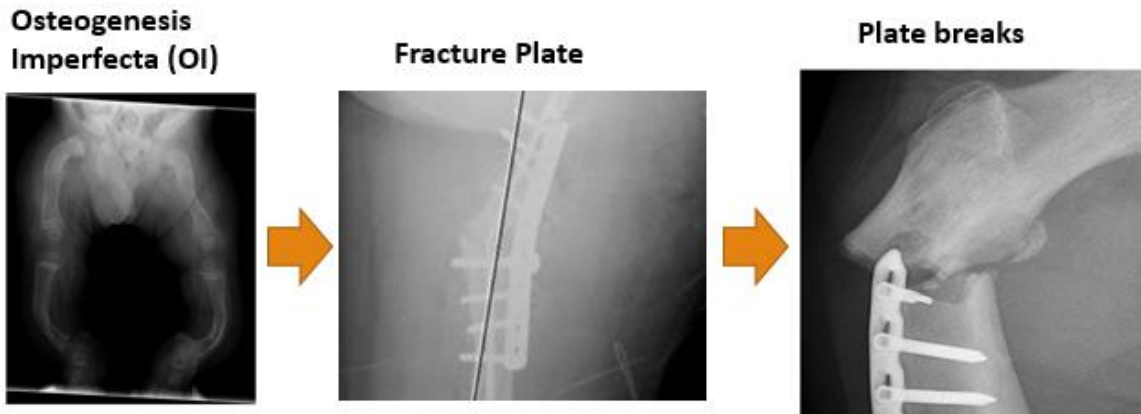
Figure 7: Images acquired from a surgeon, showing an example of the problem that the study deals with.

1.2   Hypothesis

The first part of the hypothesis is that the healed bone breaks because of a stress concentration in the bone at the edges of the plate. Secondly, It is believed that these stress peaks are most strongly related to the young's modulus of the plate than to any other implant parameter. This argument is derived by a study where the fracture fixation implant material is found to have the strongest effect on the maximum Von Mises stress in the implant (Arnone, 2013). In the current report a similar analysis is done for the maximum Von Mises stress in the bone in order to prove or disprove this hypothesis. Furthermore, we believe that by modifying the distribution of young's modulus along the length of the plate, the stress peaks can be brought down to a minimum, as shown in the figure below.

Figure 8: Hypothesis of the study. The figure shows how under pure bending, it is expected that modifying the young's modulus of the plate will allow us to minimize the peak stresses in the bone.

However, minimising the stress peaks in the bone is not the only requirement for the implant to be optimized, it also needs to be able to keep the fracture stable during the healing process. So the hy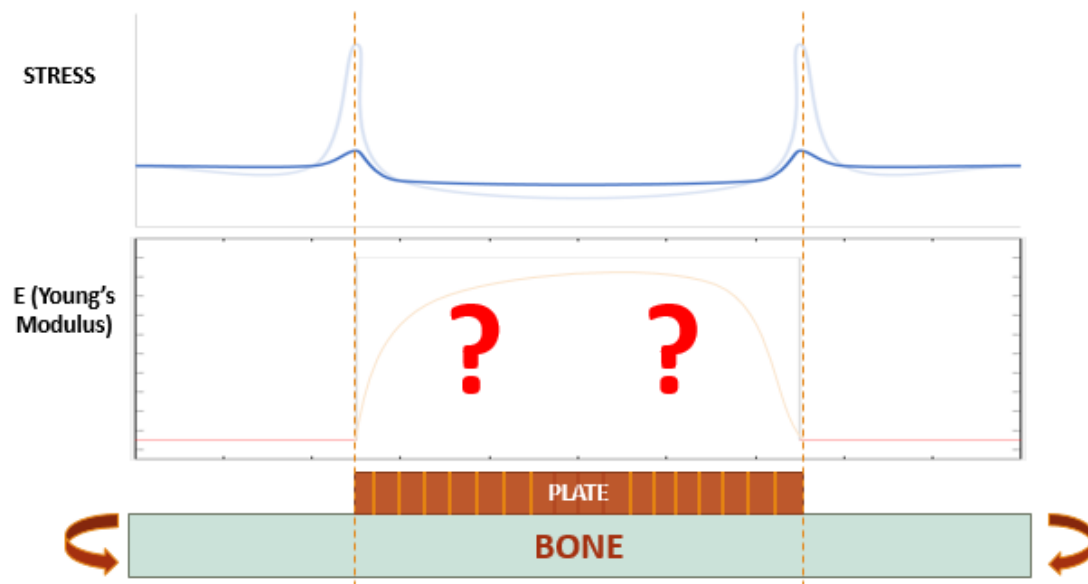pothesis is that there is an optimal young's modulus distribution along the plate that minimises the stress peaks in the bone, while keeping the fracture *stable enough* during the healing period.

Have there been other studies that address this issue?

One similar study was found but it did not have the target of minimising the stress peaks, rather to analyse how a stiffness graded plate would affect the stiffness of the construct at different healing stages (Ganesh, Ramakrishna and Ghista, 2005). Moreover, it was a 2-dimensional Finite Element study. As argued in a study aimed at comparing the 1-dimensional, 2-dimensional and 3-dimensional Finite Element studies of fracture fixation (B. R. Simon et al, 1977), 2-dimensional studies are not appropriate when analysing local stress distributions.

2   Overall Strategy:

The main steps to achieve an optimal distribution of young's modulus along the plate, are shown below. Firstly, an appropriate CAD initial geometry is developed, then, a Finite Element model is created, which consists of meshing the parts, applying loading and boundary conditions, as well as assigning initial material properties. It was chosen to use the Finite Element method, because it has been proven that this technique is very suitable to address biomechanical problems, as discussed by Huiskes and Chao (Huiskes and Chao, 1983). Lastly, an optimization routine was developed. To ensure that the implant works as predicted, producing it and testing it in the real world would be required.
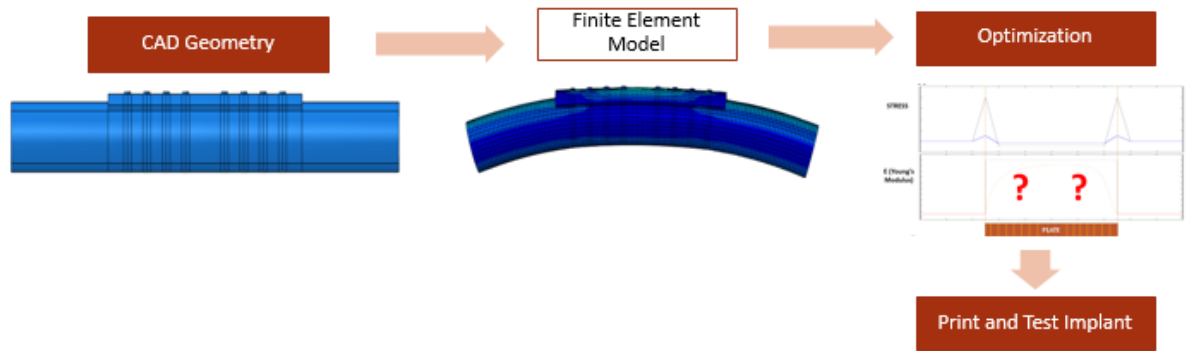
Figure 9: Overall strategy of the project.

The geometry includes both a bone and an implant. For the bone it would be ideal to have patient-specific models. Such models are addressed by A. Zadpoor and H. Weinans (Zadpoor and Weinans, 2015). They discuss the different steps involved in making patient-specific bone models, as well as how the choices made throughout the process affect the accuracy and efficiency of these models. In the current project a simplified geometry is first used before moving on to patient-specific models.

Regarding the implant, it would also increase the efficiency of the process to have an initial geometry that is generated automatically based on the bone geometry. Such a method was developed by X. Chen et al. (Chen *et al.*, 2017). They define both local and global parameters to describe the geometry of the bone, as well as how these can be measured using Computer Tomography (CT). Moreover, they developed suitable equations to link the parameters of the bone with those of a fixation plate, such that an initial patient-specific plate geometry can be obtained automatically from the CT scan of a bone. As with the bone, this project first utilizes a simplified implant before moving on to a patient-specific one.

Figure 10: Geometry acquisition and Finite Element Modelling steps.

The process of making the Finite Element Model is described in detail in the methodology below, as well as the Optimization process.
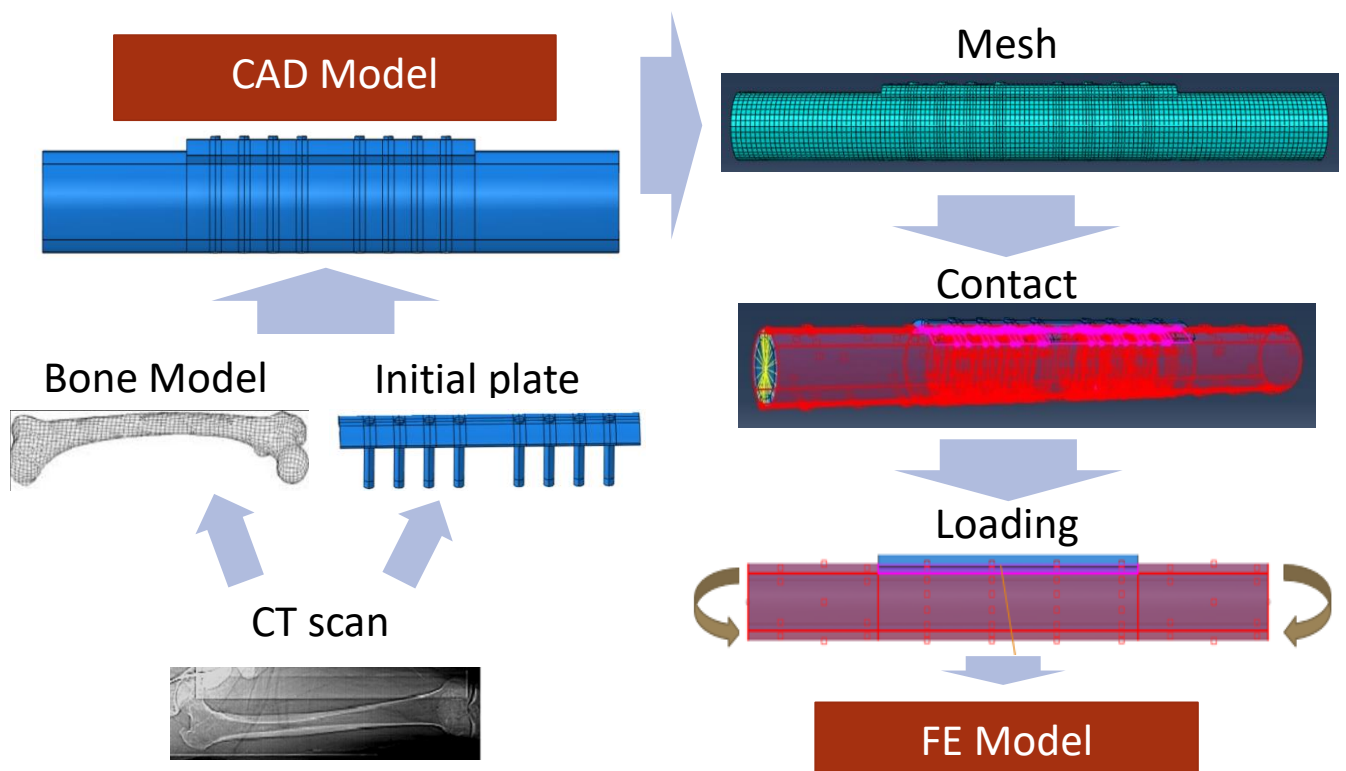
3 Finite Element Models creation:

3.1 Methodology:

For the selection of the different Finite Element properties, simplified models were used, in order to reduce the computational time, which has a big impact on the total time of the optimization. The idea is to start simple and gradually start increasing the complexity such that the implant is eventually *realistic enough*. However, this report only discusses the initial simplified model used. The software used to model the implant was ABAQUS 6.14. The documentation of ABAQUS was used extensively (Dassault Systèmes Simulia, Fallis and Techniques, 2013).

3.1.1 Geometry:

Throughout the report, the initial implant considered for improvement and eventually optimization was that of the Locked Compression Plate (LCP) 4.5 with 8 holes and made of titanium, designed and manufactured by DePuy Synthes (DePuy Synthes), which has been used by a surgeon at UMC Utrecht on some of the patients under consideration. Images of such a plate are shown below (the one under consideration has 8 holes). The geometry eventually used for the study was that of a simplified construct with screws, however, initially a model with no screws was used to develop intuition and hence why this is also presented below.
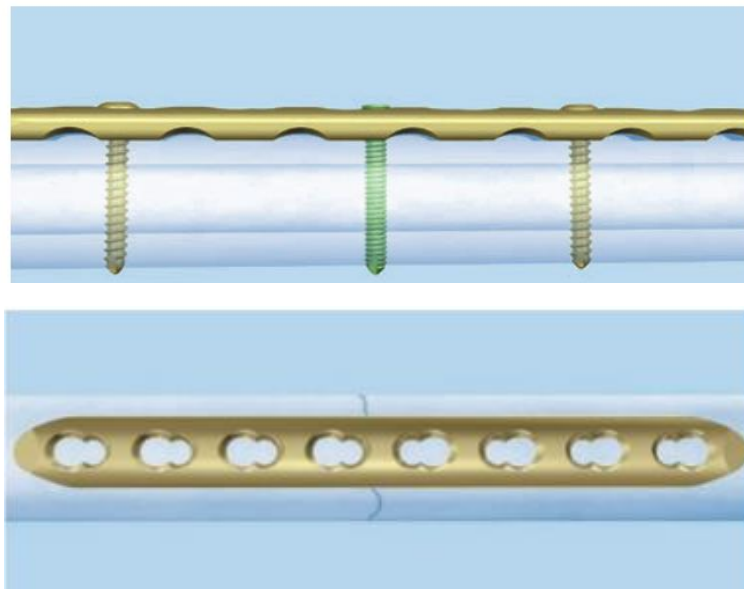
Figure 11: Synthes fracture fixation plate made of titanium. Images taken from (DePuy Synthes, 2004)*.*

Tied model:

The initial simplified model is the following. The bone was assumed to be a hollow cylinder of 35 mm outer diameter, 4 mm cortical thickness and a length of 300mm. The plate was initially assumed to be 150 mm long, 4 mm thick (constant thickness) and concentric to the bone. Initially, no screws or holes were modelled. This first model is referred to throughout the report as the 'Tied model'. The mesh for this model is shown here because it was not shown in the mesh refinement section.
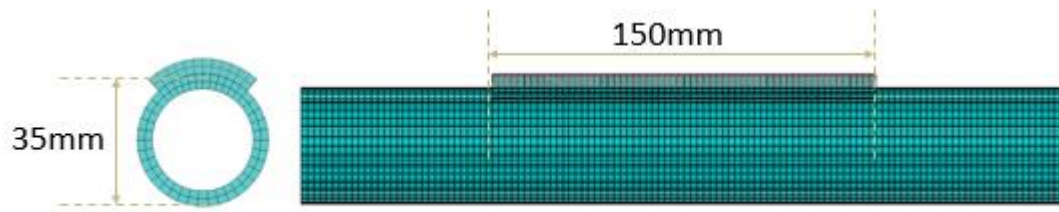
Figure 12: Geometry and mesh of the case with a plate simply tied to the bone.

Model with Screws:

Having developed an understanding for the various steps involved in the Finite Element Analysis, a more accurate model with screws was created. The geometry of this model is shown below. The screws have a diameter of 4 mm, a gap between them of 15mm and there is a gap between the bone and the plate of 1mm. All other dimensions are the same as those for the Tied model. The model below is referred to throughout the report as the model with screws.

It was chosen to model the screws as perfect cylinders because this assumption has been made in most validated Finite Element modelling of fracture fixation studies as stated in a recent review (Lehder, 2018), and led to a reasonable accuracy. The plate was modelled without fillets to start simple, but at a later stage the inclusion of fillets is studied.
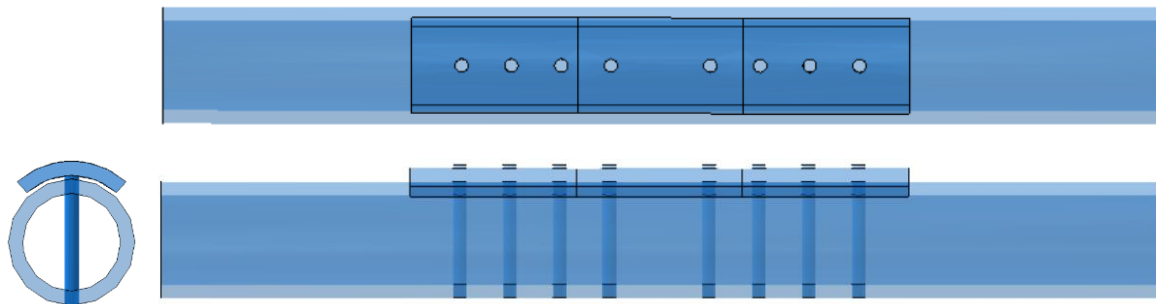

Figure 13: Geometry of the initial plate and a simplified bone (cylinder)

Model with Fracture:

Moreover, for ensuring that the optimized implant can keep the fracture stable enough, a model with a fracture was also made. The model is shown below. All dimensions are the same as those of the above model with screws, and the bone fracture was made at the longitudinal centre, with a length of 2mm (this value was chosen based on the mentioned review (Lehder, 2018)).

Fracture gap: 2mm
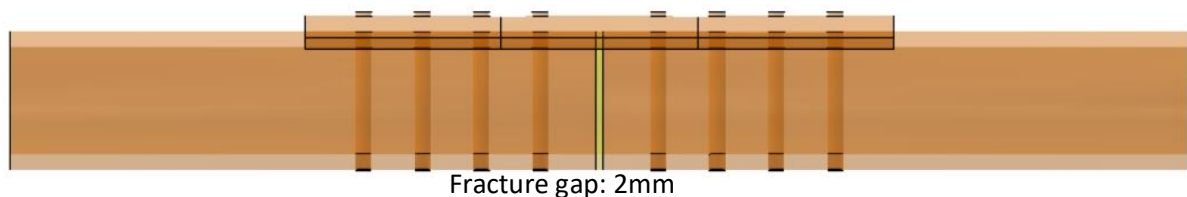
Figure 14: Geometry of the bone with a fracture and holes.

3.1.2   Material properties:

3.1.2.1   Bone:

The material properties of the bone were selected based on a recent study about the material properties of children with severe Osteogenesis Imperfecta (OI) (Albert *et al.*, 2017). Both normal bone

properties and OI bone properties were measured in that study with an accurate Micro CT scanner (0.65 micrometre resolution).

An evaluation (including experiments) done about the influence that bone homogeneity and isotropy has in finite element models (Synek *et al.*, 2015) showed that although it can be safely assumed that bone is isotropic, homogeneity may not be assumed because it greatly affects the accuracy of the results. Therefore, for a reasonable accuracy, the local density values of the modelled bone should be adapted to resemble those of the real bone as closely as possible.

Given that initially the purpose was only to test the proposed methodology, the bone was still modelled as homogeneous, isotropic and linearly elastic. Moreover, the young's modulus was chosen to be 15 GPa based on the referenced study (Albert *et al.*, 2017) and the poisons ratio 0.3.

For the model with a fracture, the segment in the middle of the bone was assigned a young's modulus of 10MPa to simulate a layer of immature callus. This value was selected because it was also used in a similar recent study (Samiezadeh, Tavakkoli and Fawaz, 2015).

3.1.2.2   *Implant:*

The materials of plate and screws were not modified relative to each other. Thus, it was assumed that the screws can always be manufactured of the same material as the plate. This assumption was made for simplicity given that the current study was merely done in order to test a proposed methodology.

The local material properties of the implant are variables, which as explained in the hypothesis, are to be optimized such that minimum peak stresses and acceptable stability are achieved. Therefore, the material properties of the implant are discussed in the optimization section of the report. It will be noted from the results that the minimum value of young's modulus of the plate segments was fixed at 3GPa, this was chosen based on two studies which measure the material properties of very porous titanium (Wang *et al.*, 2013). We assume that the only way to achieve the required strength for the connection between the plate and the screw to be sufficiently stable is by having a metallic porous titanium plate. The maximum value of young's modulus for the plate elements was fixed at 110 GPa, which was measured to be the young's modulus of pure titanium (Wauthle *et al.*, 2015).

It should however be noted that there has been a lot of research done on polymer plates as well as composite plates. A nice review of the work done is presented in a study by N.D. Chakladar et al. (Chakladar, Harper and Parsons, 2016), in which they also carry out a parametric study of a plate made of bioabsorbable glass fibre reinforced polymer composite. The main issue with polymer plates as well as polymer composite plates appears to be the lack of mechanical strength and stiffness, although studies such as the one mentioned above claim that similar mechanical performance can be achieved with optimized polymer composite plates. The study was done for an Ulnar fracture fixation implant, which has a less critical loading scenario than for instance the femur.

3.1.3   Physiological Loading and Boundary conditions:

For the loading conditions of a femoral bone, it was found that the most significant loads act along the length of the bone (Duda, Schneider and Chaot, 1997), referred to as axial loading. However, since these axial loads are not symmetrical about the two axes perpendicular to the longitudinal axes, bending moments are generated. It was further assumed that the most crucial bending moments are those acting on the plane defined by the Y and Z axes (around the X-axis), on opposite directions at either sides of the bone (see axis shown in the figure below). This loading condition is called 'pure bending', and it is the loading condition that was used throughout the simulations. Given that in the reviewed paper about the loading conditions of the bone during walking (Duda, Schneider and Chaot, 1997) the maximum absolute value of the frontal moment was found to be 0.1 times the body weight,

assuming that the patient has a body weight of 600 N, then the pure bending moment considered is 60Nm.
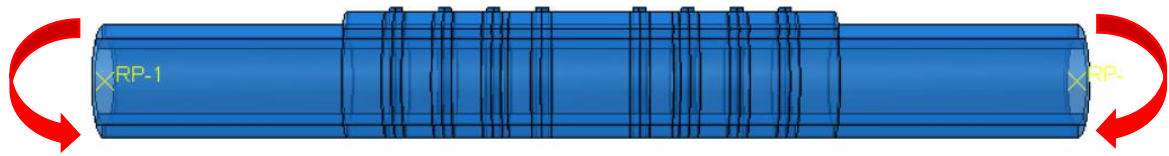
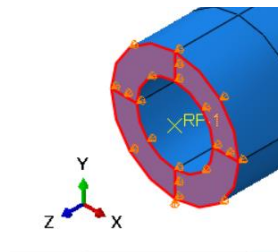**Surfaces tied to reference points:**

Figure 15: Loading used. In order to apply a moment to all sections of the bone as desired, the surfaces were tied to reference points at the centre of the circular surface, at either end. This was done through a kinematic coupling that restricts their relative movement in the translational directions.

3.1.4   Contact properties:

In the Locked Compression Plate being considered, there are usually three main contacts. (1) the contact between the plate and the bone, (2) the contact between the plate and the screws and (3) the contact between the screws and the bone.

For the model with screws, the plate and the screws were modelled as one part (this assumed that screws can always be made of the same material as the plate and ignores contact stresses between them). Between the bone and the plate, the contact was neglected since there is a spacing of 1mm between them. However, to visualize what the consequences of this assumption are, a model that uses plate contact was compared to one without. A contact was stablished between the bone and the screws. The main things to be defined in ABAQUS are: a) Master/Slave surfaces, b) Sliding Formulation, c) Discretization Method and d) Friction type. A graphic investigation was carried out in order to define the contact settings to be used at different stages of the study. The graphic results can be found in the next section.

To determine the influence of various contact setting variations, a control case was defined. The Control case was that with the screws as the master surface (most rigid), 'Small Sliding' as the Sliding formulation, 'surface-to-surface' as the discretization method and with a friction coefficient of 0.2 between the surfaces. According to the ABAQUS guide (Dassault Systèmes Simulia, Fallis and Techniques, 2013), the most accurate contact settings that can be used are these but with 'Finite sliding' instead of 'Small sliding'. However, the guide also explains that the 'Small sliding' assumption does not affect the accuracy of the results much and it speeds up the computation. Descriptions about what all these terms mean are extensively provided in the ABAQUS guide (Dassault Systèmes Simulia, Fallis and Techniques, 2013).

The contact pressure along a defined linear path was plotted for several variations of the contact settings. The contact pressure is one of the three normal components of the contact stress tensor. It is equivalent to the normal pressure between the screw surface and the contacting surface on the bone. The main variations used for comparison were: a) changing the discretization method from 'surface-to-surface' to 'node-to-surface', b) adding plate contact and c) setting the contact as

'frictionless' as opposed to the control case of having a friction coefficient of 0.2 between the bone and screw surfaces. In general, the master surface should be the most rigid body, thus the implant surfaces were always the master surface.

Lastly, two more cases were included for understanding purposes: d) using a simple tie between the screws and the bone and e) having no screws at all, using the Tied model instead. The same number of elements were used for all cases: 16000. Note that this is different from the mesh acquired through the mesh convergence study, because the contact setting was defined previous to the mesh convergence study. Furthermore, the number of elements is higher than the determined minimum number of elements so this was kept as it is.
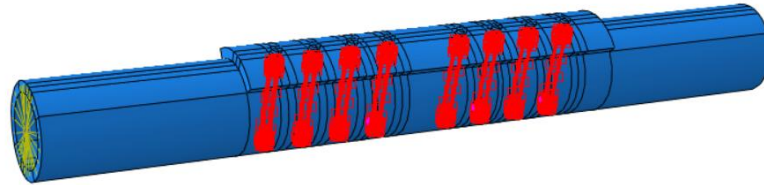
Figure 16: Contact surfaces between bone and screws in screw model. Master surface in red.
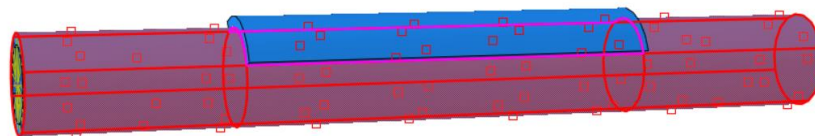
Figure 17: Master and Slave surfaces for the model where the plate is simply tied to the bone with no screws or holes. Master surface is in red, slave in purple.

Table 1: Different contact settings used in this study that attempts to find the ideal contact settings to be used. In red are the settings that were modified for that model.

Mode name	Discretization	Sliding Formulation	Plate contact	Friction formulation	Parts
Control	surface-to-surface	Small-sliding	None	Penalty-Friction	Bone, holes, Plate, screws
Node-to-Surface	Node-to-surface	Small-sliding	None	Penalty-Friction	Bone, holes, Plate, screws
Plate_Contact	surface-to-surface	Small-sliding	Plate Contact	Penalty-Friction	Bone, holes, Plate, screws
Frictionless	surface-to-surface	Small-sliding	Screws	Frictionless	Bone, holes, Plate, screws
Tied_WithScrews	surface-to-surface	Small-sliding	Screws	Tied	Bone, holes, Plate, screws

Tied_NoScrews	surface-to-surface	Small-sliding	Bone	Tied	Bone,Plate
HolesOnly	-	-	-	-	Bone,holes

3.1.5 Mesh study: What is the minimum allowed number of elements?

Usually, a mesh convergence study is crucially important to determine the number of global and local elements needed to represent the continuous system with enough accuracy. In this study the intention is only to understand how parameters of the plate can minimise the peak stresses observed in the bone (while allowing for proper healing). Thus, it is the difference in maximum stress values between successive models that we are interested in rather than the real size of the stress peaks. Moreover, for further analysis it was deemed important that the overall shape of the stress distribution along the bone was also close enough to the real distribution. Given that an optimisation was to be carried out, a low computational time was desired, hence a low number of elements would be preferable.

Therefore, a mesh study starting at a very low number of elements was carried out. With the objective of the study being to find the number of element required to represent the overall shape of the Von Mises stress distribution along the shown path in a reasonable manner, while allowing for a very low computational time. Below is a table presenting the mesh sizes used as well as some figures showing how the mesh varies. Note that the number of elements around the screw sections remains somewhat constant, this was done to ensure a reasonable result even with very low number of elements, given that these are the most critical regions.

Table 2: Number of elements used for each of the meshes used in this mesh study.

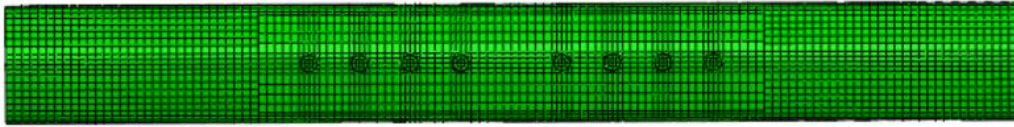| Mesh Model	Total Number of Elements
M1	3000
M2	3500
M3	4000
M4	5000
M5	7000
M6	9300
M7	12000
M8	16000
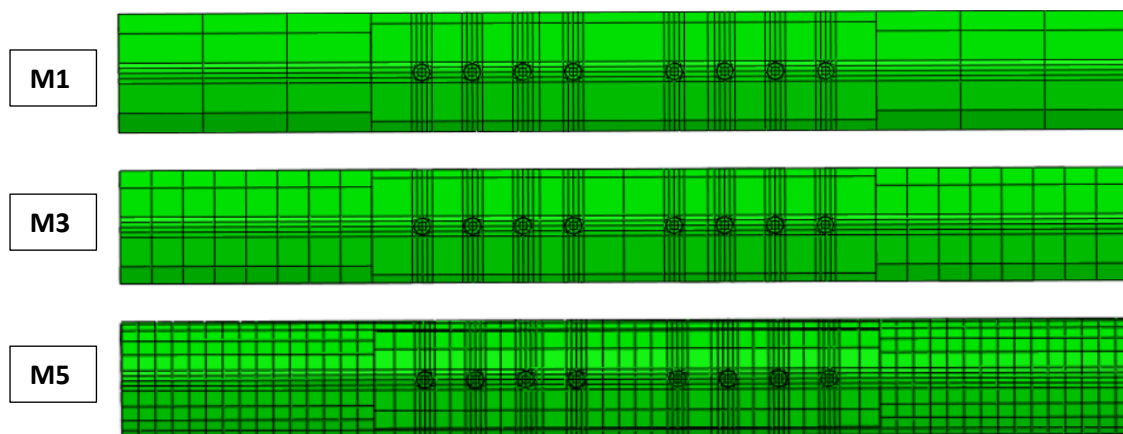
M8

Figure 18: Top view of four of the eight meshes used.
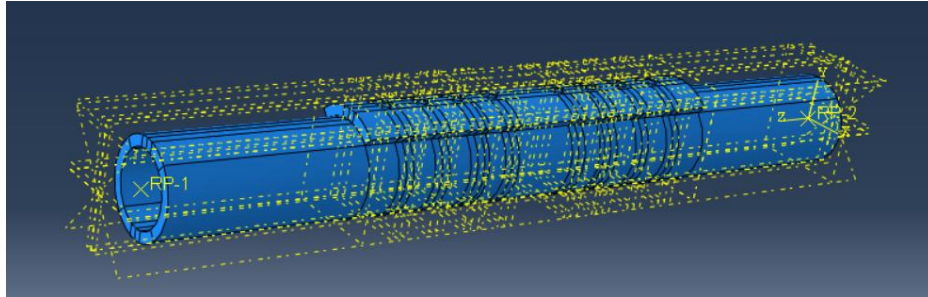

Figure 19: All the different planes used to section the construct in order to mesh it as desired.

3.2   Results:

3.2.1   Contact settings:

As can be seen in the graph below, changing the discretization method to 'Node-to-surface' and adding a plate contact appear to have an insignificant influence on the maximum contact pressure. However, adding plate contact clearly causes some inconsistencies in the distribution. This is because the moments applied here were high enough for there to be contact between the plate and the bone. Changing the contact to be frictionless appears to increase the contact pressure peaks (by about 20%). Moreover, setting the contact between the screws and the bone as 'Tied' (this restricts any deformation of the nodes of each contact surface to be equal for either part) caused a very large decrease in the contact pressure as well as causing the contact pressure distribution to be highly asymmetrical about the central radial axis.
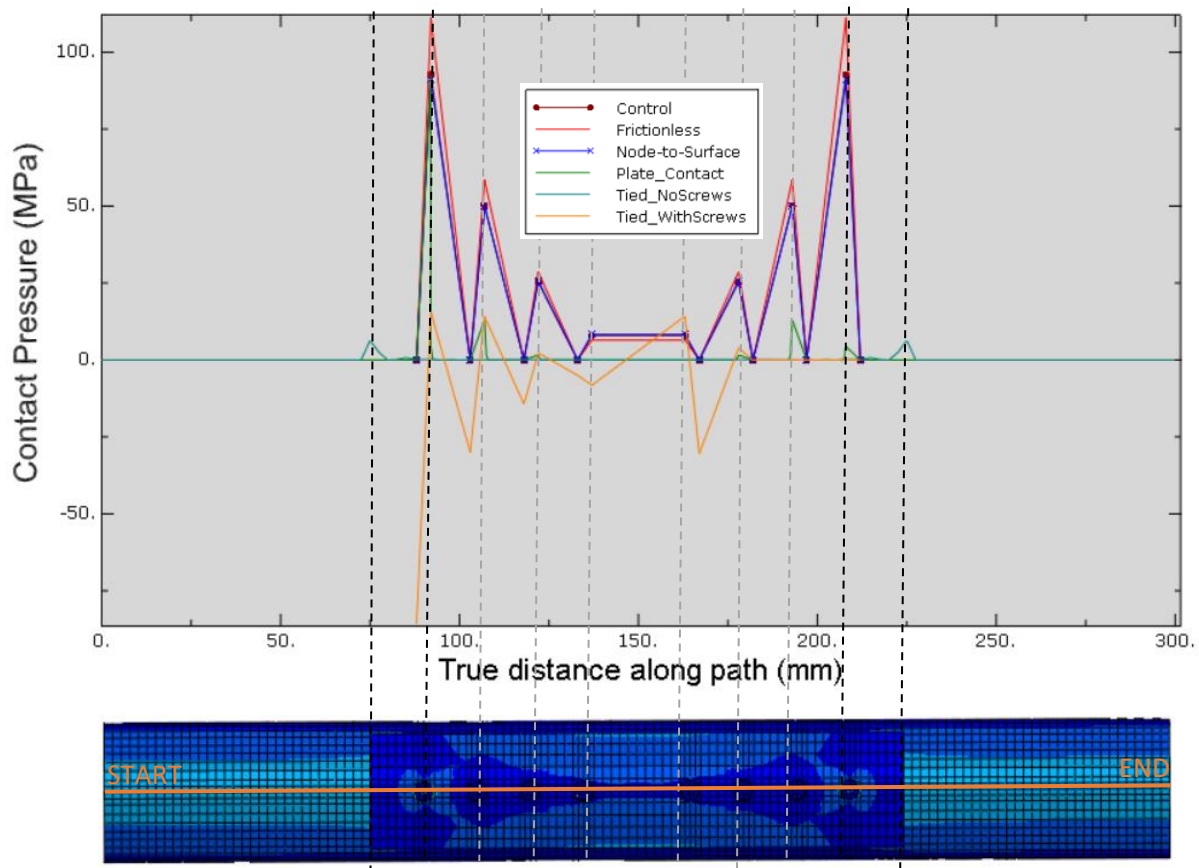
Figure 20: Contact pressure plotted against the distance along the shown path, for various cases. The cases are explained thoroughly in the methodology section. As can be observed, some plots only have values between the outer-most screws because these are the only regions where contact stresses actually exist.

Having the plate tied to the bone without any screws at all (as shown in the geometry section) also produced contact pressure peaks at the edges of the plate, but their magnitude was much lower (a reduction of about 90%). A further simulation without the use of screws but adding holes to the bone, showed that the main difference in magnitude between the peaks of the case with screws and the case without screws, is due to the presence of the holes rather than that of the screws themselves (see figure below). In this case the measurement variable was the Von Mises stress, which as shown later takes into accounts the principal stresses in all directions.
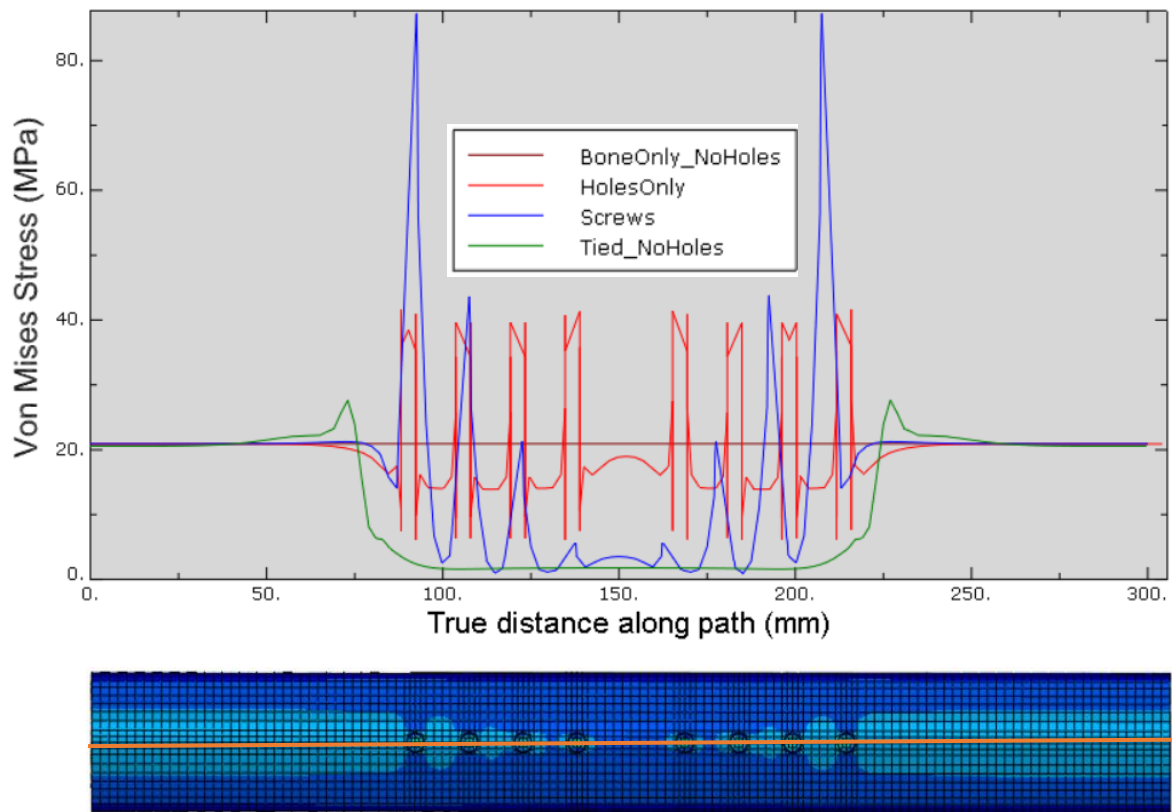
Figure 21: Von Mises stress against distance along the shown path, for the described cases. 'BoneOnly_NoHoles' refers to the case of having only a bone with no holes and without a plate. 'HolesOnly' refers to a model that also does not have a plate but has holes in the bone. The 'Tied_NoHoles' model has no holes nor screws, and the plate is simply tied to the surface of the bone. The 'Screws' model has screws, holes in the bone, and the only contact defined is between the screws and the bone as described previously, using the contact settings.

A timing analysis was carried out to compare the results in terms of their computation time as well and the results are presented below. Surprisingly, using the 'Node-to-surface' discretization method took almost 15% longer than using the 'surface-to-surface' approach. Using the 'frictionless' formulation decreased the duration of the simulation by about 25%. Tying the screws surface nodes to those of the bone holes surfaces reduces the duration even further, however, this option causes large errors as seen previously. Another surprising result was that of the case with the plate Tied to the bone, using no screws or holes. It took longer than using the frictionless approach for the model with the screws. However, a lower number of elements is required for the 'Tied model'.

Table 3: Time taken with different contact properties.

Mode name	Simulation time (s)
Control	50
Node-to-Surface	59
Plate_Contact	96
Frictionless	38
Tied_WithScrews	21
Tied_NoScrews	42

Figure 22: Bar plot of Simulation time for each of the contact settings used.

The approach that was thus adopted was to first use the most accurate settings, and if the optimization took too long, to use the frictionless approach. Moreover, if an even quicker optimisation was required, the plate was Tied to the bone and a lower number of elements used. The case of Tying the screws to the bone was not used due to the highly unsymetric result.
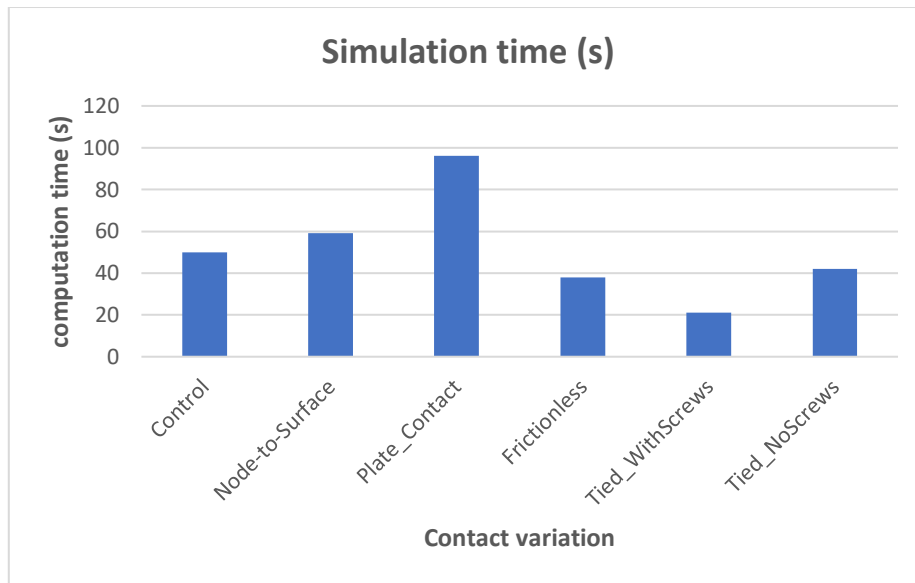
3.2.2   Mesh study: What is the minimum number of elements required?

Table 4: Mesh refinement results.

Mesh Model	Total Number of Elements (#)	Maximum Stress (Mpa)	Computation time (s)
M1	3000	123.4	12
M2	3500	121.4	13
M3	4000	117.6	14
M4	5000	114.5	21
M5	7000	110.4	24
M6	9300	109.8	33
M7	12000	109.3	49
M8	16000	109.2	54

The table above presents single value results that are more clearly represented by the graphs below. It can be observed that as the number of elements decreases, the maximum stress decreases in an almost exponential manner. More intuitively, as expected, the computation time increases as the number of elements increases. It is important to note that the most realistic result is that given by M8, the model with the most number of elements. Looking only at these single value results a conclusion about what model to use cannot be made, thus stress distributions were again plotted along a path as shown further below.

The Von Mises stress distribution plots show that although there is less of a decrease in stress between the holes, the overall shape of the curve is preserved even with a total number of elements of 3000 (it is likely that this is due to the fine local meshing at the screw regions). Moreover, the contact pressure plot shown indicates an even lower variation with decreasing the number of elements. Therefore, although the single value plots show a significant increase in the maximum stress when decreasing the number of elements, the stress distributions allow us to understand that this does not

signify a wrong distribution, and if the exact magnitude of the stress is not important then even 3000 elements may be used. Since as low a simulation time as possible is desired, 3000 elements were used for the optimisation.
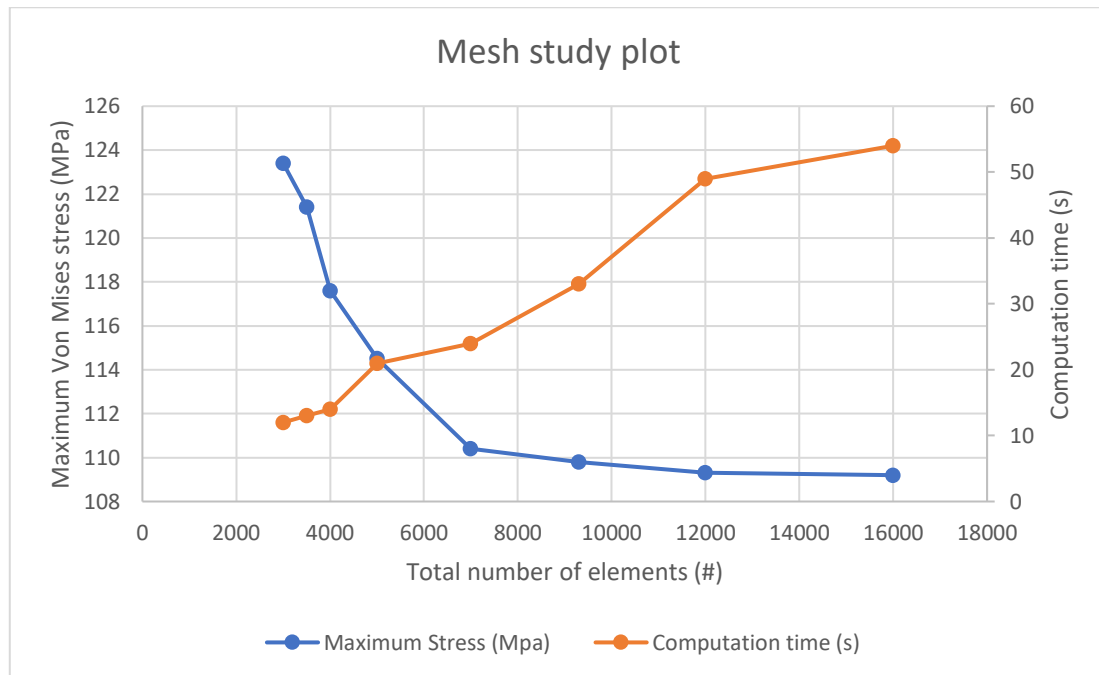
Figure 23: plots of the maximum Von Mises stress and computation time of successive mesh sizes.
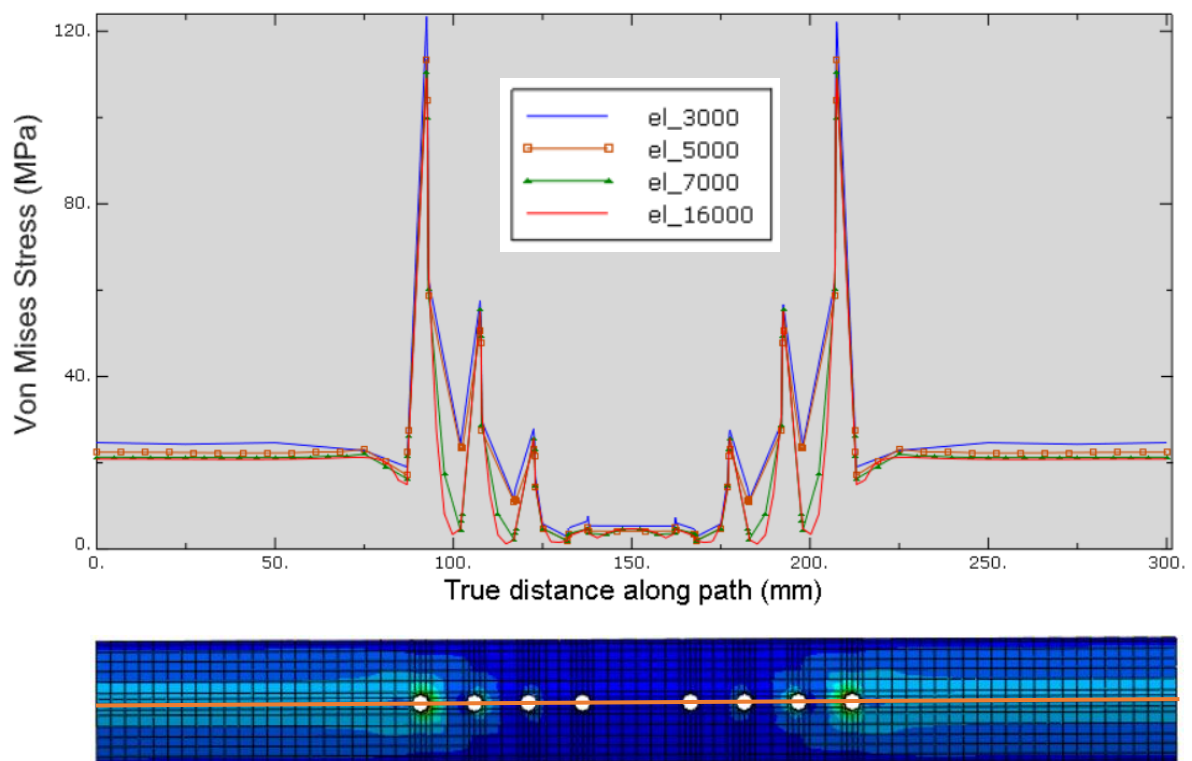
Figure 24: Distribution plot of the Von Mises stress along the path shown, for the different meshes used.
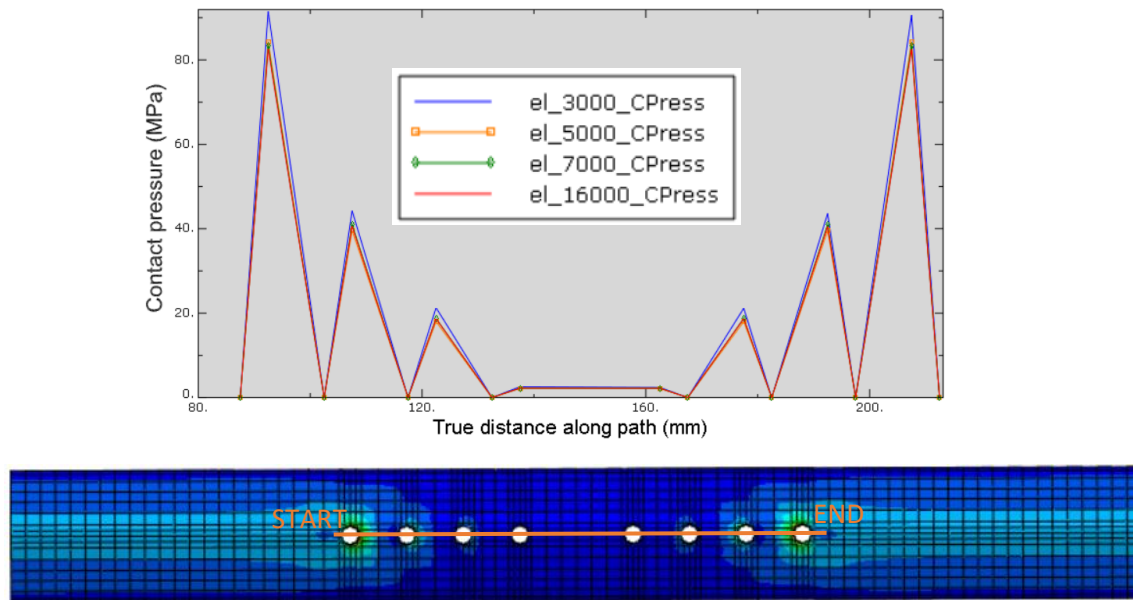
Figure 25: Distribution of contact pressure along the path shown.

4 Parametric study: Is the material the most influential parameter to the implants performance?

4.1 Methodology:

One of the hypotheses defined above was that the most influential implant parameter was the implant's material, thus why the focus of this report is on the material of the implant. With the target of finding out whether this hypothesis is correct, the current parametric study was carried out. The procedure followed in this section was the same as that followed in a study by J.C. Arnone et al. (Arnone, 2013) which aimed to create a methodology for parametric investigation of locked plating systems. In the latter, several combinations of implant parameters were tested through a Finite Element Analysis using ABAQUS. The parameters considered by them were four, and three levels for each, thus the total number of possible combinations was 81. However, through the use of the L9 Taguchi orthogonal array (Wysk, R. A., Niebel, B. W., Cohen, P. H., and Simpson, 2000) the nine simulation conditions that statistically represent all possible conditions required were calculated, and only those were evaluated. In the mentioned study, the risk of failure of the implant was evaluated by means of the factor of safety (maximum Von Mises Stress divided by the yield strength of the material). They found that the material of the implant has the most significant impact on the factor of safety as shown through the ANOVA table below.

Source	Degree of freedom	Sum of square, Sx.	Mean square Vx = Sx/D.F.	$\rho\%$
Material	2	207.64	103.82	60.94%
Thickness	2	102.25	51.13	30.01%
Inserts	2	5.06	2.53	1.49%
Oblique screw	2	25.76	12.88	7.56%
Total	8	340.71	170.36	100.00%

Figure 26: ANOVA results for parametric study conducted by J.C. Arnone et al (Arnone, 2013). Image is taken directly from their report. The % on the right represents the influence that each parameter had on the maximum stress experienced by a fracture fixation implant.

Similarly, four parameters were also investigated in the current study and each was also assigned three levels. The parameters investigated were: A. The material of the implant, B. The thickness of the implant, C. The number of screws present and D. The radius of fillets at the longitudinal edges of the implant. The first two parameters were chosen because they have been reported to be the most influential to the performance of the implant (Arnone, 2013)(Uhthoff, Poitras and Backman, 2006). The last two parameters were chosen because no article was found that investigates their influence in the chosen performance parameters outlined below. Looking at the plates manufactured by DePuy Synthes it can be observed that they use fillets at the edges of the plate. The levels for the three first parameters were chosen by either adding or subtracting 25% fragments of the initial level successively. Initial levels were based on commonly used parameters by DePuy Synthes. Since only nine simulations were done, it could be afforded to use a relatively fine mesh of 15000 elements. We believe this finer mesh would help us better capture the geometry variations.

Two parametric studies were done, one using the model without a fracture gap and a second one using the model with the fracture gap. The design performance measure selected for the study that used the model without a fracture was the maximum Von Mises stress experienced by the bone. The design performance measure selected for the model with a fracture was the maximum normal strain experienced at the fracture interface (Interfragmentary strain). For an explanation of why these variables were selected, please see the Optimization section. Below is an image showing where the maximum interfragmentary strain (IFS) is taken from and the path used for distribution plots.
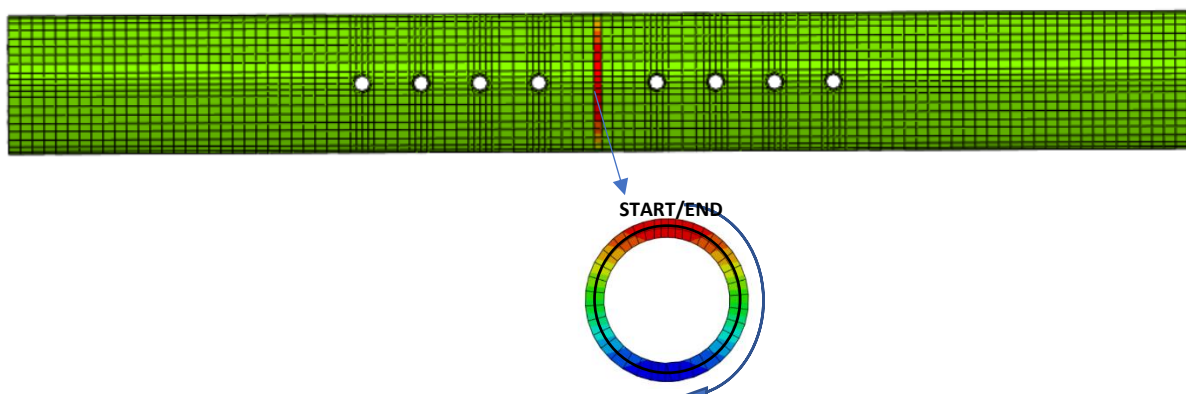

START/END

Figure 27: Bone fracture section used to calculated the Interfragmentary strain (IFS). As explained in the methodology, this small section of the bone (exactly at the longitudinal middle of the bone) was assigned a young's modulus of 10MPa such that it is virtually non existent but the strain in it may be measured.

However, as suggested by the Taguchi method, these performance measure variables were converted into signal-to-noise ratios using the formula shown below (Tiwari, Bajpai and Dewangan, 2017). 'Y' stands for the difference between a given response and the mean response, for any given measurement variable. 'n' for the number of simulations carried out (nine in this case). Below are tables showing the levels used for the different studied parameters and the nine statistically most significant simulations chosen based on the Taguchi method. It should be stated that the Taguchi method assumes that there is no interaction between the variables investigated.

$$\frac{S}{N} = -10 * Log10\left((R) * \left(\frac{1}{n}\right)\right)$$
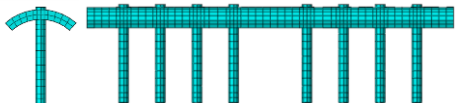
$$if\ larger\ is\ better, R = \frac{1}{Y^2}, if\ lower\ is\ better, R = Y^2$$
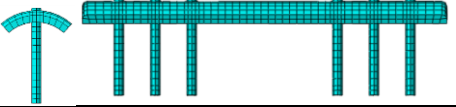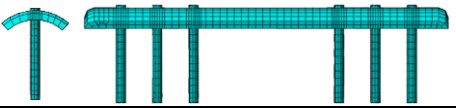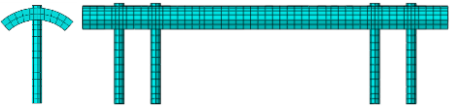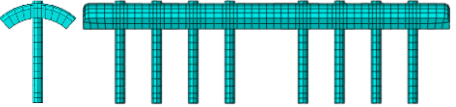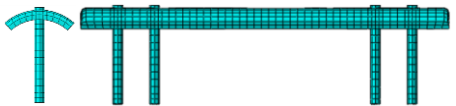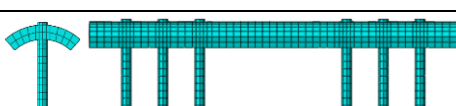
The influence that each parameter had on the signal-to-noise ratio of the chosen response measurement variable was calculated using an ANOVA table. This was made by writing all the required formulas for the sum of squares (Sx), the Mean square (Vx) and the influence (rho) into EXCEL and the results are presented in the next section.

Table 5: Chosen levels for each parameter investigated in the analysis. For the first three parameters the increase or decrease in successive levels is in steps of 25% of the initial level.

	Levels		
Factors	**1**	**2**	**3**
A. Material	110 Gpa	82.5 GPa	55 Gpa
B. Thickness	2 mm	3 mm	4 mm
C. Number of screws	4 screws	3 screws	2 screws
D. Fillet radius	None	2mm	4mm

Table 6: The nine simulations that statistically represent the 81 possible combinations of these 4 parameters (each with three levels) according to the Taguchi method *(Wysk, R. A., Niebel, B. W., Cohen, P. H., and Simpson, 2000)*. The CAD model shown is only that of the implant, in the actual model there is the bone with the respective holes.

L9 Orthogonal array					
Simu #	A.Material	B.Plate thickness	C. Number of Screws	D. Fillet radius	CAD model and Mesh
1	Pure Titanium (110 Gpa)	2 mm	4	None	

2	Pure Titanium (110 Gpa)	3 mm	3	2 mm	
3	Pure Titanium (110 Gpa)	4 mm	2	4 mm	
4	82.5 Gpa	2 mm	3	4 mm	
5	82.5 GPa	3 mm	2	None	
6	82.5 GPa	4 mm	4	2 mm	
7	55 GPa	2 mm	2	2 mm	
8	55 GPa	3 mm	4	4 mm	
9	55 GPa	4 mm	3	None	

In order to better understand the influence that the young's modulus of the implant has on the maximum Von Mises Stress of the bone, as well as on the interfragmentary strain (IFS) at the fracture, further plots were made of these variables against an unevenly spaced increase in young's modulus from 3 to 110 GPa using 8 intervals. The results are presented in the next section. The intention of this final parametric study was also to address a common misconception about the 'stress shielding phenomenon'. Some researchers believe that this is caused solely by the difference in young's modulus between the implant and the bone. If this were true, an isoelastic plate would achieve the same stress distribution as a bone alone, meaning there would be no stress peaks at all. The results below present an answer to this question. This is also discussed by J. Kuiper et al. (Kuiper and Huiskes, 1996) and H. Weinans et al. (Weinans, Huiskes and Grootenboer, 1992).

4.2   Results:

The table below shows the Maximum Von mises stress as well as the maximum interfragmentary strain (IFS) for every one of the nine simulations. Moreover, the signal-to-noise ratio (S/N) is also presented for both. By selecting the S/N ratio of the Von mises stress achieved by every level of every parameter, this data can be grouped into the tables below, which effectively shows the lowest S/N ratio of the Von Mises Stress achieved by every level of the respective parameter. The table also shows some statistics (blue values), including the sum of squared differences, which represents the variation from the global mean. The same procedure was followed for the IFS, and the results of that are presented further below.

Table 7: Results for the nine simulations that statistically represent (according to the Taguchi method *(Wysk, R. A., Niebel, B. W., Cohen, P. H., and Simpson, 2000)* all possible 81 combinations of the chosen levels of parameters. The two columns of the right represent the signal-to-noise ratio of the respective variable, calculated as shown in the methodology.

Parametric study results							
Simu #	A.Material	B.Plate thickness	C. Number of Screws	D. Fillet radius	Max Von Mises Stress (Mpa)	Max IF Strain (%)	S/N VM Stress	S/N IF Strain
1	Pure Titanium (110 Gpa)	2 mm	4	None	131.9	0.828	10.79	-8.40
2	Pure Titanium (110 Gpa)	3 mm	3	2 mm	140.0	0.853	-7.64	-10.31
3	Pure Titanium (110 Gpa)	4 mm	2	4 mm	135.8	0.895	-0.10	-14.96
4	82.5 Gpa	2 mm	3	4 mm	120.2	0.881	-12.44	-13.21
5	82.5 GPa	3 mm	2	None	141.9	0.910	-9.67	-17.44
6	82.5 GPa	4 mm	4	2 mm	137.3	0.839	-3.59	-9.22
7	55 GPa	2 mm	2	2 mm	130.9	0.935	4.12	-24.54
8	55 GPa	3 mm	4	4 mm	128.2	0.874	-3.65	-12.40
9	55 GPa	4 mm	3	None	128.7	1.575	-2.64	5.40
Mean					132.8	1.0	-2.8	-11.7

Table 8: On the left (in black) are the signal-to-noise ratios of the Von Mises stress (MPa) for each level of each parameter. On the right (blue values) are (from left to right) the mean, difference between mean and global mean, the latter squared and the sum of squares; for every row of values. All the data in this table is only for the Model without a fracture.

Global mean: 3.8	Levels			Stats			
Factors	1	2	3	Mean	DM	DMS	SSDT_i
A. Material	10.79	-3.59	4.12	3.8	0.0	0.00	103.4
B. thickness	10.79	-3.65	-0.10	2.3	-1.4	2.07	119.4
C. Number of screws	10.79	-2.64	4.12	4.1	0.3	0.09	90.4
D. Fillet radius	10.79	4.12	-0.10	4.9	1.2	1.32	64.2

The table below shows the results of an Analysis of Variance (ANOVA) study for the model without a fracture. This shows that the thickness of the implant has the highest influence in the maximum Von mises stress calculated via the Finite Element Models (32%). It also shows that the next most influential parameter, in terms of the risk of fracture of the bone, are the material of the implant and the number of screws present, respectively.

Table 9: The ANOVA table showing the influence that each parameter has on the maximum Von Mises stress experienced by the bone. Data is for the Model without fracture.

Source	Degrees of Freedom, D.F.	Sum of square, Sx	Mean square Vx=Sx/D.F.	Influence, rho(%)
A. Material	2	103.45	51.72	**27.41**
B. thickness	2	119.35	59.68	**31.62**
C. # of Screws	2	90.43	45.21	**23.96**
D. Fillet radius	2	64.17	32.09	**17.00**
Total	8	377.40	188.70	100.00

Table 10: On the left (in black) are the signal-to-noise ratios of the IFS (MPa) for each level of each parameter. On the right (blue values) are (from left to right) the mean, difference between mean and global mean, the latter squared and the sum of squares; for every row of values. All the data in this table is only for the Model with a fracture.

Global mean: -10.8	Levels			Stats			
Factors	1	2	3	Mean	DM	DMS	SSDT_i
A. Material	-8.40	-9.22	5.40	-4.1	0.9015	0.8127	137.414
B. thickness	-8.40	-10.31	5.40	-4.4	0.5408	0.2925	147.779
C. Number of screws	-8.40	5.40	-14.96	-6.0	-1.0098	1.0198	219.016
D. Fillet radius	5.40	-9.22	-12.40	-5.4	-0.4325	0.1870	180.823

Looking at the ANOVA table below, one can observe that the material has the least significant influence on the stability of the fracture (as measured by the IFS). This is somewhat contradictory to the influence on the maximum stress experienced by the bone. The parameter with the largest influence on the stability was the number of screws, but not significantly. All this data is also shown through the use of pie charts further below.

Table 11: The ANOVA table showing the influence that each parameter has on the IFS experienced by the bone at the fracture interface, in the normal direction. Data is for the Model with a fracture.

Source	Degrees of Freedom, D.F.	Sum of square, Sx	Mean square Vx=Sx/D.F.	Influence, rho(%)
A. Material	2	137.41	68.71	**20.06**
B. thickness	2	147.78	73.89	**21.57**
C. # of Screws	2	219.02	109.51	**31.97**
D. Fillet radius	2	180.82	90.41	**26.40**
Total	8	685.03	342.52	100.00
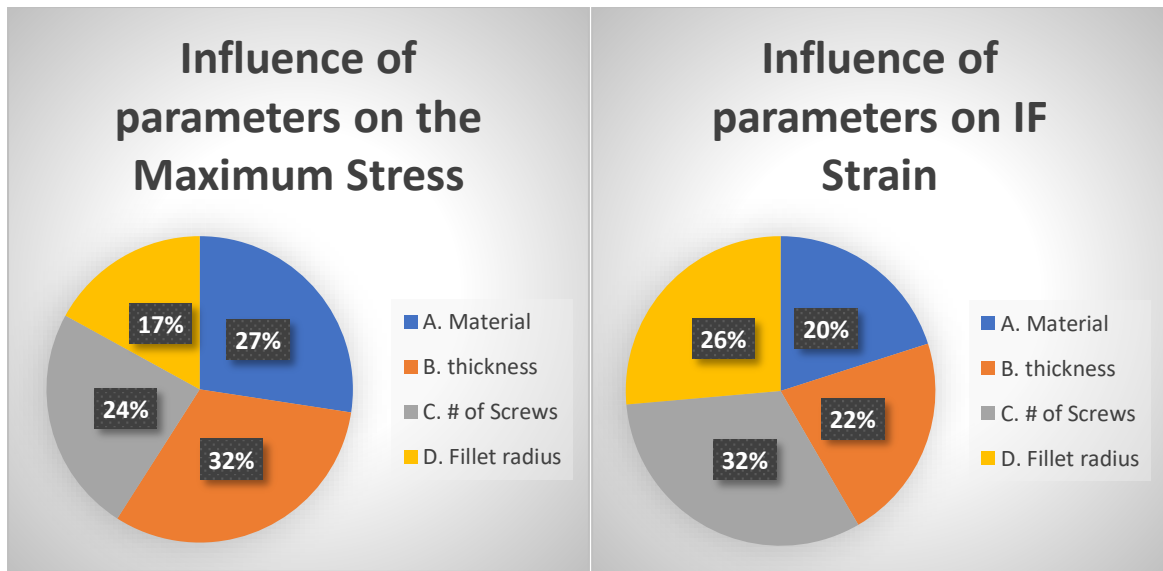
Figure 28: Graphical representation of the data presented on the ANOVA tables. On the left is the data for the model without a fracture and on the right the data for the model with a fracture. As stated previously, IFS stands for the Interfragmentary strain.

Given how similar the influences of the material and the thickness appeared to be from the analysis above, further plots were made to compare these. The plots are presented below. It appears that although at first the material has more of an influence in decreasing the maximum stress, eventually the thickness takes over. Nevertheless, as also visible in the distribution, the difference seems to be very small. For similar graphs considering also the other two parameters, see Appendix A.
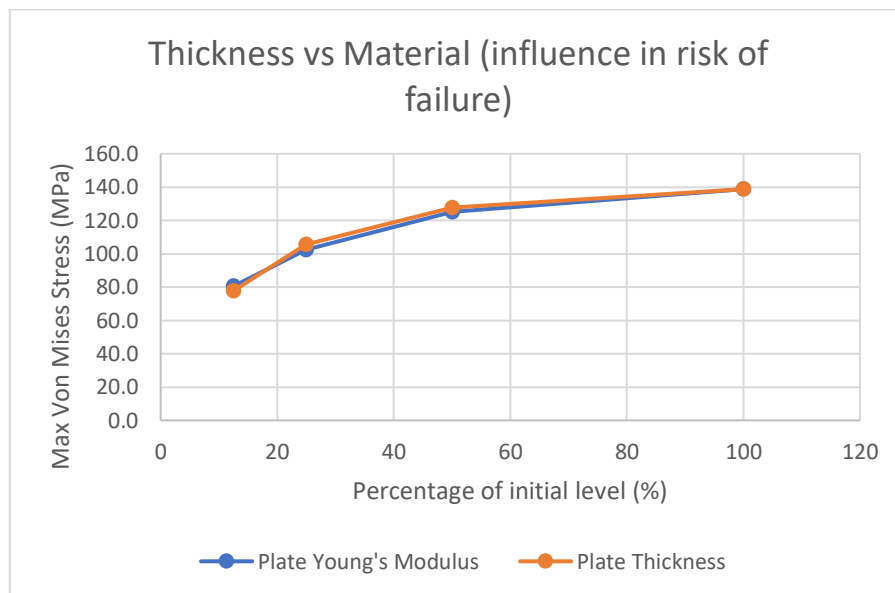
Figure 29: Single-value plots of the maximum Von Mises stress in the bone vs the percentage of thickness of the initial level for both plate thickness and young's modulus. The initial young's modulus was 110 GPa and the initial plate thickness was 4mm.
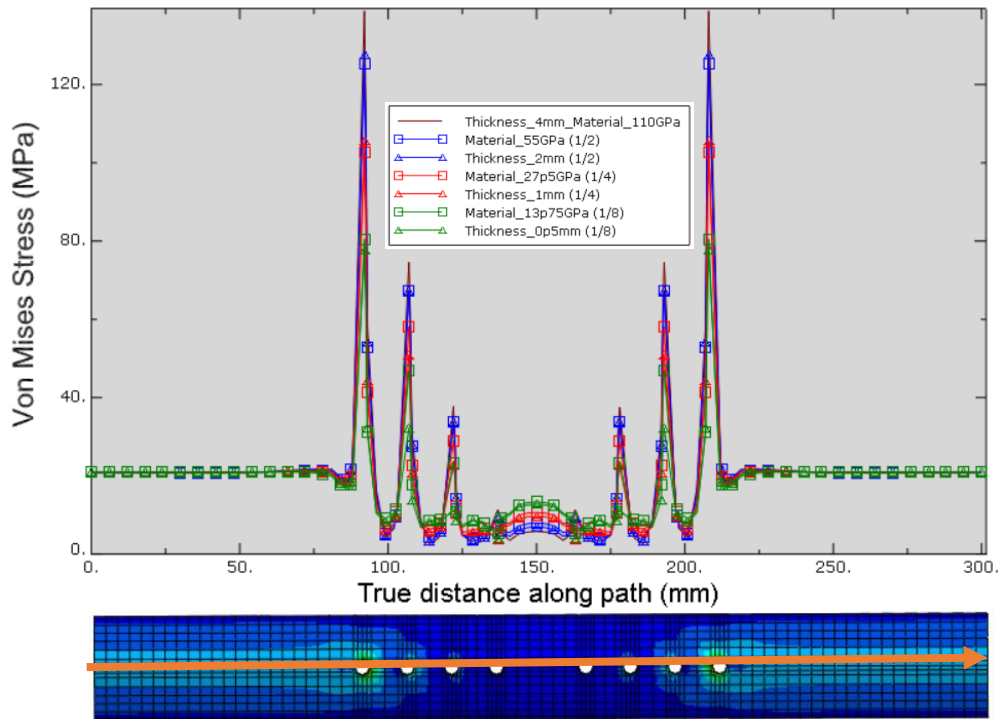
Figure 30: Distribution plots of all the cases plotted in the previous figure. As can be seen, each color corresponds to a given percentage of the initial levels. Squares represents the material plots and triangles represent the thickness plots.

Further results showing how the maximum stress and the maximum IFS vary when modifying only the young's modulus of the plate even further, are presented below. As the young's modulus of the implant decreases, the maximum stress in the bone decreases and the maximum IFS increases. Furthermore, the magnitude of the negative gradient of the maximum Von mises stress curve increases as the young's modulus decreases. The gradient of the IFS curve also increases as the young's modulus of the implant decreases, but positively.
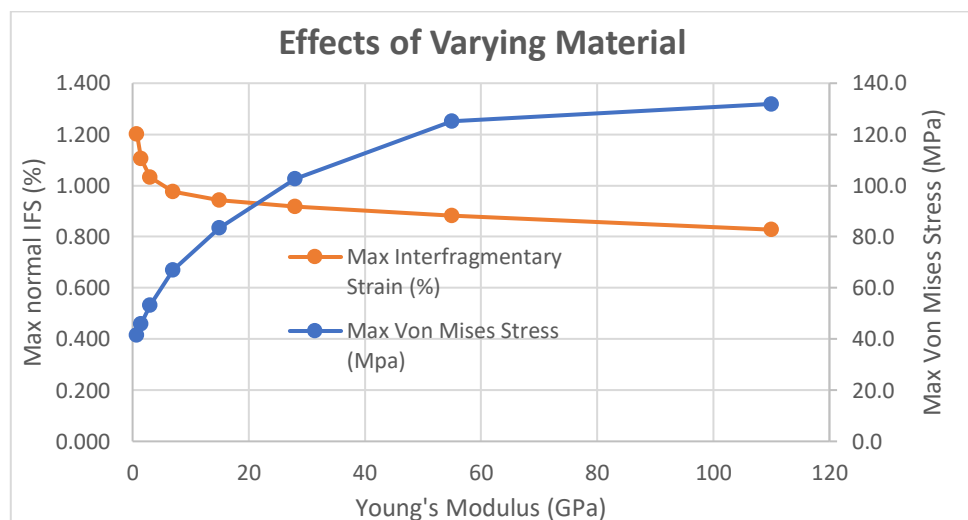
Figure 31: Graph of the effects that varying the young's modulus of the implant has on both the maximum Von Mises stress and the maximum normal IFS.

Below are graphs showing the distribution of Von Mises stress and Interfragmentary strain (IFS) along a defined linear path. As with all the cases where IFS is presented, this was computed using the model with a fracture. When the Von Mises stress is presented this has been computed using the model without a fracture and with screws. It can again be observed that the peak stresses along this path are

lowered when the young's modulus of the plate is lowered. Most notably is the decrease in the peak stresses from the isoelastic plate (15 GPa) to the 3 GPa plate, where the stress peaks are reduced by about 50%.

Furthermore, at the middle section of the bone (where the fracture used to be) the Von Mises Stress rises with decreasing the young's modulus. Lastly, to refer directly to the believe some researchers have about 'stress shielding' being caused solely by the difference in young's modulus between plate and bone, it can be seen below that this is clearly not the case since the isoelastic plate also has significant stress shielding and peak stresses.
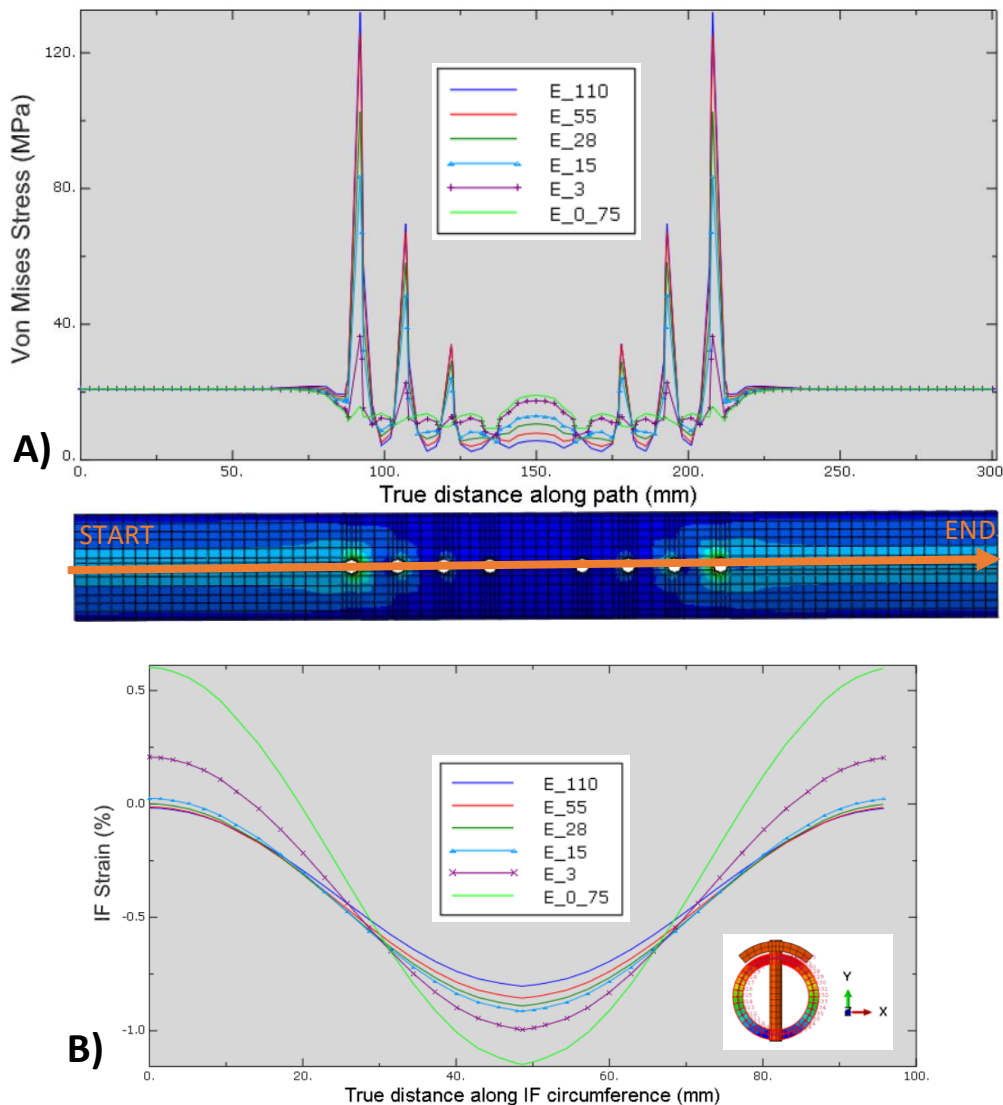
Figure 32: A) distribution of Von Mises stress along the surface path shown in orange. The variation of the distribution with changing young's modulus is shown. B) Interfragmentary strain distribution along the circular path shown on the bottom right of the figure. This is the normal strain acting on the z axis of the middle segment. The variation of the distribution with changing young's modulus is shown.

5   Optimization:

The aim of this report was to find a suitable way to minimize the risk of fracture of a bone fixed with a plate, while ensuring that when fractured the bone heals properly. As shown in the parametric study, although decreasing the material's stiffness has a large influence in the stress peaks, this also causes

the interfragmentary strain (IFS) to increase significantly, thus inhibiting appropriate healing to take place at the fracture gap (The reason for having chosen the IFS is addressed in this section).

As discussed in the Hypothesis, we believe that by modifying the young's modulus distribution throughout the plate, we can minimize the maximum stress experienced by the bone, while ensuring that the bone heals properly when there is a fracture gap. There are four main questions to be answered before proceeding: (1) What would be a suitable objective function to minimize? (2) what constraint/s can we apply to ensure that the bone heals appropriately during the period when there is a fracture gap? (3) how can we control the young's modulus distribution in the implant? And finally, (4) How can we find the optimal young's modulus distribution? These questions are addressed in the respective order below. The last question is addressed with three successive optimization techniques which influence each other. Their relevant 'methodology' and 'results' sections are presented within their own section.

5.1   (1) What would be a suitable objective function?

The different stresses present in the bone are plotted below for the shown path along the surface of the bone. They all follow the same pattern: stress peaks at all the holes, but the stresses of largest magnitude are those at the outer holes.

The stresses can also be divided into just two: Contact stresses and internal stresses. The Von Mises Stress shown below can be used as a way of considering the stresses in all directions, as shown also by the equation below. The main contact stress is the contact pressure (CPress) between the surfaces, although there is also some shear contact stress as shown in the graph. Thus, the Von Mises stress and the Contact Pressure are the main two parameters of interest.

If one compares the two in the graph below it can be observed that the main difference is that in the contact pressure plot there is no reduction of stress along the length of the implant. This reduction in stress is important to observe and understand, however it is not the variable that we are interested in for this analysis, hence, the variable to be minimised could be either the maximum contact pressure or the maximum Von Mises stress. Given that the latter was used in other similar studies, this was used (Samiezadeh, Tavakkoli and Fawaz, 2015)(Chakladar, Harper and Parsons, 2016)(Arnone, 2013).

$$\sigma_v = \sqrt{\frac{1}{2}[(\sigma_{11} - \sigma_{22})^2 + (\sigma_{22} - \sigma_{33})^2 + 6(\sigma_{12}{}^2 + \sigma_{23}{}^2 + \sigma_{31}{}^2)]}$$
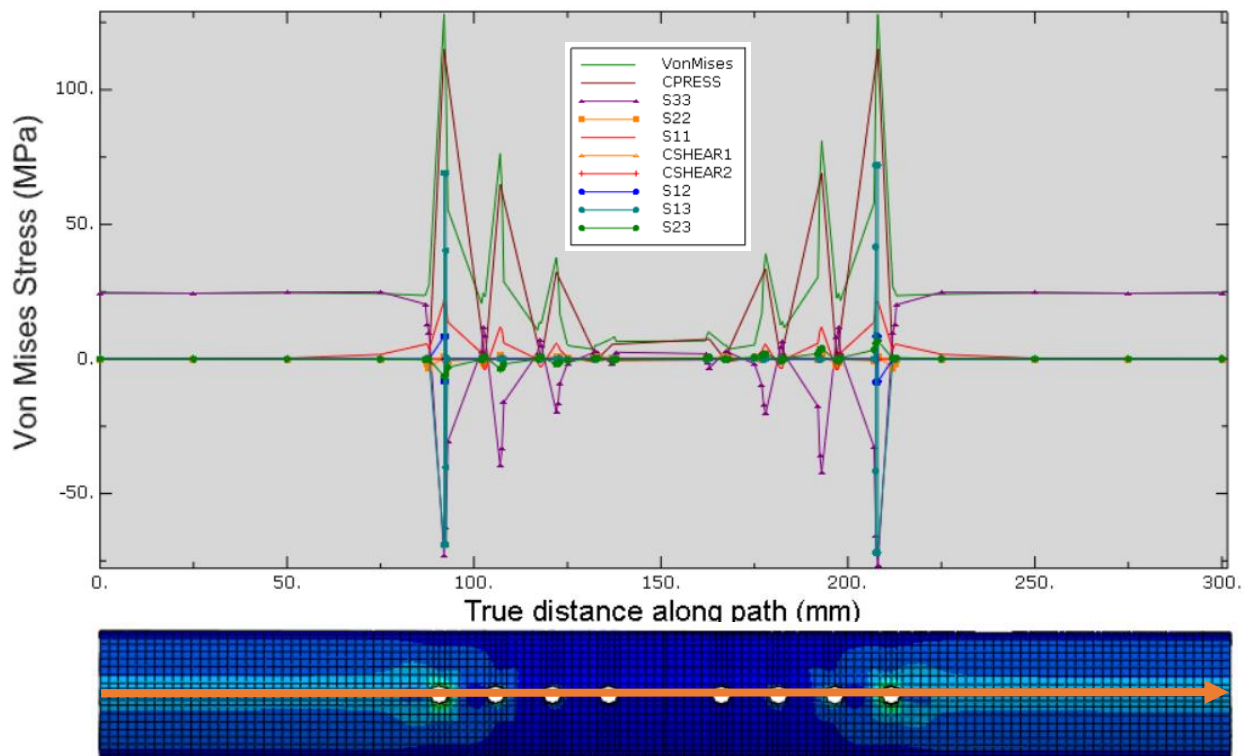
Figure 33: Different types of stress in the bone, along a central path. Stress is in MPa and distance along path is in mm.

5.2   (2) What constraint/s can we apply to ensure that the bone heals appropriately during the period when there is a fracture gap?

The question of what determines appropriate healing of a fracture gap was addresses extensively, and in a publication titled "Magnitudes of local stress and strain along bony surfaces predict the course and type of fracture healing" (Claes and Heigele, 1999) suitable criteria was developed. As can be seen in the figure below, their main idea was that by knowing the interfragmentary strain and hydrostatic pressure, one could predict the type of healing that would occur. However, in a later publication (Steiner *et al.*, 2014) M. Stainer, L. Claes and others state that the main contributing factor is the Interfragmentary strain (IFS) and this alone may be used to predict the type of healing. In this more recent paper they also devised alternative criteria for healing based on the axial and shear stiffness of a given fracture fixation construct, with the axial stiffness being most important. The two proposed criteria are presented graphically below.
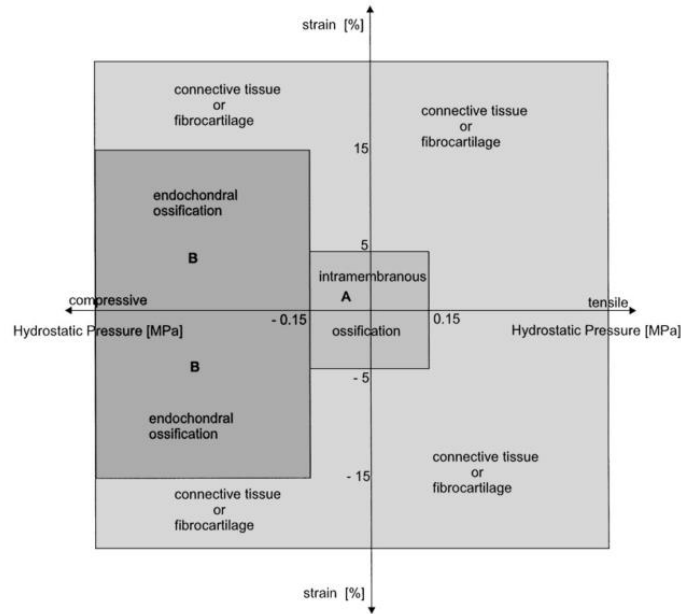
Figure 34: Conditions for primary healing (intramembranous ossification) and secondary healing (endochondral ossification) as described in *(Claes and Heigele, 1999).*
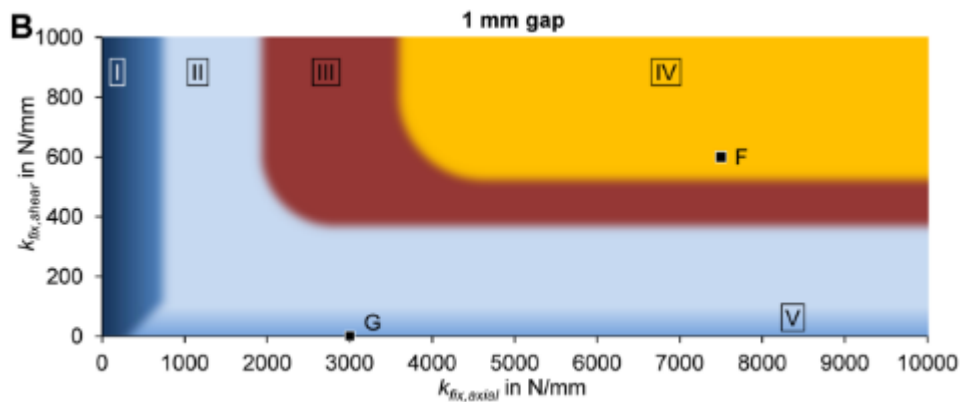
Figure 35: Healing criteria as determine in the publication mentioned above *(Steiner* et al*., 2014).* Yellow or IV shows the region of optimal healing. $K_{fix, axial}$ represents the axial stiffness of the construct and $K_{fix, shear}$ represents the translational shear stiffness of the construct.

A common objective of the presented studies is to create healing criteria to predict the type of tissue that will be generated under given conditions, in order to simulate the healing process with enough accuracy. This is also done in another study (Steiner *et al.*, 2013) where the type of tissue differentiation is predicted based on the type of loading. Although the present study does not attempt to simulate the healing process at various stages, to increase the reliability of the method this could be done in the future.

Thus, based on the referenced studies, the main choice to make is between the interfragmentary strain (IFS) and the Axial stiffness of the construct. Given that the IFS can be calculated directly from the deformation of the Finite Elements in the fracture gap, and that it was suggested by L. Claes (Steiner *et al.*, 2013) as a suitable measure, this was chosen as the measure for appropriate healing. The maximum compressive or tensile strain required to ensure direct healing takes place, as described by Claes and Heigele (Claes and Heigele, 1999), is 5%. However, this threshold was defined based on a two-dimensional Finite Element Model that used different material properties and a different gap size than we do here.

Assuming that an implant made entirely of pure titanium yields appropriate healing, it seems suitable to define the criterium for appropriate healing as follows: The maximum axial IFS should not be higher than 110% of the IFS calculated with an implant made entirely of titanium, nor lower than 90% of it. Moreover, the higher the IFS is, within these limits, the better. These are by no means reliable limits, but the current study is only concerned with a suitable methodology to solve the presented problem. For accurate and thus more useful results, a more realistic model should be created, and it should be validated through an in vitro experiment.

Below is the interfragmentary strain plotted along the circumference of the fracture gap (The top figure shows the starting point and direction of the plot). It is clear from the figures that the maximum axial IFS occurs at the region closest to the lateral middle of the plate. This can also be intuitively deduced by considering the deformed shape. Thus the only IFS (magnitude is taken, irrespective of whether it is compressive or tensile) that needs to be evaluated is that of the middle bottom element shown on the figure below.
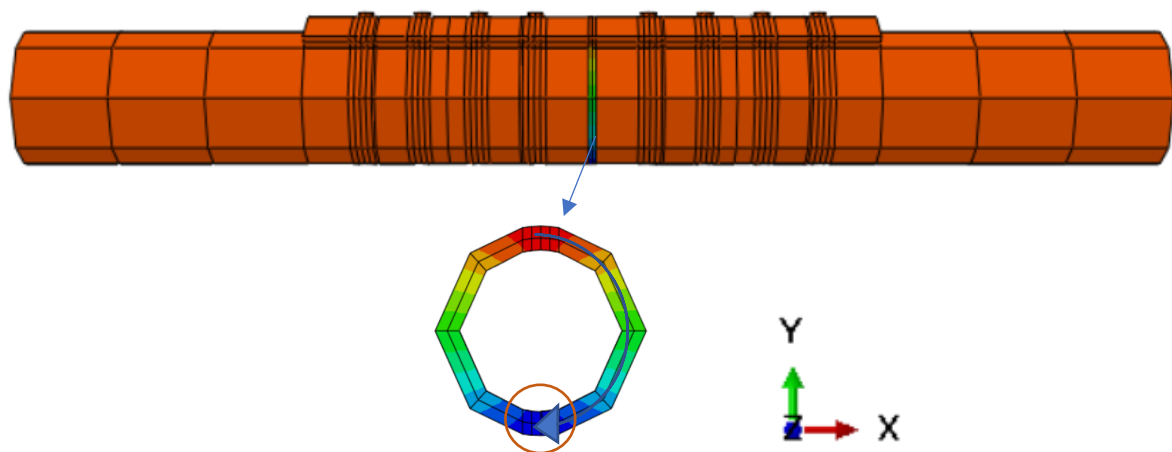
Figure 36: Section of the bone used for measuring the IFS. The blue arrow shows half of the path used for the plots shown below. The orange circle encircles the element that always has the maximum IFS.
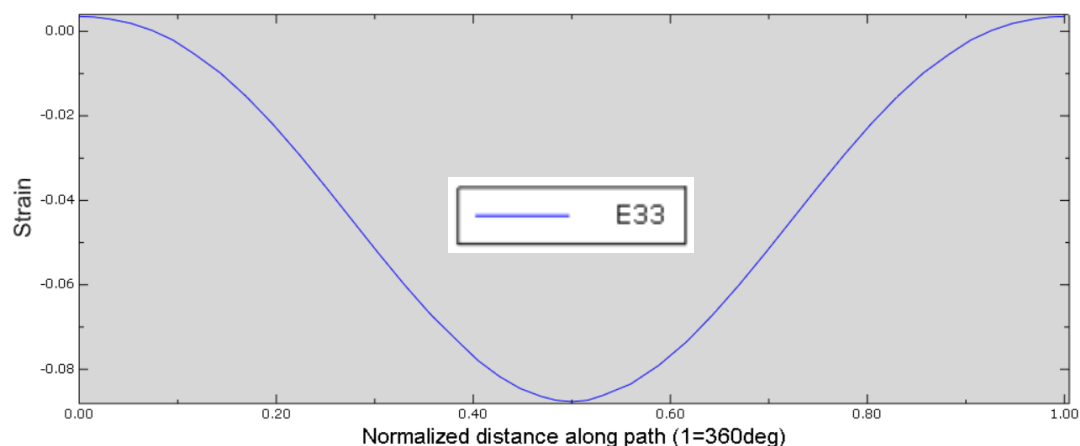
Figure 37: Normal strain (in the z axis from the axes shown above) results in the fracture gap plotted against the degrees along the circumference of the fracture segment. As shown, the horizontal axis of the plot consists of the normalized circumferential length along the fracture gap. 1=X, 2=Y and 3=Z, E11 is the normal strain in the x axis and so on.

5.3   (3) How to control the young's modulus distribution throughout the implant?

Given that the Finite Element Method divides the implant into a Finite number of elements, one could simply assign different young's modulus values to every element, effectively creating a distribution

along every one of the three orthogonal axes. In the plate shown below for instance, there are 12 elements along the X axis, 60 along the Y axis and 2 along the Z axis. Thus, the distribution of young's modulus along a given direction can be controlled using a number of intervals which is equal to the number of elements in the respective direction. The graph below shows an example of how a longitudinal distribution can be control with a Finite Number of elements. Clearly, the higher the element density, the smoother the curves would become. Concluding, the most accurate way to control the distribution of material properties is by having an infinite number of elements and assigning different material properties to each.
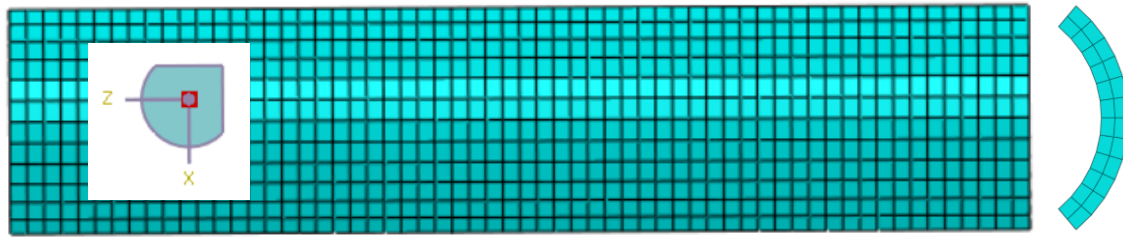
Figure 38: Meshed plate. The number of elements is 12 by 60 by 2 as explained above.
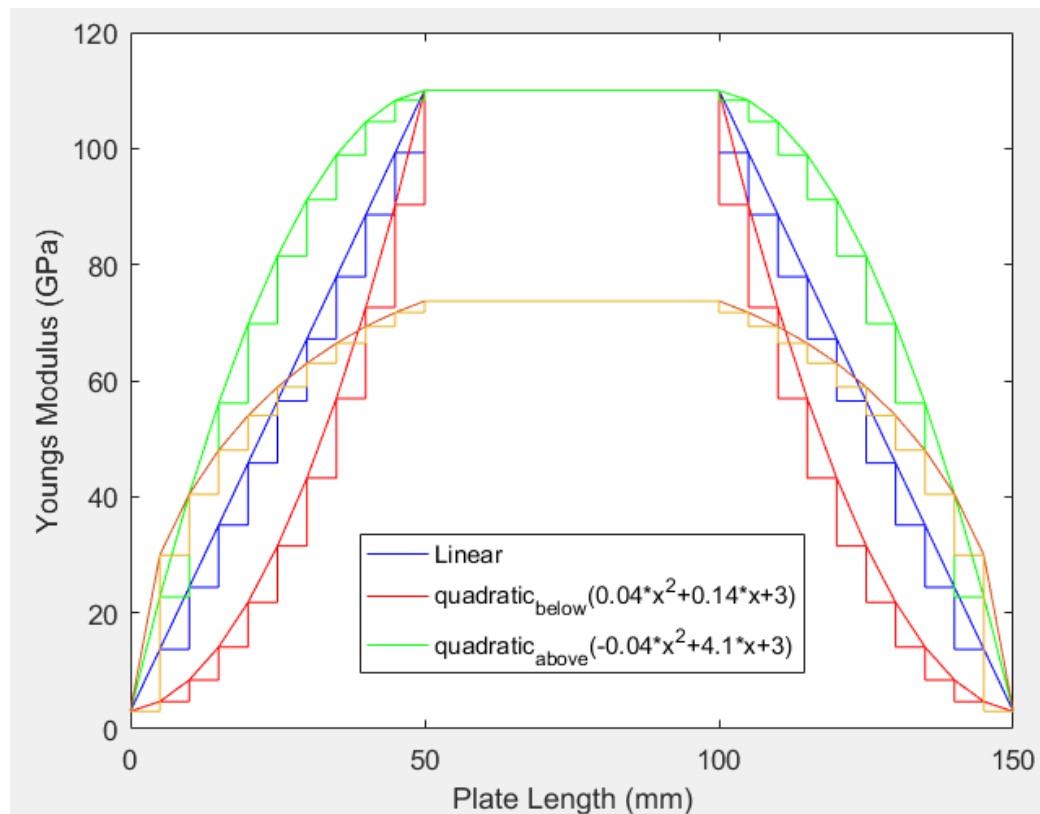
Figure 39: Different distributions of young's modulus along the plate length.

Unfortunately, however, while increasing the number of elements does increase the accuracy of the distribution representation, it also increases the dimensionality of a discrete solution space. To illustrate this the figure below is presented. If the shown part of the plate is divided into 15 segments as shown, and every segment can have any one of 10 possible young's modulus values between 3 and 110 GPa, the number of possible combinations would be 10^{15}. Running all these models would take 10^8 years for my computer. This is precisely why an optimization algorithm can be very handy in order to search through this incredibly large space of solutions in a smart way and thus arrive at the desired

solution without having to run too many models (as fast as possible). The optimization decisions are discussed in the next section.
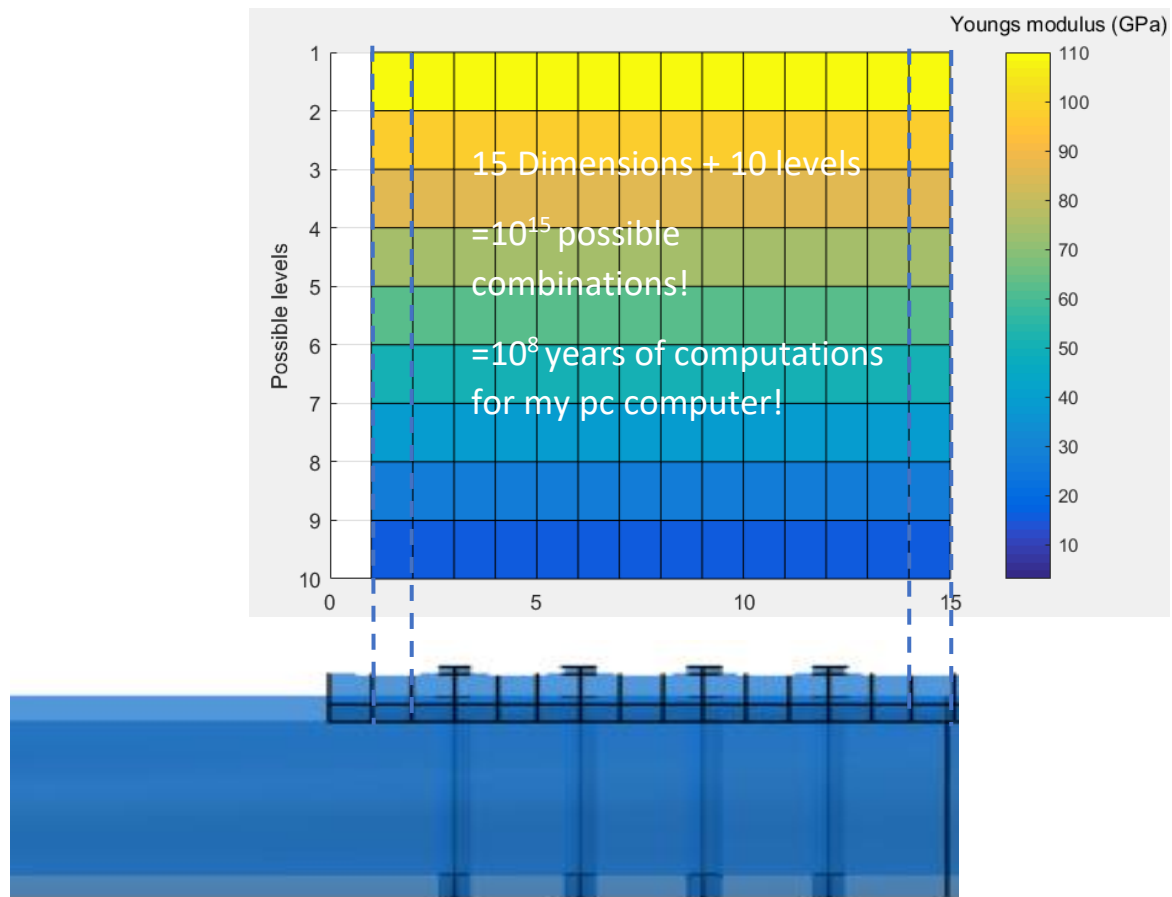
Figure 40: (above) graph showing the possible levels for each section of the plate, (below) plate and bone showing the number of elements. Note that no screws are shown here, but the model used has screws as has been presented previously, this is used only for simplicity.

In order not to allow the dimensionality of the solution space to be directly related to the mesh size, the plate was sectioned independently of the mesh and material properties were separately assigned to these sections, as illustrated below. Each section may contain many elements, but all elements will share the same material properties within a given section. As described in the Finite Element Models creation section, the minimum and maximum values for the young's modulus were set at 3 and 110 GPa respectively. The plate was eventually divided into more than three sections as explained in the next part of the report.
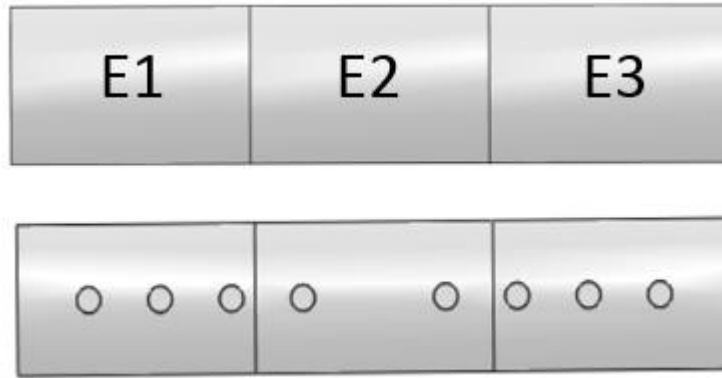
Figure 41: Initial segmental division of plate. E stands for young's modulus. (above) Model without screws and (below) model with screws.

5.4 (4) How to find the optimal young's modulus distribution throughout the implant?

5.4.1 2D visual optimization

5.4.1.1 Methodology:

As briefly discussed above, the optimal young's modulus distribution, for a discrete space of 10 intervals, happens to be one out of 10^n combinations, where n is the number of sections considered, and thus the dimensionality of the solution space. Intuitively, the only solution space that can be visualized in terms of the output variable is a two-dimensional solution space. To get some initial insights, the implant was divided into three segments as shown in the figure below, but the young's modulus of the outer sections (E1) was assumed to be equal. Thus, only two variables need to be optimized, E1 and E2, and the possible combinations can be represented in a 2D space. Each variable was allowed to have any one of ten values between 3 and 110 GPa, making the number of possible combinations 10^2=100. The mesh used was that found to be the quickest in terms of computation time during the Mesh refinement study.
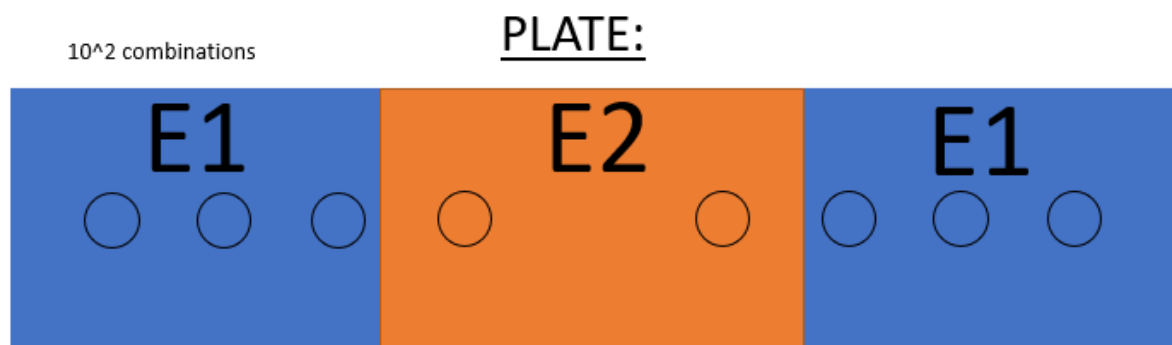
Figure 42: Plate division for the 2D optimization and variables representing the young's modulus at each of the sections.

The maximum Von Mises Stress was plotted for all the 100 possible combinations and the results are shown in the next section. For every combination the model was ran in ABAQUS but through a routine written in MATLAB, which accesses the input and output files of ABAQUS. The plots were also created

using MATLAB. For every iteration, the chosen measure for appropriate healing, the Interfragmentary strain (IFS) was also calculated, and wherever it was above 110% of the IFS calculated with an implant made purely of titanium, it was decided that such a combination would not be allowed. This produces the constrained solution space as shown in the results, which allows for visually finding the optimal combination. Various post-processing plots were also made and are described in the results section.

5.4.1.2 Results:

As explained in the methodology, the maximum stress as well as the maximum Interfragmentary strain (IFS) was plotted for a 2D solution space, with the third dimension being the maximum Von Mises Stress or IFS. The plot is presented below. It can be observed that the maximum Von Mises stress decreases with decreasing the young's modulus of either the outer or the inner section. However, the gradient of the decrease in Von Mises stress due to decreasing the outer young's modulus (E1) seems to be much steeper. And in fact overall it seems that the young's modulus of the outer section has much more of an influence in the maximum stress. It should be noted that the minimum value for either material axis is three (from 3 GPa) and not zero. Moreover, looking at the locations where one material is at its minimum value (3) and the other at its maximum (110), it can be observed that the case when the outer material is at its lowest point produces a lower maximum Von Mises stress in the bone.
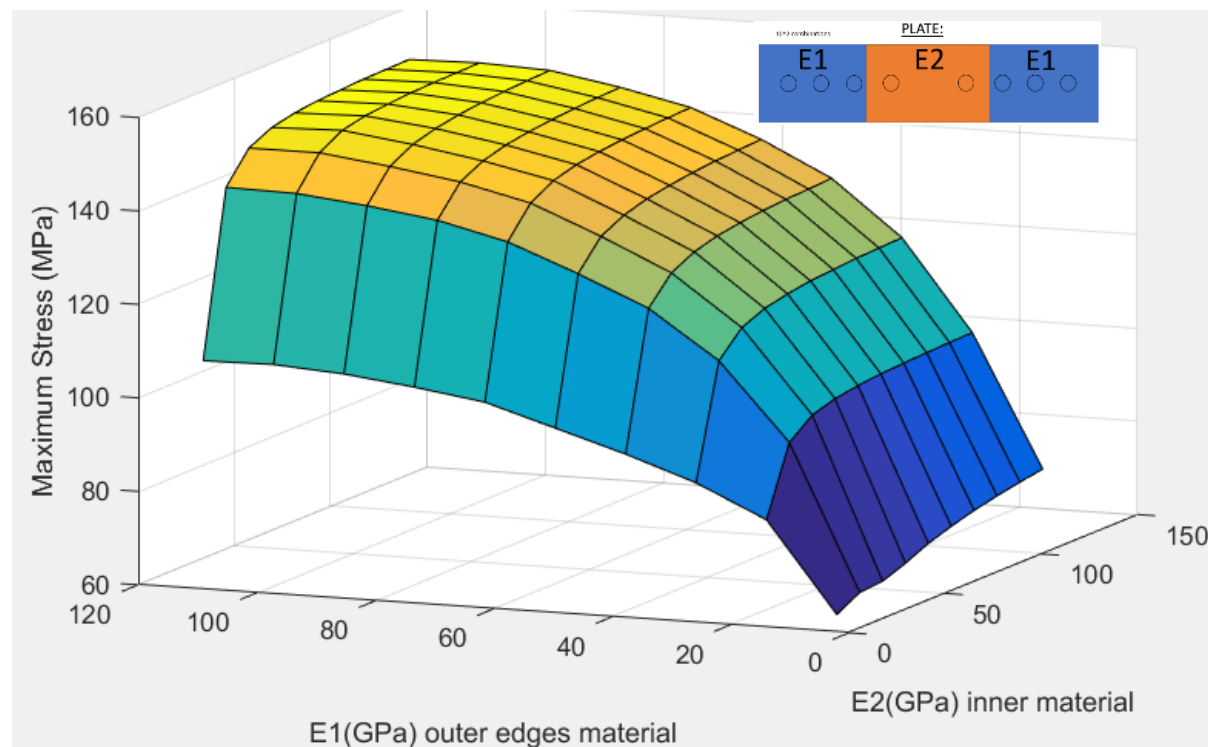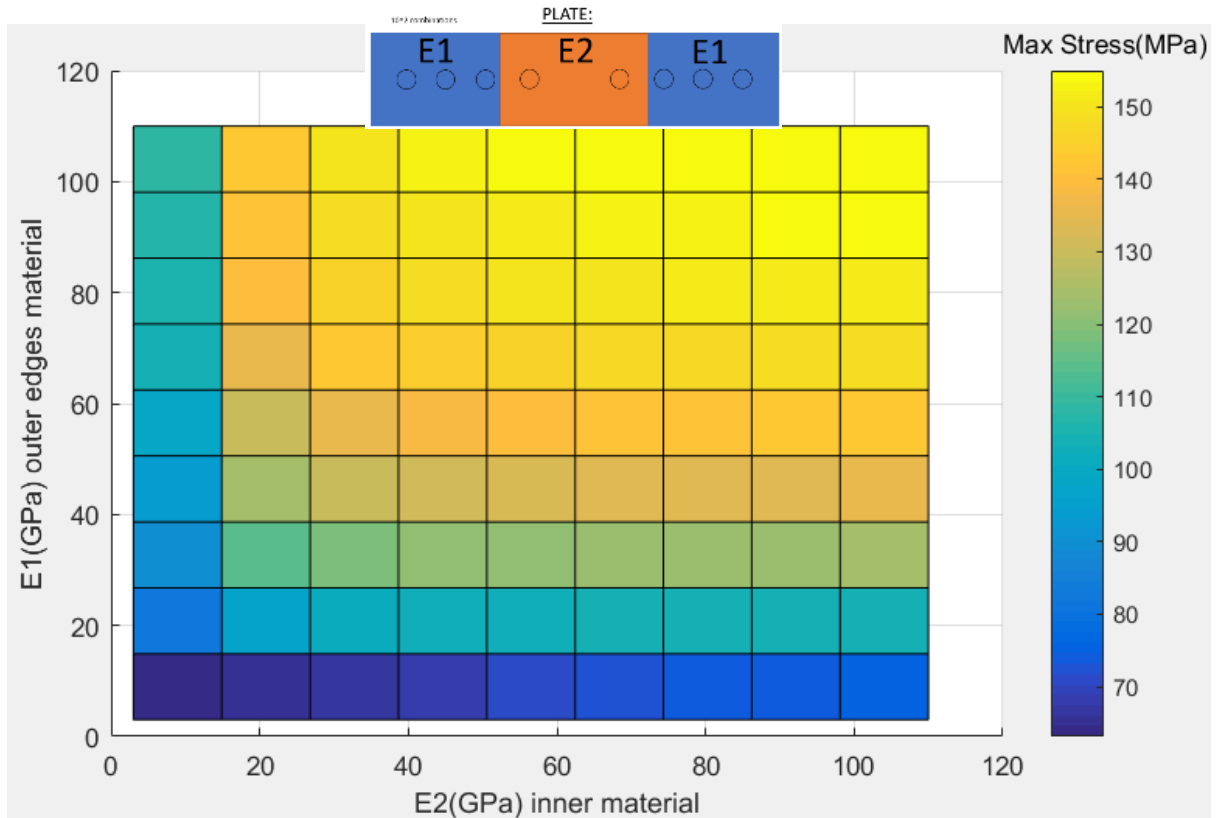
Figure 43: Maximum Von Mises stress calculated at every single one of the 100 possible combinations of E1 and E2. The calculation was done using Abaqus but ran through MATLAB, hence the plots are made in MATLAB. <u>Above</u> is the plot in 3 dimensions, and <u>below</u> is the same plot but using only colour as the third dimensions as this is easier to interpret.

For the normal interfragmentary strain, it can be seen from the figures below that it varies quite similarly with varying either the inner (E1) or outer (E2) value of young's modulus, although as can be seen more clearly from the figure with a colour bar, E2 seems to have more of an influence in increasing the IFS than E1 does.
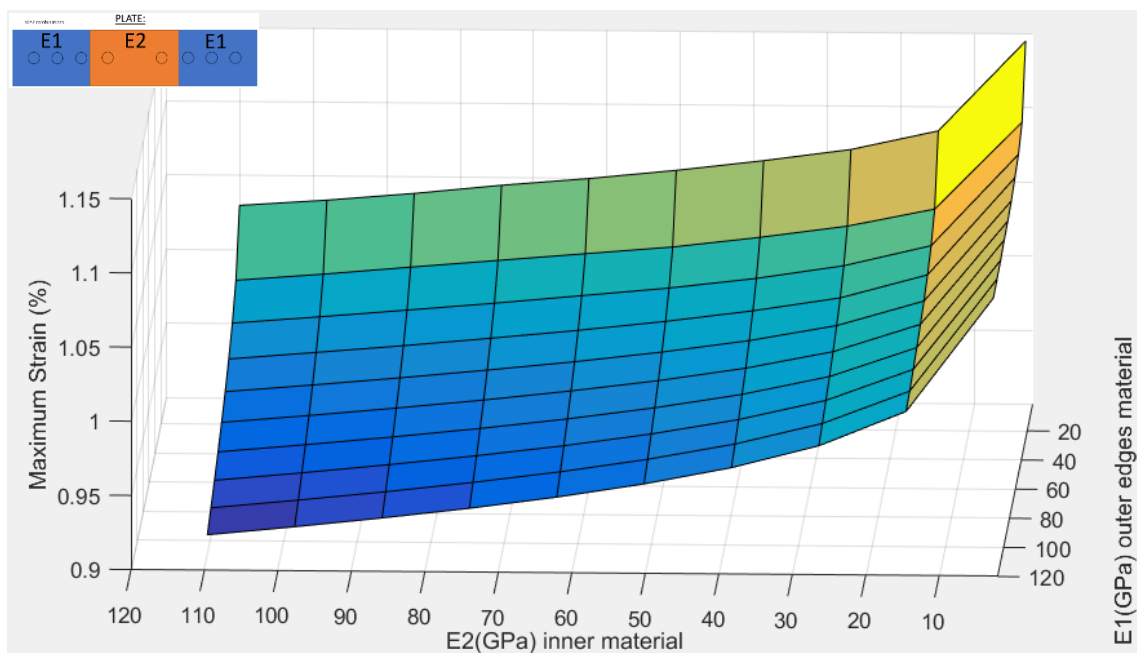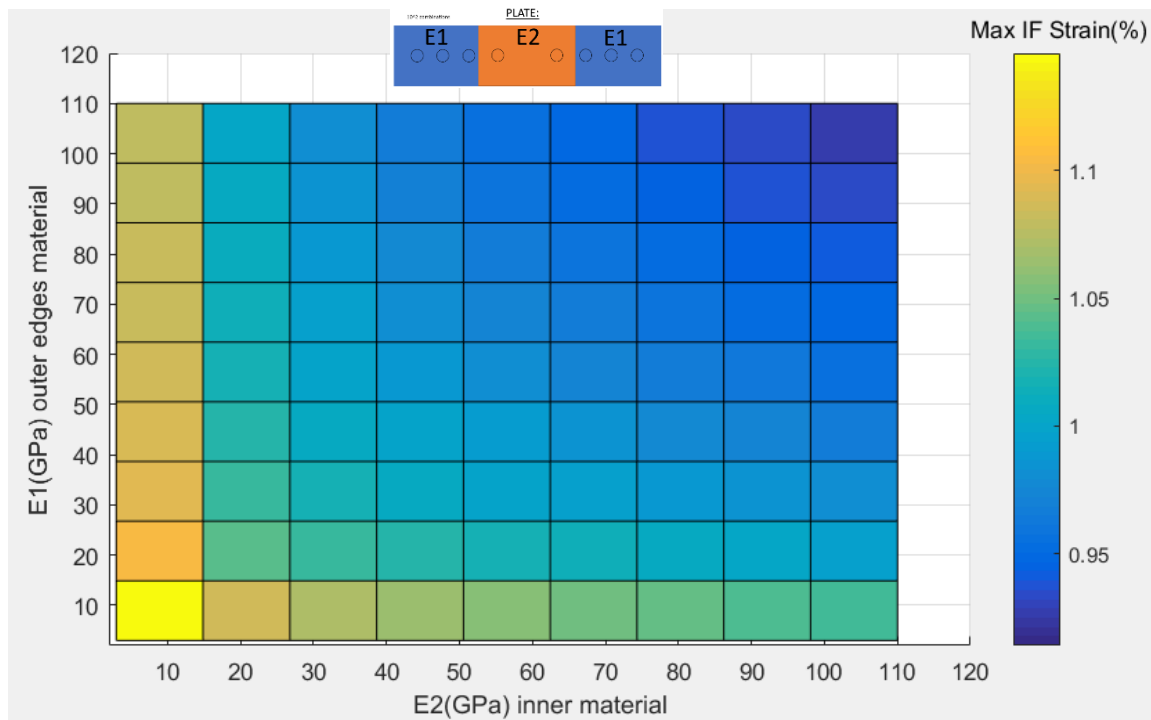
Figure 44: Maximum interfragmentary normal strain calculated at every single one of the 100 possible combinations of E1 and E2. The calculation was done using Abaqus but ran through MATLAB, hence the plots are made in MATLAB. Above is the plot in 3 dimensions, and below is the same plot but using only colour as the third dimensions as this is easier to interpret.

The following plot represents the constrained solution space. The goal is to find the lowest maximum stress possible while ensuring that the strain is low enough. Using the criterion described earlier which stated that the strain shouldn't be any higher than 110% of the strain obtained with a titanium implant, which is equivalent to a strain of 1.093%, the red area below could be computed as the area where the strain would be too high to ensure appropriate healing. Due to the low dimensionality of the problem at hand, it is possible to visually find the constrained optimum, which in this case would be: E2=3GPa and E1=74.3GPa. This yields a maximum Von Mises stress of 73.4 MPa.
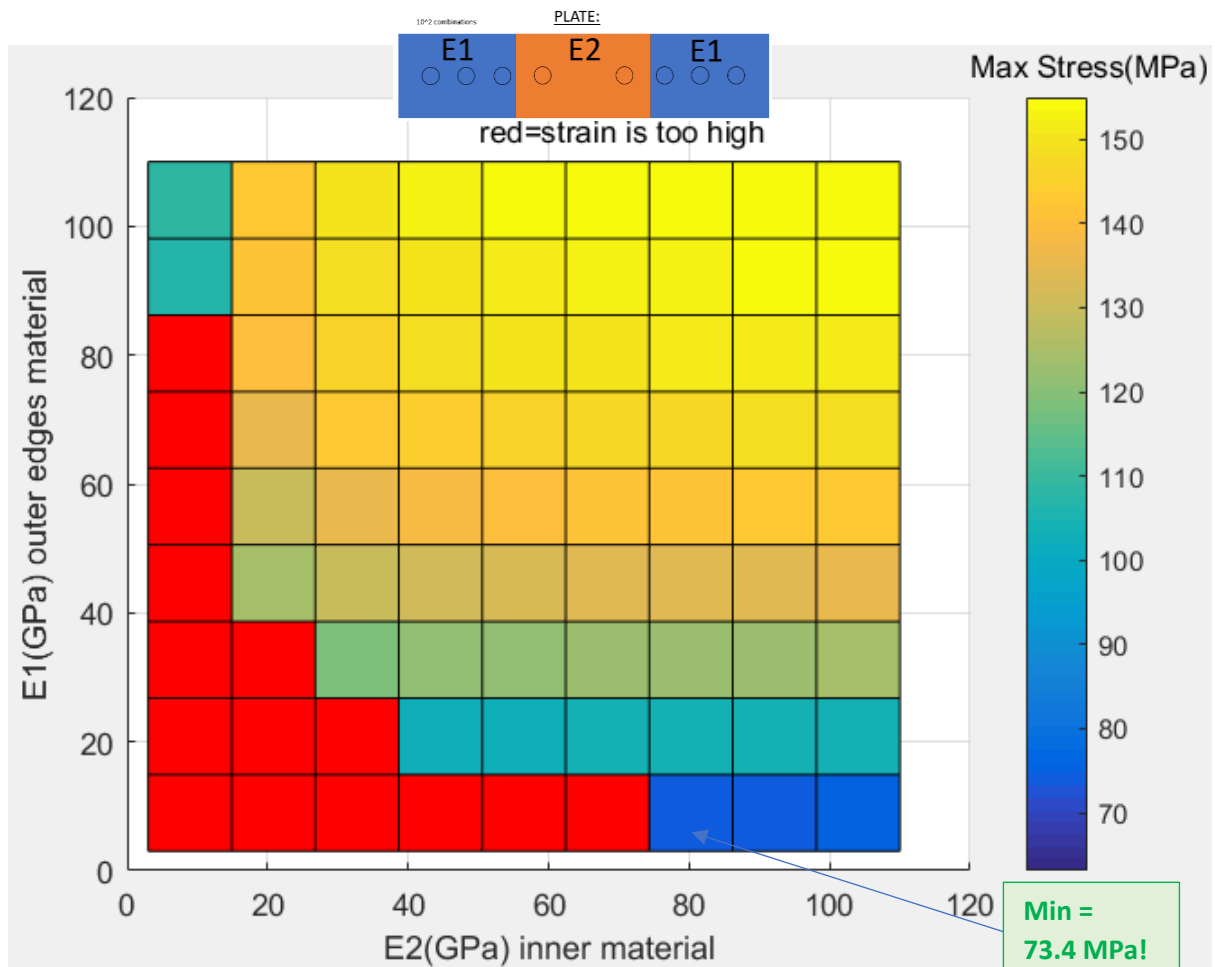
Figure 45: Maximum interfragmentary normal strain calculated at every single one of the 100 possible combinations of E1 and E2. The plot uses colour as the third dimension (Maximum Von Mises stress). The red squares represent combinations of E1 and E2 that would stimulate a IFS which is too high to allow for appropriate healing, according to the proposed criterium.

What a smart optimization algorithm would do is find this constrained optimum without having to search through the whole space, for instance a gradient-based optimization routine could begin at 110GPa, and follow a path of descending gradient until arriving at the constrained minimum (where the magnitude of the gradient is low enough). In which case the space would not have intervals but rather be made into a continuous one. Such a technique is discussed in a later stage of the report.

Further below a distribution plot was again made to show how the distribution of Von Mises Stress for a fully titanium implant compares to that of the optimised implant (E1=3GPa and E2=74.3GPa). It can firstly be noted that the plot further proves that the stress peaks are in fact reduced significantly. It can also be noted that the stress peaks at the screws near the fracture are now higher, and if one kept decreasing the outer young modulus, it is clear that the inner peaks would become the highest ones. This is because reducing the stiffness of the outer sections too much is almost like making a plate one third of the original length, and the inner peaks are now the outer peaks of that plate. Altogether, the stress shielding is also reduced, which is a further benefit of this optimised fracture fixation implant.
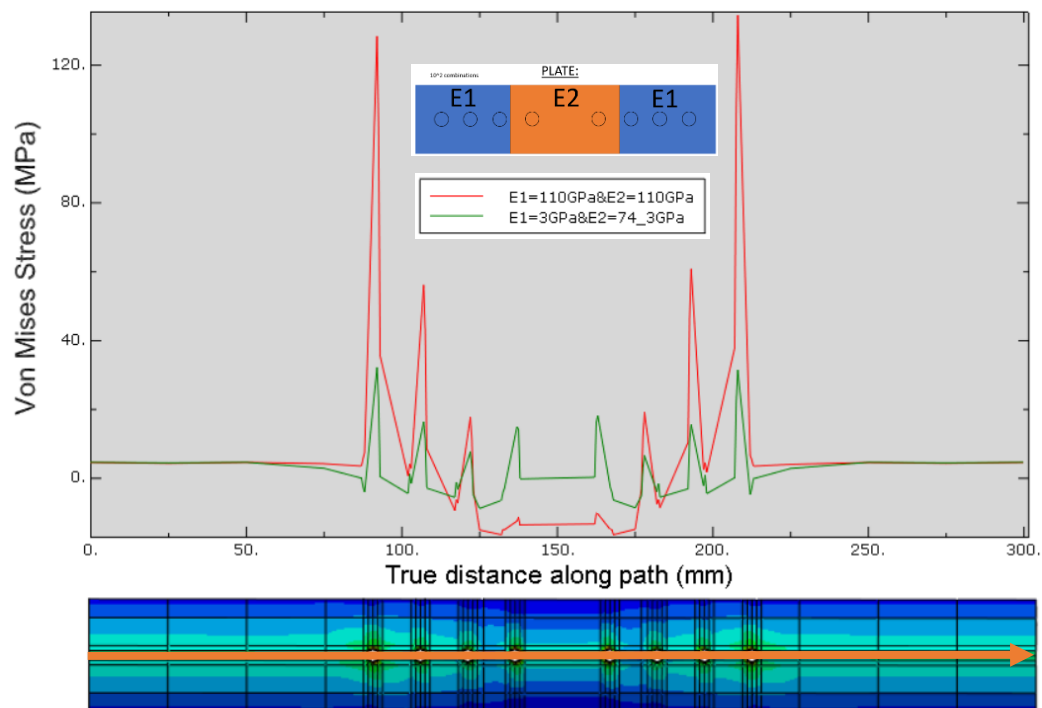
Figure 46: (green) Distribution of stress for final simulation along the path shown, (red) Distribution of stress for plate made fully of titanium along the path shown. 74_3 stands for 74.3.

Further plots were made to analyse how varying the material of the whole plate compares to varying only the material defined by E2 or that defined by E1 and the results are presented below, which are derived from the results shown on the 3D plots. Varying the value of E1 (the young's modulus of the outer sections) has clearly almost the same effect on the maximum stress as varying the young's modulus of the whole plate, whilst varying only the inner material (E2), has a much weaker effect on the maximum stress. When it comes to the Interfragmentary strain (IFS), both E1 and E2 have a very similar effect, as seen previously in the 3D plot, and as seen perhaps more clearly in the 2D plot below. As can be expected, increasing the young's modulus of the whole plate causes a more pronounced increase in the IFS. Lastly, a distribution plot was again made that compares the extreme cases for all three Von Mises stress curves discussed in this paragraph.
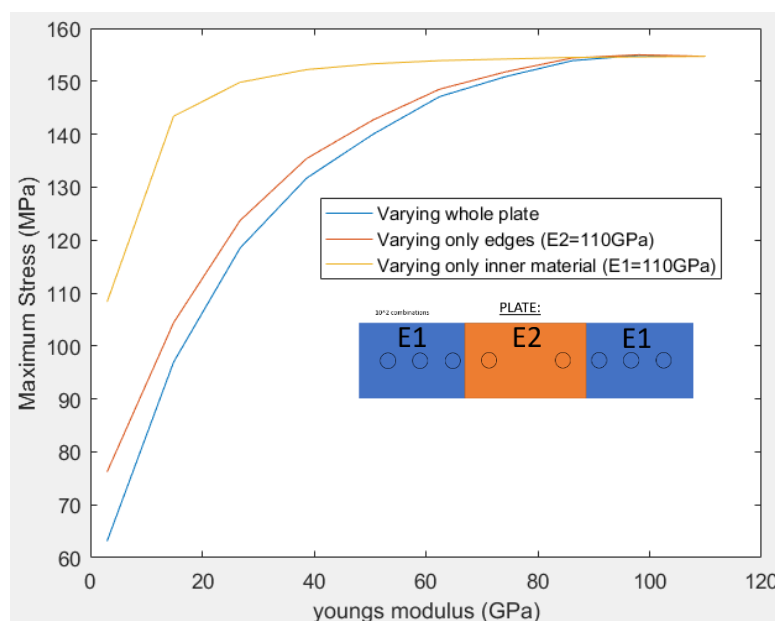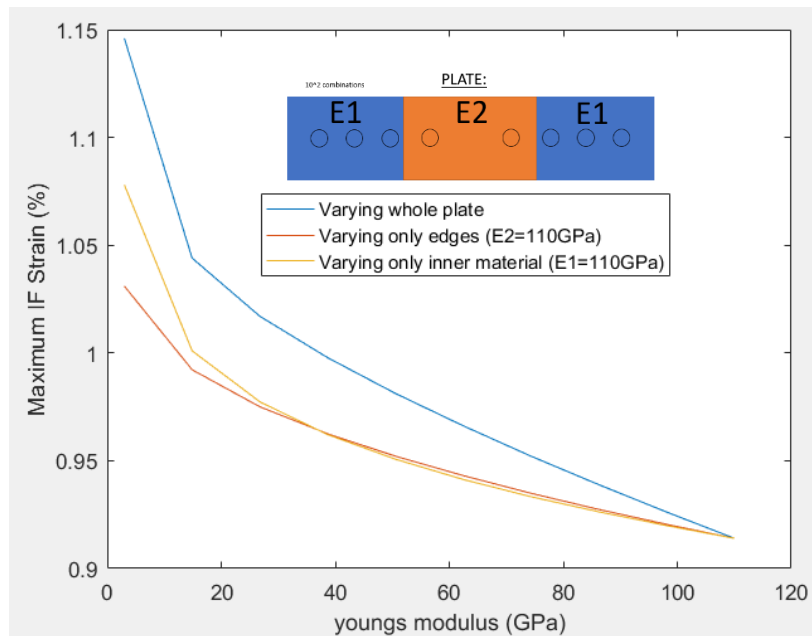
Figure 47: 2D plots comparing the influence of varying the young's modulus of the plate and varying the young's modulus of only inner or only outer sections. (above) influence in maximum Von Mises Stress, (below) influence in interfragmentary strain.
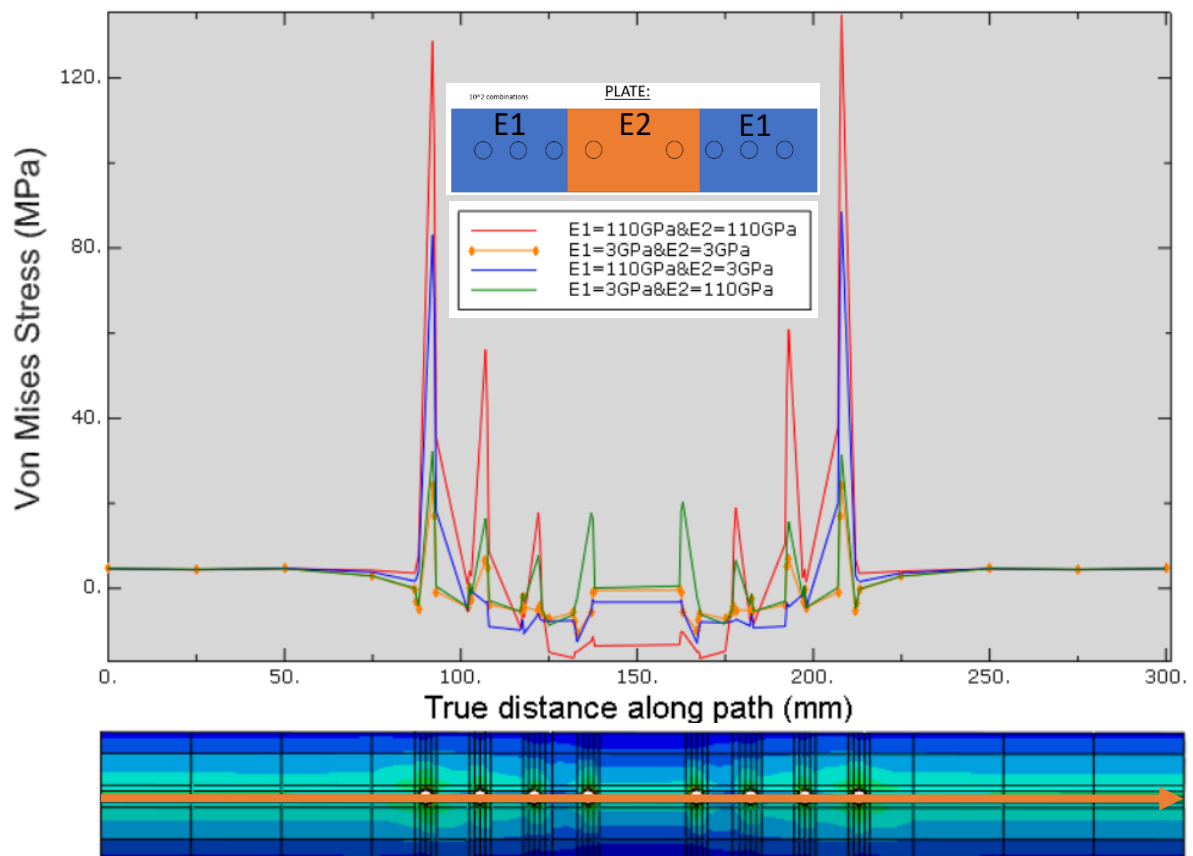
Figure 48: Distribution plots of the extreme cases from the maximum Von Mises stress 2D plots shown above. E1 and E2 represent young's modulus values for the implant.

5.4.2 4D investigation

5.4.2.1 Methodology:

As was previously done for certain implant parameters, the Taguchi method was again used in order to perform a 4D investigation. The plate was divided into eight sections, but the material properties of one half of the plate were assumed to be the mirrored properties of the other half, hence only four parameters had to be analysed as shown below. Each parameter was again assigned three different levels in order to use an L9 Taguchi orthogonal array. This time all four parameters had the same three levels as shown below; 3, 55 and 110 GPa respectively.

The aim of this analysis was to find out how much of an influence did every one of the four sections have on reducing the maximum Von Mises stress for the case of the model without a fracture, and which had more of an influence on the maximum strain at the fracture surface for the case of the model with a fracture. Thus, the same performance measures were used as in the parametric analysis and two studies were needed.
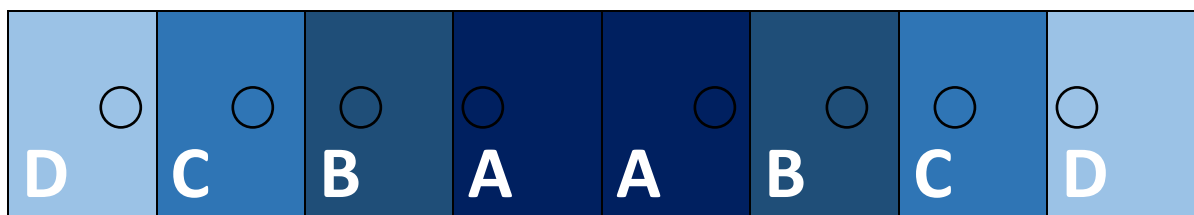
Figure 49: Plate division made for the current 4D material influence investigation.

Table 12: The possible levels that any one of the sections shown above could have. The levels are young's modulus values.

	Levels		
Factors	**1**	**2**	**3**
Plate Section A	3GPa	55GPa	110GPa
Plate Section B	3GPa	55GPA	110GPa
Plate Section C	3GPa	55GPa	110GPa
Plate Section D	3GPa	55GPa	110GPa

Table 13: The nine combinations which according to the Taguchi method, statistically represent the 81 possible combinations between the levels of each plate section shown above.

L9 Orthogonal array				
Simulation #	Plate Section A	Plate Section B	Plate Section C	Plate Section D
1	3GPa	3GPa	3GPA	3GPA
2	3GPa	55GPa	55GPa	55GPa
3	3GPa	110GPa	110GPa	110GPa
4	55GPa	3GPa	55GPa	110GPa
5	55GPa	55GPa	110GPa	3GPA

6	55GPa	110GPa	3GPA	55GPa
7	110GPa	3GPa	110GPa	55GPa
8	110GPa	55GPa	3GPA	110GPa
9	110GPa	110GPa	55GPa	3GPA

5.4.2.2   Results:

The ANOVA tables below present the influence that the different parameters had on the Von Mises Stress and Interfragmentary strain respectively. Further down a figure with an implant shows clearly the results for each segment of the implant. It is clear that the outermost section has the largest influence on the Von Mises Stress (54.3%), while the other sections have all the same influence (15.2%). Regarding the IFS, section A appears to be slightly more influential than the rest, but not significantly.

Table 14: Max Von Mises stress and Maximum IFS results for the nine selected combinations of material properties according to the L9 Taguchi orthogonal array of the three material levels for each section.

Parametric study results for plate sections									
Simu #	Plate Section A	Plate Section B	Plate Section C	Plate Section D	Max Von Mises Stress (Mpa)	Max IF Strain (%)	S/N VM Stress	S/N IF Strain	Diff VM	Diff IFS
1	3GPa	3GPa	3GPA	3GPA	61.8	1.253	42.12	26.99	-42.6	0.1
2	3GPa	55GPa	55GPa	55GPa	106.9	1.173	17.67	34.86	2.5	0.1
3	3GPa	110GPa	110GPa	110GPa	113.8	1.164	29.05	36.44	9.4	0.0
4	55GPa	3GPa	55GPa	110GPa	108.2	1.124	21.25	55.19	3.8	0.0
5	55GPa	55GPa	110GPa	3GPA	128.1	1.072	37.06	36.14	23.7	0.0
6	55GPa	110GPa	3GPA	55GPa	95.5	1.080	28.50	37.77	-8.9	0.0
7	110GPa	3GPa	110GPa	55GPa	103.1	1.098	11.49	43.19	-1.3	0.0
8	110GPa	55GPa	3GPA	110GPa	101.9	1.066	17.33	35.09	-2.5	-0.1
9	110GPa	110GPa	55GPa	3GPA	119.9	1.039	33.38	31.50	15.5	-0.1
Mean					104.4	1.1	26.4	37.5	0.0	0.0

Table 15: Signal-to-noise ratios for the Von Mises Stress results acquired. Each result of every level corresponds to the highest S/N ratio for every level of every parameter. DM stands for mean difference, DMS for mean difference squared and SSDT_i stands for the sum of differences squared. The later is used for the calculation of the ANOVA table.

Global mean: 36.4	Levels			Stats			
Factors	1	2	3	Mean	DM	DMS	SSDT_i
Plate Section A	42.12	37.06	33.38	37.5	1.1	1.15	42.0
Plate Section B	42.12	37.06	33.38	37.5	1.1	1.15	42.0
Plate Section C	42.12	33.38	37.06	37.5	1.1	1.15	42.0
Plate Section D	42.12	28.50	29.05	33.2	-3.2	10.37	150.0

Table 16: ANOVA table showing the influence of the different plate sections on the maximum Von Mises stress.

Source	Degrees of Freedom, D.F.	Sum of square, Sx	Mean square Vx=Sx/D.F.	Influence, rho(%)
Plate Section A	2	42.04	21.02	**15.22**
Plate Section B	2	42.04	21.02	**15.22**
Plate Section C	2	42.04	21.02	**15.22**
Plate Section D	2	150.05	75.02	**54.33**
Total	8	276.18	138.09	100.00

Table 17: Signal-to-noise ratios for the IFS results acquired. Each result of every level corresponds to the highest S/N ratio for every level of every parameter. DM stands for mean difference, DMS for mean difference squared and SSDT_i stands for the sum of differences squared. The later is used for the calculation of the ANOVA table.

Global mean: 44.5	Levels			Stats			
Factors	1	2	3	Mean	DM	DMS	SSDT_i
Plate Section A	36.44	55.19	43.19	44.9	0.3893	0.1516	180.811
Plate Section B	55.19	36.14	37.77	43.0	-1.5152	2.2957	229.748
Plate Section C	37.77	55.19	43.19	45.4	0.8344	0.6963	160.928
Plate Section D	36.14	43.19	55.19	44.8	0.2914	0.0849	185.663

Table 18: ANOVA table showing the influence of the different plate sections on the maximum IFS.

Source	Degrees of Freedom, D.F.	Sum of square, Sx	Mean square Vx=Sx/D.F.	Influence, rho(%)
Plate Section A	2	180.81	90.41	**23.88**
Plate Section B	2	229.75	114.87	**30.34**
Plate Section C	2	160.93	80.46	**21.25**
Plate Section D	2	185.66	92.83	**24.52**
Total	8	757.15	378.57	100.00

Max VM stress Influence=	54.3%	15.2%	15.2%	15.2%	15.2%	15.2%	15.2%	54.3%
Max IFS Influence=	24.52%	30.3%	21.3%	24.5%	24.5%	21.3%	30.3%	24.52%
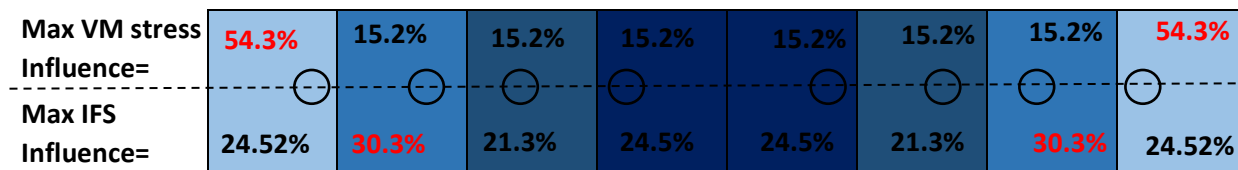
Figure 50: Plate sections showing the influence they have on the maximum Von Mises Stress (above) and on the maximum interfragmentary strain (IFS)(below).

5.4.3   10D optimization

5.4.3.1   Methodology:

In order to control the distribution of young's modulus more precisely, the plate was now divided into 20 sections and it was assumed that the material properties of one longitudinal half of the plate were the mirrored properties of the other half. Hence, only half the section's material properties need to be defined as shown below. This is similar to the problem presented previously, only now there are 10 sections and each one has 5 possible values (intervals), producing a total of 5^{10} (9765625) possible combinations.
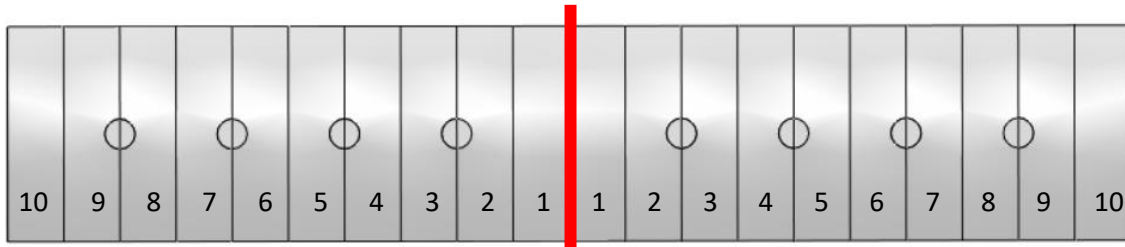
Figure 51: Plate division for final 10D optimisation

In order to solve this problem an optimization algorithm is required. A recent paper titled "On optimisation of a composite bone plate using the selective stress shielding approach" (Samiezadeh, Tavakkoli and Fawaz, 2015) dealt with a similar problem in a smart manner. 14 plate sections were to be optimized, each of which had four possible levels. Therefore their solution space consisted of 4^{14} possible combinations, larger to that considered in the present study, but comparable. The approach used to solve the problem was as follows: (1) The use of 6 constraints reduced the solution space to a much smaller number of combinations: 279,990. (2) The use of a bending stiffness criterion for the plate (minimum of 8Nm^2 for proper healing) reduced this to only 199,905 combinations. (3) Finally, these combinations were organized into intervals of 1Nm^2 and only the combination of each interval with the highest Stiffness Efficiency Factor (SEF) was chosen. This leaves only 13 combinations to be analysed, which is done through Finite Element Analysis. Since the calculation of the stiffness values can be done very quickly in a program such as MATLAB, the most time-consuming part is running the 13 models in an FEM program such as ABAQUS. But even that, given the low number of models, can be done very quickly.

This procedure might be a smart one, but it is not very flexible to the changing of various parameters, because the stiffness calculations are only valid for a simple slim beam as that shown. However, the idea of excluding many combinations using an appropriate constraint was used in this study. An assumption was made which states that combinations where the outer elements are not equal or lower to the inner elements, should not be evaluated. This is based on the 4D – Investigation results, where it was concluded that lowering the outer material has the highest influence in reducing the maximum stress in the bone, and so it follows that cases where the young's modulus is low at the middle sections and high at the ends are not worth considering.

```
for ii=1:9
    if E(ii)<=E(ii+1)
        g(ii)=1;%Inclusion criterium
    else
        g(ii)=0;%Exclusion criterium
    end
end

if sum(g)==9 %Include this
```

Figure 52: Loop through the nine inner most sections of the plate (the plate is mirrored so there are actually 18 inner sections) checking whether the young's modulus of the given section is lower or equal to the next section. If it is, then the relevant combination is included, if it is not it is excluded. E is a vector of 10 elements, each containing the young's modulus of one section. Numbering begins at the central section.

This assumption reduces the number of possible combinations from 5^{10} (9765625) to 1001. In other words, only 0.0103% of the initial combinations are now left to be analysed. For the initial position of the optimization, the 2D optimization was used. From the 2D optimisation it became clear that the global minimum of the unconstrained optimization is found where the plate is as porous as possible, which in this case, given the minimum value of young's modulus, is a plate with all elements having a young's modulus of 3GPa. Thus, this was assigned to be the initial state of the current optimization.

The way that the exclusion technique was implemented in MATLAB was through the use of a 10-dimensional analysis. 10 loops were created within each other as shown in the figure below. Each loop had 5 steps to access each of the 5^10 (9765625) combinations. The order that this process used can be intuitively deduced by looking at the loops, firstly the inner sections increase the young's modulus until the maximum, then the next sections towards the outside increase their young's modulus value by one step and the initial process is repeated, etc. For every combination, the constraint mentioned above was first checked in order to exclude the combinations that did not comply with it. The combinations that pass the criterium were stored in a vector of 1001 elements.

```matlab
%These are all the 10 dimensions (each of 5 steps)
for i10=E_chh; for i9=E_chh
for i8=E_chh;for i7=E_chh
for i7=E_chh;for i5=E_chh
for i4=E_chh;for i3=E_chh
for i2=E_chh;for i1=E_chh
n=n+1;%count all simulations
E=[i1,i2,i3,i4,i5,i6,i7,...
    i8,i9,i10];%the 10 mirrored material section variables
E=[fliplr(E),E];%Mirroring the material properties

for ii=1:9
    if E(ii)<=E(ii+1)
        g(ii)=1;%Inclusion criterium
    else
        g(ii)=0;%Exclusion criterium
    end
end

if sum(g)==9 %Include this
m=m+1;%Count combinations that meet criteria
E_todo(m,:)=E;%Store them in a matrix
end

end;end;end;end;end;end;end;end;end
```

Figure 53: MATLAB code used to loop through the 10-dimensional space of nearly 10 million combinations, thus accessing each combinations. It then used the criterium described earlier to only include the desired combinations in a vector 'E_todo'.

Usually, an ideal optimization routine to use would be an iterative gradient-based routine such as that used by R. Huiskes and R. Boeklagen (Huiskes and Boeklagen, 1989) on a shape optimization for a hip prosthesis. The iterative method they used is presented in the image below. As can be seen, the FE model is ran iteratively until the objective function converges to a minimum. The smart part about this technique is that the direction that the search algorithm takes is dependent on the gradient at any point, it follows that slope until a minimum is found. To address the risk of getting stuck at a local minimum, various starting positions may be used and their respective minima compared. The design variables that produced that global minimum are then taken as the optimal design variables. In the current study however, this was not done, because the solution space being considered is discrete.

This is so because we want to be able to validate the method by running all the combinations, something impossible for a continuous space as the combinations are infinite.
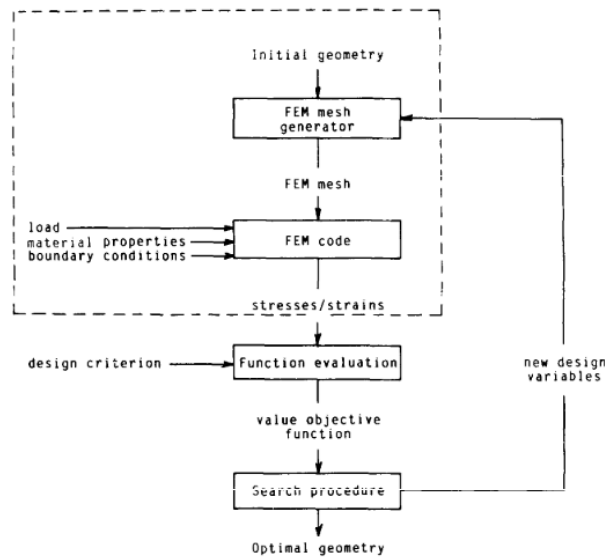

Figure 54: The schematic for the iterative algorithm used by R. Huiskes and R. Boeklagen (Huiskes and Boeklagen, 1989) when optimising the shape of a hip prosthesis.

Instead, MATLAB's genetic algorithm was used (Documentation, 2012), which is based on a natural selection process that mimics biological evolution. It starts with an initial generation of candidate solutions, for which the objective function is calculated. Afterwards, through processes such as selection, crossover and mutation, subsequent generations of candidate solutions are generated (this gives the direction). By using a 'Fitness function value', the respective candidates are evaluated. Ultimately, it leads to a global minimum by natural selection. A figure showing how the process for a 2D space would work is shown below.
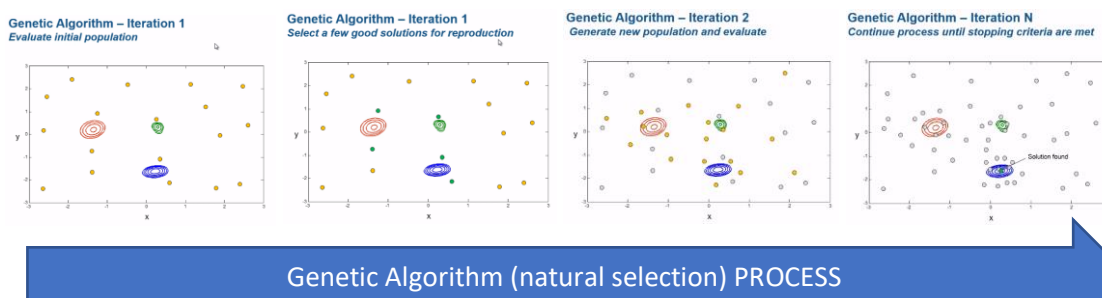
Figure 55: computation process of the genetic algorithm, for a 2D solution space. The figures were taken from MATLAB's documentation (Documentation, 2012).

Like with any optimisation algorithm, lower and upped bounds had to be supplied. These were 1 and 1001 respectively, the minimum and maximum row indices of the vector that contains all the allowed material combinations (with the 20 implant sections as its columns). In order to incorporate the Interfragmentary strain (IFS) constraint described previously (maximum IFS should not exceed 1.093%), the objective function was modified as shown in the figure below. Any combination for which the maximum IFS was higher than 1.093% was neglected using an if-statement, and only the rest were considered for the minimisation. The function shown below as 'VM_max(E(I,11:20))' runs the model with screws in ABAQUS by taking as inputs the young's modulus values of the 10 mirrored segments (ABAQUS was ran from MATLAB by accessing its input and output files) contained within the 'E' vector, in the relevant stored row 'I'. It produces as an output the maximum Von Mises stress in the bone

('S'). The 'IFS_max(E(I,11:20))' runs the model with a fracture with the same inputs as 'VM_max(E(I,11:20))' but the output in this case is the maximum Interfragmentary Strain in the element described in an earlier section. The genetic optimiser then found the global minimum in this constrained space, producing the optimal row of 'E' values, 'I'. To validate the results, the 1001 models were ran (this took about 20 hours) and the results were plotted, allowing us to find the global minimum graphically and compare it with the result obtained with MATLAB's genetic optimiser. Below is an image showing how the MATLAB function was used.

```
Opt=ga(@MaxVonMises_ConstMaxIFS,1,[],[],[],[],...
    1,1001,[],1);

%Function for calculating the constrained maximum Von Mises Stress
function S=MaxVonMises_ConstMaxIFS(I)
global VM_max IFS_max %The functions that call ABAQUS
IFS_Max=IFS_max(E_todo(I,11:20));%Calculating the max IFS in ABAQUS
if IFS_Max>1.093 || IFS_Max<0.894%Is the max IFS within the accepted values?
    S=NaN;
else
    S=VM_max(E_todo(I,11:20));%Calculating the max VM stress in ABAQUS
                             %for the combinations that have an acceptable
                             %max IFS
end
end
```

Figure 56: (below) MATLAB function used as the objective function (or fitness function) of the genetic algorithm. As described above, IFS_max() and VM_max() are functions which were prepared to write input into ABAQUS files, run the FE model and then extract the desired output value. (above) call to the genetic optimiser of MATLAB by providing it with the required inputs.

5.4.3.2   Results

The genetic algorithm of MATLAB solved the problem in a total of 65 iterations (72 minutes), 6.5% of the maximum number of models. The initial optimal solution found was the 835th row, which is equivalent to an E vector [83.25,83.25,56.5,56.5,56.5,29.75,29.75,29.75,29.75,29.75], equivalent to the plate's young's modulus distribution shown below. The global minimum was a Maximum Von Mises stress of 122.4 MPa.
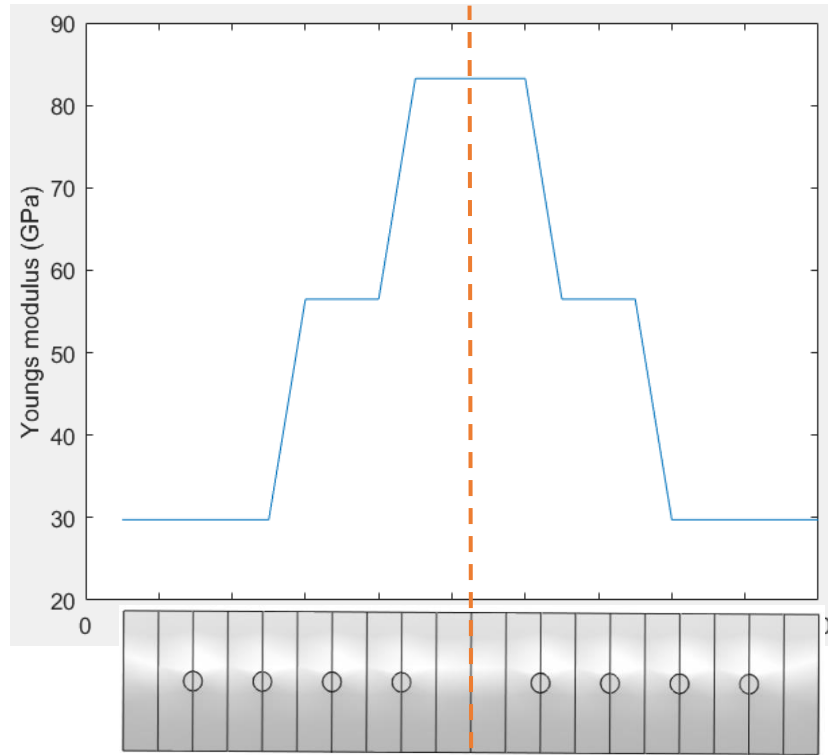
Figure 57: Optimal young's modulus distribution along the implant's length, as computed by the genetic algorithm. Starting at the centre and extending towards the outer most segment (on only one half), the relevant values are *[83.25,83.25,56.5,56.5,56.5,29.75,29.75,29.75,29.75,29.75].*

As explained in the methodology, this result was validated by calculating the entire solution space and finding the optimum graphically. The plot of the maximum Interfragmentary strain is shown below. The models that produced an Interfragmentary strain higher than 1.093% were all from the 1st until the 734th. These models were excluded from the visual search in the Maximum Von Mises stress plot shown below and the constrained global minimum was found to be 122.4 MPa as shown, the 835th model. This proves that the genetic algorithm did in fact find the global minimum.
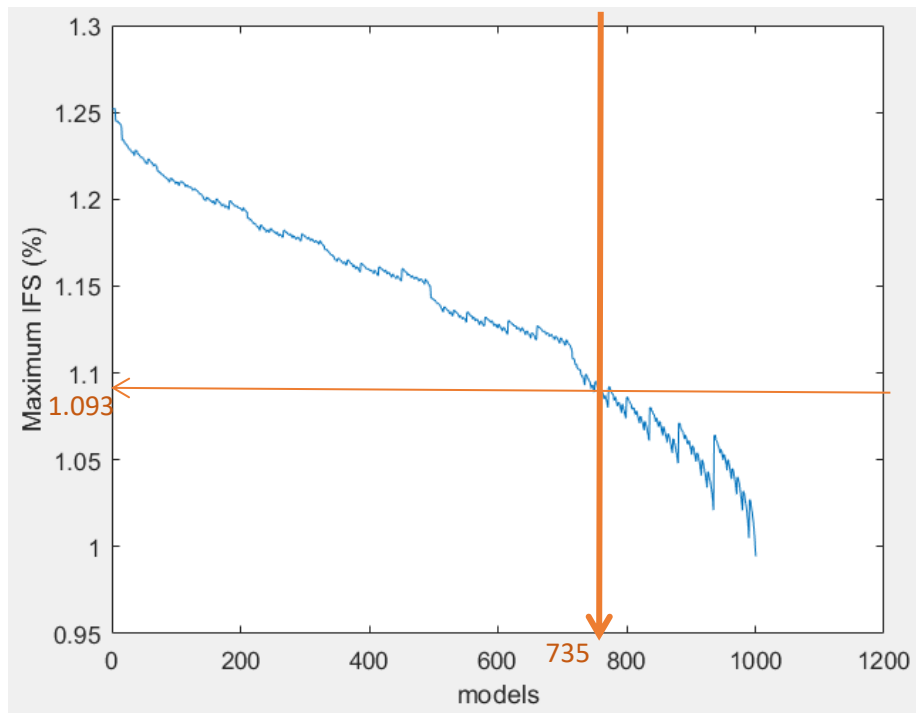
Figure 58: Maximum Interfragmentary strain of each of the 1001 models that passed the initial test. The horizontal orange curve shows the 1st interfragmentary strain value of all the models (from left to right) which meets the defined stability criterium. Thus, all models from the 735th on to the right are allowed and all those to the left of this model are not allowed (as seen more clearly below).
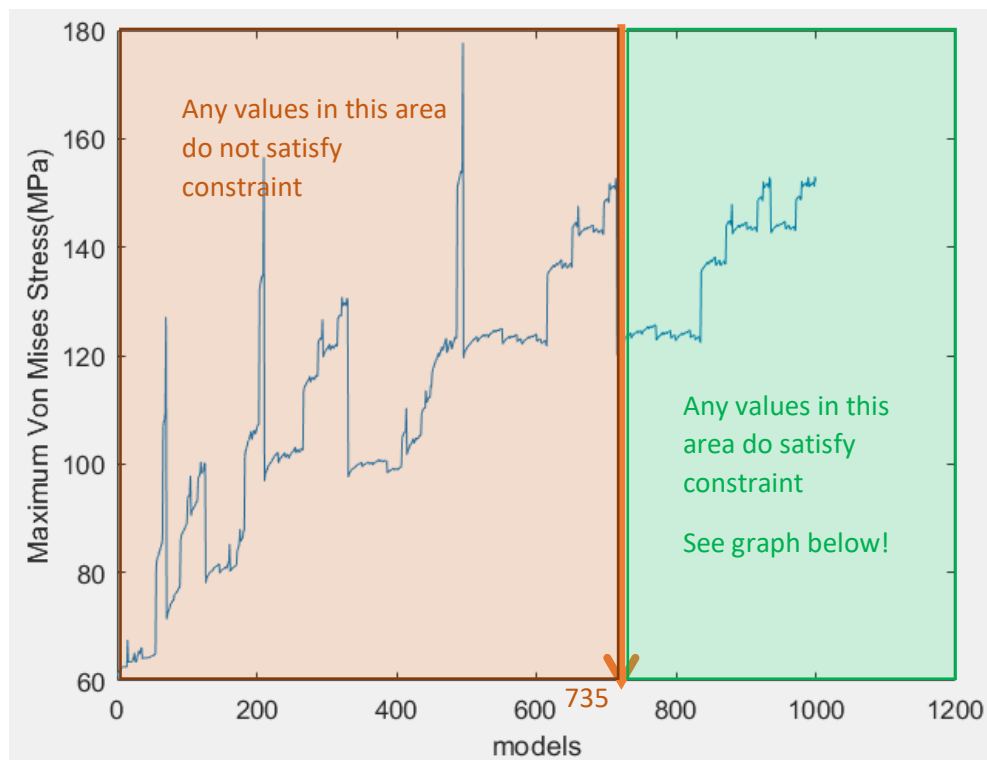
Figure 59: Maximum Von Mises Stress of all the 1001 models ran. By using the index of the first model that allowed for proper healing (735), it was possible to define the range of Von Mises Stress values which are allowed (green) and the range of values that is not allowed (red).
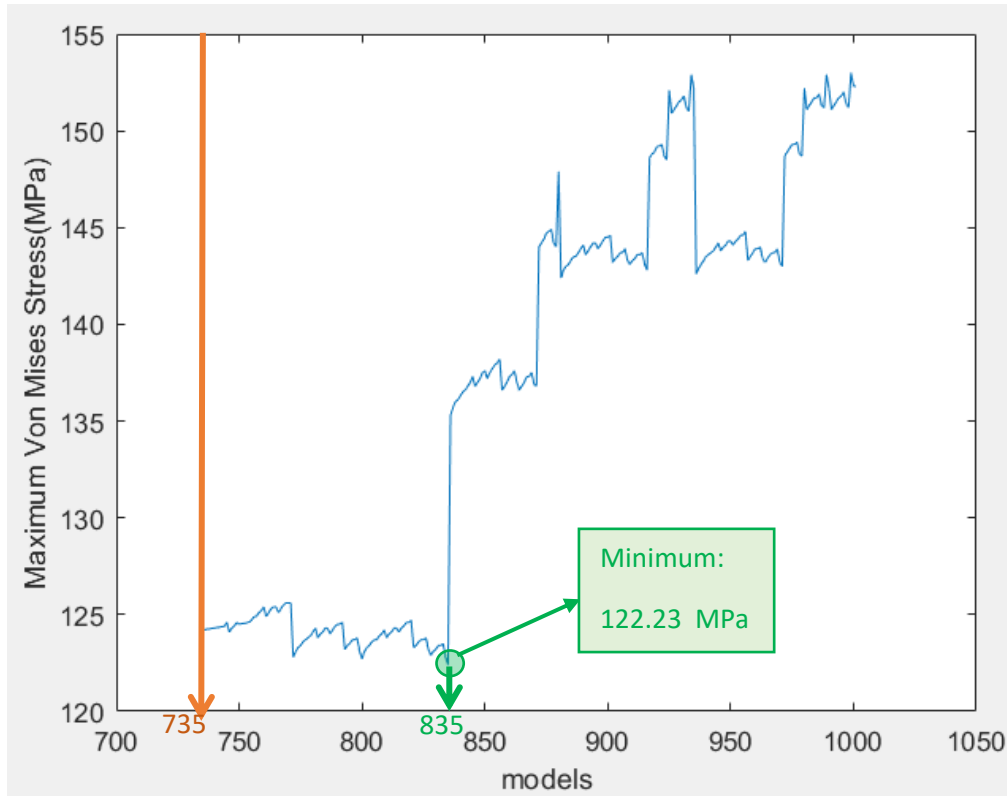
Figure 60: These are only the Von Mises Stress values of the models which met the first criteria and furthermore also allow for appropriate healing according to the IFS criterium. Therefore this is the constrained solution space and the global minimum can be easily found by taking the minimum of this vector which happens to be the 754th model with a Von Mises Stress of 75.92MPa and a young's modulus distribution shown earlier.

However, given that the minimum found is a lot higher than the minimum found with the 2-Dimensional optimisation, it was decided to modify the strategy. The reason why the minimum found is so high is because of the low number of intervals used (5). In the 2D optimisation, there are only two possible variables but each has 10 intervals. In other words, the step size for the 10D optimization was 11.89 GPa while that for the 10D optimization was 26.75 GPa. In order to reduce the step size for the 10D optimization, the result of the 2D optimization was now used, such that the outer 6 segments at either side were always kept at 3GPa and the inner segments could only vary between 62.4 and 74.3 GPa. The solution space then becomes 4-dimensional hence one can afford to use 10 intervals. Thus the step-size is now 2.22 GPa. The code used to achieve this is shown below:

```
%These are all the 10 dimensions (each of 5 steps)
for i10=3; for i9=3
for i8=3;for i7=3
for i6=3;for i5=3 %The outer 6 segments are now 3GPa
for i4=E_chh;for i3=E_chh
for i2=E_chh;for i1=E_chh
n=n+1;%count all simulations
E=[i1,i2,i3,i4,i5,i6,...
    i7,i8,i9];%the 10 mirrored material section variables
E=[fliplr(E),E];%Mirroring the material properties

for ii=1:5
    if E(ii)<=E(ii+1)
        g(ii)=1;%Inclusion criterium
    else
        g(ii)=0;%Exclusion criterium
    end
end

if sum(g)==5 %Include this
m=m+1; %Count combinations that meet criteria
E_todo(m,:)=E;%Store them in a matrix
end

end;end;end;end;end;end;
end;end;
end;end
```

Figure 61: Adapted code for 10D optimization. The ends are now constrained to stay at 3GPa and the middle sections are constrained to vary only between 60 and 80GPa in 10 steps.

The optimal young's modulus distribution was then found to be the one shown below. The Maximum Von Mises Stress now found was 71.68 MPa.
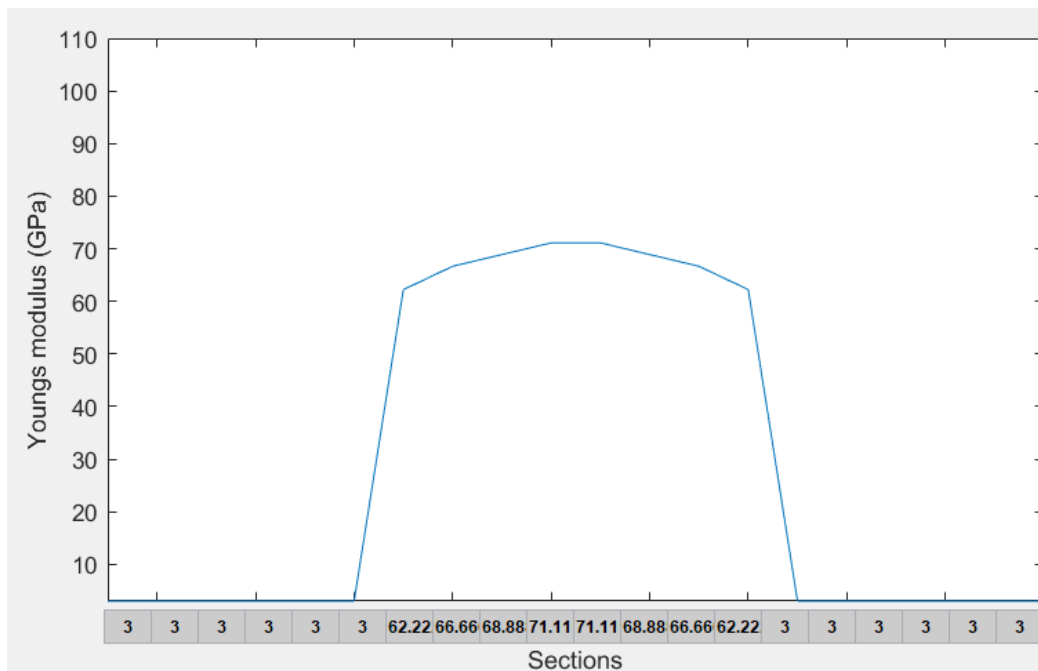
Figure 62: Optimal young's modulus distribution found with the new strategy. Note that the rectangles on the x-axis represent that young's modulus at the respective sections in GPa

With the purpose of comparing the result of the 2D optimisation to that of the 10D optimization, the graph below is presented. The optimal distributions found with either optimisation were plotted below. For reference, the young's modulus distribution of a plate made fully of titanium was also plotted. It appears that the optimal distribution found with the 2D process (10 intervals) has almost no difference to that found with the refined 10D approach (10 intervals). However, looking further

down at the bar plot showing the maximum stress, it can be appreciated that the maximum stress found with the 10D optimisation is in fact better.
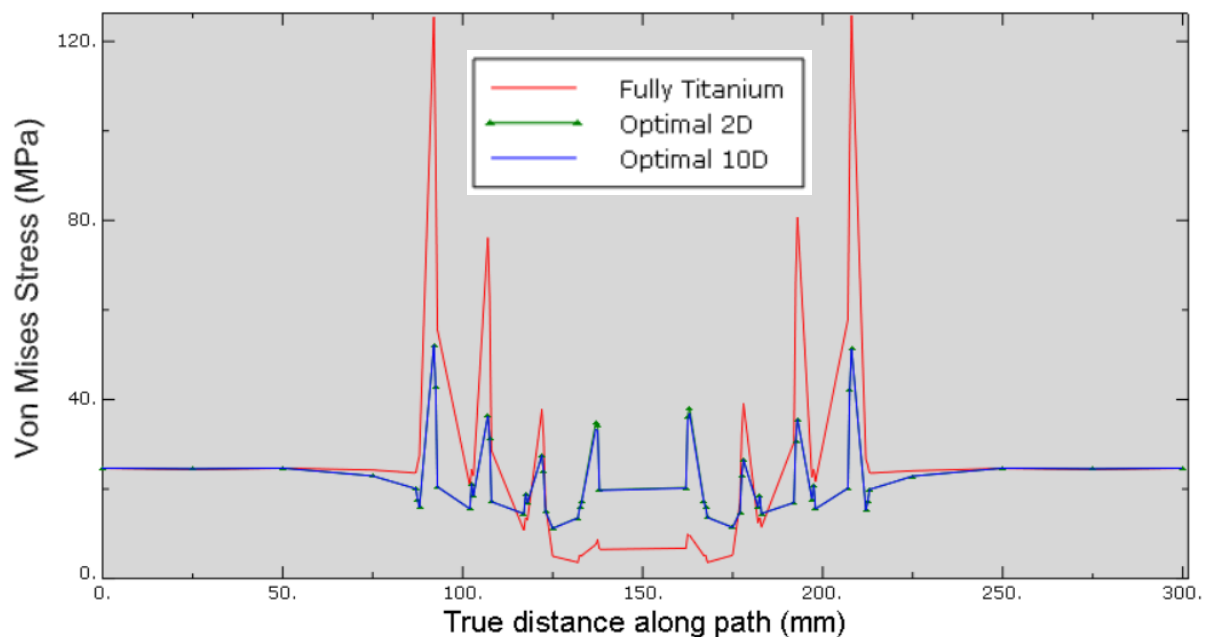
Figure 63: Von Mises stress distributions for a) titanium implant, b) optimised implant through the 2D optimization of 10 intervals and c) optimized implant through the 10D optimisation of 5 intervals.
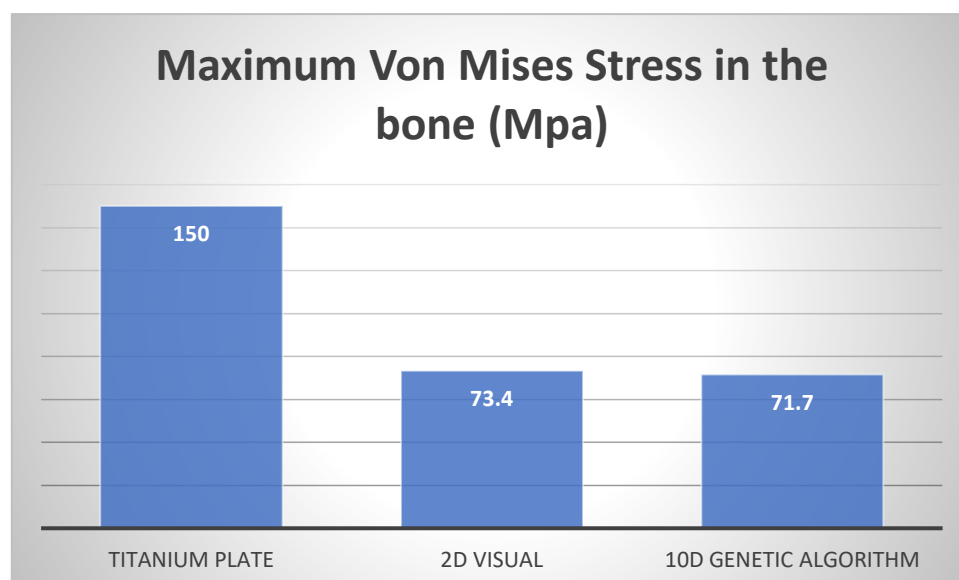
Figure 64: Bar plot comparison of the different optimization techniques used as well as comparing them to the maximum stress of the titanium plate. Values are in MPa.

5.4.4   Using Abaqus's Topology Optimization

Abaqus has its own optimization module. Detailed information about how it works can be found in the ABAQUS guide. However, it does not seem possible to define the constraint as the output of a second model if one uses this module. Therefore, a different constraint must be used. In the optimization study of Samiezadeh et al. (Samiezadeh, Tavakkoli and Fawaz, 2015) the rigidity is used as a constraint, and in the also discussed mathematical optimization of a hip prosthesis (Huiskes and Boeklagen, 1989) the Strain Energy Density is used as the objective function. Moreover, it was also

described in the healing constraint selection section of the report that the stiffness of the construct may be used as the criterion for healing of the fracture gap (Steiner *et al.*, 2014). The rigidity is given by the product of the young's modulus E and the Inertia I. The ABAQUS variable that seems to relate best to the rigidity is the total strain energy of the construct (ALLSE) which I referred to here as TSE. The general equation for the TSE, where M is the applied moment, is as follows (*CODE COGS*, 2004):

$$TSE = \int \frac{M^2}{2EI} dx$$

In order to visualize how this constraint compares to the previously used Interfragmentary strain (IFS) constraint, the following comparison plot was made. It can be observed that the relationship between these two variables and the young's modulus of the implant is in fact very similar. Therefore it is suitable to use this as the constraint. Using the same assumption about appropriate healing occurring if the variable's magnitude does not exceed 110% of that achieved with a titanium plate (E=110GPa) and does not fall below 90% of that either; the new criterion is defined as follows (values in Nm):

$$684.20 \leq TSE \leq 836.24$$
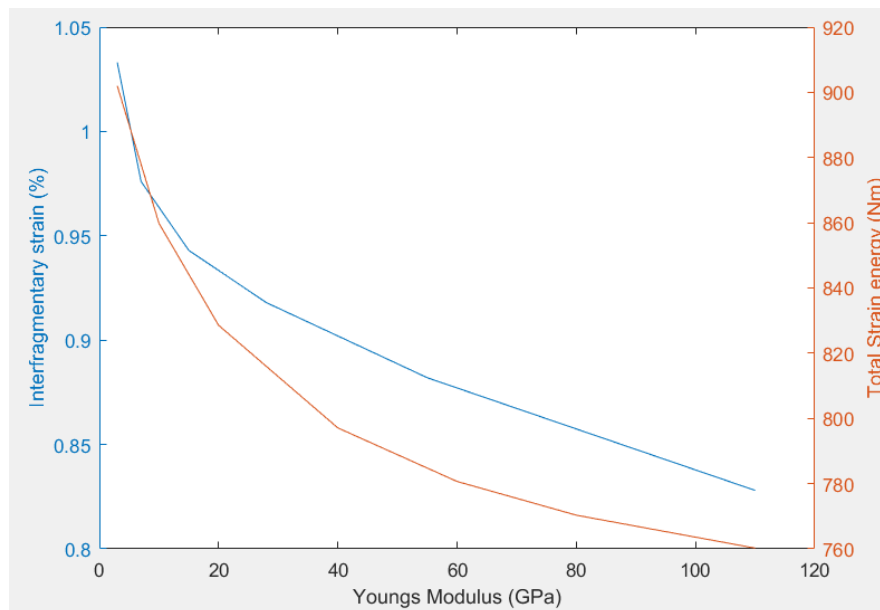
Figure 65: Plot of Interfragmentary strain and Total strain energy against the young's modulus.

With the objective function again being the Maximum von mises stress, the topology optimization was carried out. The topology optimization of ABAQUS optimizes the density of the elements in order to minimize the chosen objective function, while satisfying the given constraints. The optimizer ran a total of 26 iterations as shown below, converging to a minimum of 92.20MPa which was achieved with the density distribution shown below.
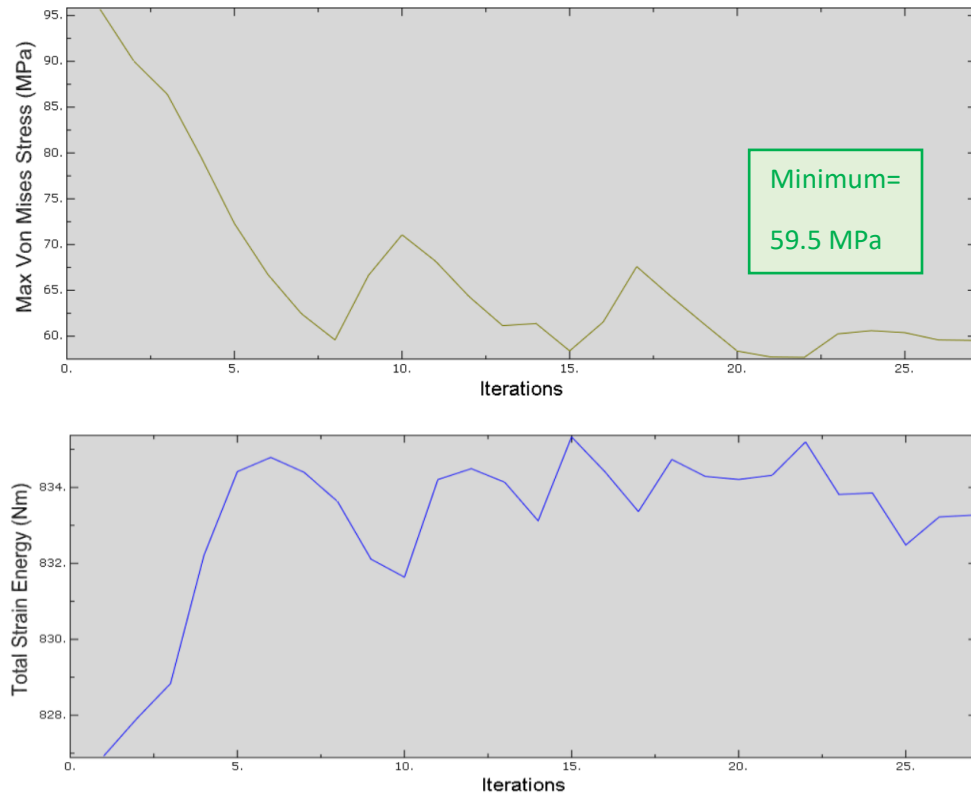
Figure 66: Above: Plot of the maximum von mises stress for the 26 iterations of the ABAQUS optimization. Below: Plot of the total strain energy for the 26 iterations.

It should firstly be noted that the optimization was not done only along the length of the implant this time but rather for all elements. The most surprising thing about this result can be seen by looking at the right side of the figure, where it can be observed that the lower half of the implant (along the thickness direction) did not vary much at all, its density was kept at around 100% (as explained below, the density is given as a ratio of the initial value to the assigned value, hence 1 is equivalent to 100%). Furthermore, it can be seen that along the length, on the left side the density was decreased very much at this edge, much like in the previous optimization. However, on the right side the result is not as expected. The density distribution was expected to be symmetric about the longitudinal centre because of the symmetry of the stress distribution.
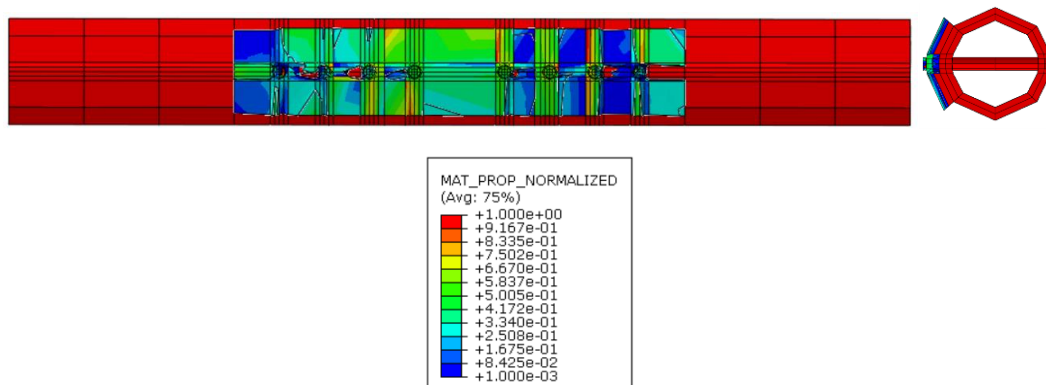
Figure 67: Optimal density distribution of the implant. The density is given in the ratio of the initial density to the current density. 1 can be seen as 100% of the initial density. If the material has been removed it means the section reached the minimal density that ABAQUS takes as zero.

The following table compares the minimum value of the peak Von Mises Stress found by the topology optimization routine of ABAQUS to that found on the 2D optimization and that found in the 10D optimization. It can be seen that the lowest minimum was found with the ABAQUS topology optimisation.

Table 19: Comparison of minimum results

Case/Optimization	Maximum Von Mises Stress in the bone (Mpa)	Percentage of max with Titanium (%)	Models required
Titanium plate	150.00	-	-
2D visual	73.40	48.93	100
10D genetic algorithm	71.68	47.80	65
ABAQUS	59.50	39.67	26

6   Discussion:

6.1   Overall Strategy:

How much of this strategy was implemented?

The patient-specific analysis described in the 'Overall strategy section' was not carried out in this report, however, the goal is to ultimately adapt an optimization such as the one presented, to be patient-specific by using the proposed strategy. The available techniques to actually manufacture the implant though additive manufacturing were also not the focus of the current study, but a future study should focus on this, given that the performance of the implant will most probably also be affected by manufacturing parameters.

A thorough review of patient-specific 3D printing in medicine was done by D. Akilbekova and D. Mektepbayeva (Kyobula *et al.*, 2017). They concluded, amongst other things, that Selective Laser Sintering (SLS), inkjet printing and micro extrusion printing are the most common 3D printing techniques used for medical applications. Moreover, post-processing of the results collected in the review of P. Tack et al. (Tack *et al.*, 2016) about the influence that 3D printing has had in the medical setting proved that 96% of the selected articles which dealt with 3D printed implants, reported an improved clinical outcome. This review also concluded that 3D printing was more expensive than traditional manufacturing.

Regarding the heterogeneous composition of the proposed implant, a recent paper summarizes the latest developments in this area (Udupa, Rao and Gangadharan, 2014). One of the most promising processes to achieve a functionally graded parts through additive manufacturing (FGAM) appears to be that of varying the density segmentally as described in the image below. However, there are other ways to achieve this as described in the article. Amongst other things, the article concluded that "the potential of FGAM for future manufacturing is limitless".
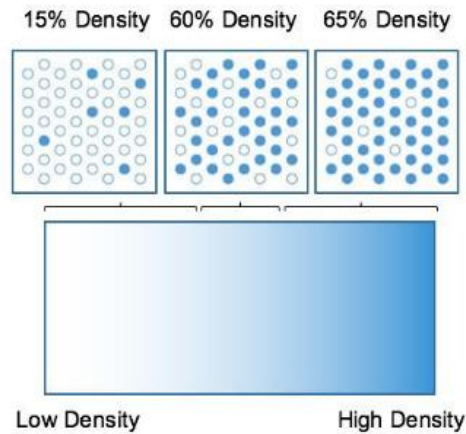
Figure 68: Image taken from (Udupa, Rao and Gangadharan, 2014) showing how the density can be altered to manufacture a functionally graded part.

The rest of the steps described in the overall strategy section were carried out in this study (CAD geometry, Finite Element Model and optimization).

6.2   Finite Element Model creation:

Why was the model generally simplified?

As described, the idea was to start simple, develop a thorough methodology, and in future studies increase the complexity, such that it is possible to analyse how different parameters affect the performance of the implant as well as the efficiency of the methodology. However, a parametric study was also carried out already to understand how some parameters affect the performance of the implant. Moreover, a simplified model allows for a quicker optimization, which as shown on the last optimization section, was crucial in order to be able to validate the optimization process.

How is the simplicity of the geometry expected to affect the results?

Making the geometry of the bone be a perfect tube has been done in validated Finite Element studies and it did not affect the performance of the implant much (Oh *et al.*, 2009)(Shirurkar, Tamboli and Jagtap, 2017). The same was the case for making the geometry of the screws be perfect cylinders, in fact most (71%) validated Finite Element studies of Fracture fixation plates reviewed recently (Lehder, 2018) were found to make this assumption. This review also related the simplicity of the Finite Element modelling choices to the validation accuracy achieved, and it was further found that simplifying the geometry of the plate to a plate that can be defined with three parameters (apart from the holes) also does not influence the accuracy significantly. Overall, no geometry simplification was found to affect the accuracy significantly according to this review (Lehder, 2018). A transverse fracture gap such as the one used was also used by 53% of the reviewed studies and 50% of all the studies used a gap between 1 and 4 mm.

How is the simplicity of the material model expected to affect the results?

Bone has been shown to experience a viscoelastic behaviour (Ziheng Wu, Timothy C. Ovaert, 2013). In the latter study, the viscoelastic properties of bone were measured and amongst their findings was the curve shown below. If bone was linearly elastic, the displacement would increase linearly with the increase in loading, and when the load were released at the same rate, the displacement would be reduced at the same rate until zero. However, none of these things happen as is clearly observed, and especially the elasticity assumption seems to be very ambitious. Nevertheless, the average accuracy of the validated Finite Element studies of fracture fixation was 89%, and all 21 studies used a linear

elastic material model for the bone, therefore it was still deemed acceptable to use a linear elastic material model (Lehder, 2018).
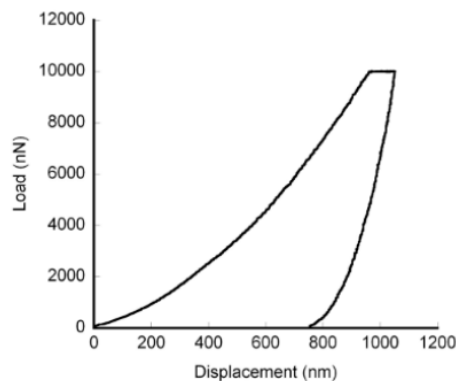

Figure 69: Load-displacement curve for cortical bone. Taken from (Ziheng Wu, Timothy C. Ovaert, 2013).

About 30% of the mass of bone is type I collagen (Ziheng Wu, Timothy C. Ovaert, 2013). Collagen is an organized fibrous matrix that is much stronger along the fibre direction than perpendicular to them (Ziheng Wu, Timothy C. Ovaert, 2013). Therefore, its mechanical properties are bound to be quite different along the longitudinal direction than along the radial directions. Hence why cortical bone is often assumed to be transversely isotropic (Ferguson, Wyss and Pichora, 1996). C. Albert et al. (Ferguson, Wyss and Pichora, 1996) measured the anisotropic properties of bone and post-processing of these results show that bone was 62% less stiff in the transverse direction than in the longitudinal direction. However, 86% of the reviewed validated studies (Lehder, 2018) were found to use a fully isotropic model without significant effects on the validation accuracy. Thus, once again, although in theory this is a bold assumption, in practice, when considering all other modelling decisions too, it appears to be a reasonable one.

When it comes to the homogeneity, all but one of the 21 reviewed articles (Lehder, 2018) modelled the bone as homogeneous and the accuracy was not seen to be significantly affected by this choice. This is in disagreement with the conclusion drawn by A. Synek et al. (Synek *et al.*, 2015) on his study about the influence of bone homogeneity and anisotropy on the accuracy of the results. They concluded that whilst anisotropy can be safely assumed, homogeneity can lead to significant errors. Nevertheless, given that 20 validated studies used a homogeneous bone model and still obtained a good validation accuracy, the homogeneity assumption is also justified.

What about the loading assumptions?

Most of the reviewed studies (62%) (Lehder, 2018) used a relatively simple loading scenario where only 1-dimensional or 2-dimensional loading was considered. This also did not seem to affect the results significantly. Moreover, as discussed, using pure bending is well justified and this has also been used by other studies (Claes, 2011).

What about the contact assumptions?

Ignoring the Screw-Plate contact and thus assuming these surfaces to be fully merged, was done by 85% of the reviewed studies (Lehder, 2018) without major effects on the validation accuracy. Hence it is justifiable to do it here. A Locking Compression Plate (LCP) usually has dynamic compression screws as well as threaded or 'locked' screws as shown below. Thus it seems reasonable to suggest that when a locked screw is modelled, a Tie may be assumed, but when a dynamic screw is modelled

a more realistic contact setting, taking into account friction effects seems more appropriate. This was not done in the current study but is suggested as a modification to a future study.
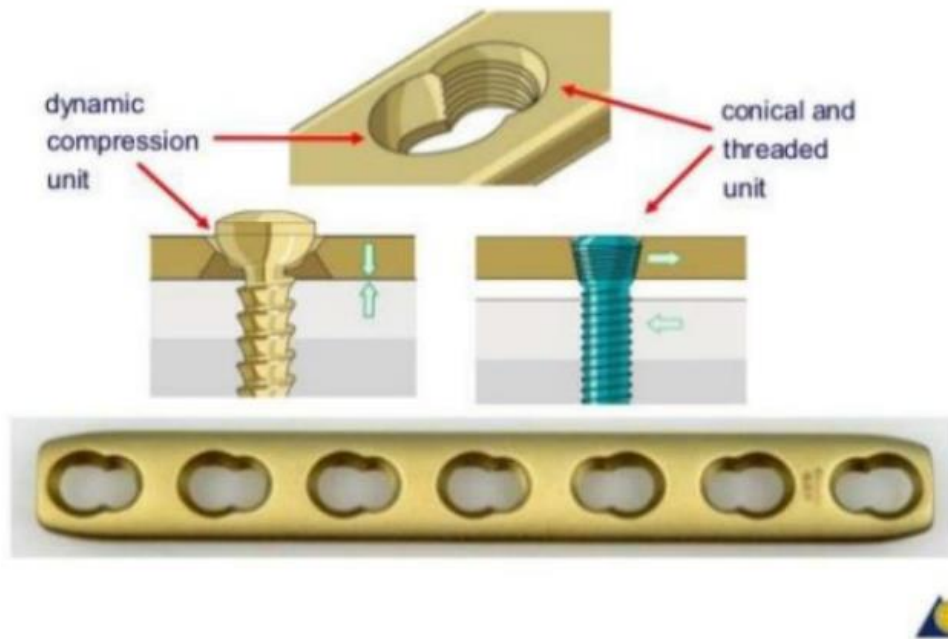

Figure 70: Compression and locked screw types. Images taken from the AO website.

The contact between the bone and the plate was not modelled because it was assumed that these two parts never come into contact. This was also assumed in another study titled "Validated computational framework for efficient systematic evaluation of osteoporotic fracture fixation in the proximal humerus" (Varga *et al.*, 2018) and it caused no significant effects in the validation accuracy. The reason this assumption was made in the current study is because in reality a contact between the plate and the bone would greatly affect the results, but then we would not know whether the change in the output variable is because of the change in the respective input parameter or because of a contact between the bone and the plate. This is however something that should be taken into account in a future study.

Regarding the contact between the bone and the screw, 70% of the reviewed studies modelled this as a Tie (Lehder, 2018). Overall, these studies found that modelling this contact as a Tie did not affect the validation accuracy significantly and the computation time was much lower. As seen in the contact settings comparison study presented in this report however, using a Tie constraint for these surfaces greatly affects the contact pressure results and does not improve the simulation time significantly. Given that so many studies have assumed a Tie and this did not affect the validation accuracy of the model, it is clearly justifiable to use a frictionless contact. For details about what a frictionless contact is in ABAQUS see their guide (Dassault Systèmes Simulia, Fallis and Techniques, 2013).

The 'Tied model' also briefly discussed in the contact settings comparison section, is a much simpler model when it comes to the meshing process as the geometry definition. Given that it provides us with stress distributions that follow the same trend as that of a model with screws, it may be used for a study that is concerned only with the analysis of the stress peaks at the edges of the plate. However, given that in this study the interfragmentary strain is also of great importance, it was deemed more accurate to use a model with screws. Moreover, the advantage that the 'Tied model' should have regarding the computation time was not clear from the presented comparison study (a study that takes into account the necessary number of elements for each model might be more relevant for this).

The literature review mentioned (Lehder, 2018) also included some results regarding the mesh convergence criteria used, it showed that most studies used a stress parameter to define the convergence criterion. M. Ni et al. (Ni *et al.*, 2016) for instance, carried out a mesh convergence test by ensuring that the deviations of the maximum Von Mises stress were lower than 2%. This is generally how a mesh convergence study is carried out, a sort of optimization of the number of elements. However, as explained in the current study, this is only relevant if exact stress values are desired. The purpose here is merely to compare the results of various simulations, thus it is only important that the overall effects of the various parameters are well represented with the output variables, as it is the case even with a coarse mesh (shown in the figure of the mesh refinement study). Other studies have also avoided doing such a mesh refinement study for simple geometries (Huiskes and Boeklagen, 1989). This mesh refinement study might seem counterintuitive but it is justifiable for the purpose of this report.

6.3   Parametric study:
Was the material really the most influential parameter for minimising the peak stresses?

As explained, a parametric study was carried out comparing the influence of various parameters on the risk of fracture as well as the interfragmentary strain, namely: material, thickness, number of screws and fillet radius. A special purpose of this section was to find out whether the material properties of the plate are the most influential to the peak stresses found at the edges of the plate. The results proved that this was in fact not the case, the material had 27.4% (second most influential out of the four parameters) of the influence, whilst the parameter with the highest influence was the thickness of the plate with an influence of 31.6%.

Why is the thickness the most influential parameter?

The stress peaks seen in this report have been previously reported in relation to total hip arthroplasty, in a chapter titled "Stress Patterns, Failure Modes and Bone Remodelling" (Huiskes, 1988). In the latter study it is reported that the stress peaks are dependent on the stiffness (as well as stem taper and cement-layer thickness for the intramedullary stem, but these do not exist in the fracture fixation plate), which is roughly equal to the product of the young's modulus multiplied by the inertia.

The figure of a study that was done using the 'Tied model' is presented below. It also shows that the Inertia at the section where the plate is, increases dramatically because of the added inertia of the plate, I2. This inertia increases proportional with h^3 where h is the thickness of the plate. Therefore it makes sense that the thickness of the plate has a larger influence in the peak stresses. A study where the plate thickness would be segmentally modified would in fact be very interesting, or perhaps one where both the thickness and the material distributions are optimized simultaneously.

Another aspect that both the figure below as well as the results of the parametric analysis show, is the fact that reducing the young's modulus does in fact reduce the peak stresses (more clear from the results of the model with screws as well as the single value plots) and it does so exponentially, such that decreasing the young's modulus from 15 to 5GPa for instance has a much larger influence in reducing the maximum stress than going from 110 to 100 GPa. Moreover, the figures also show that the 'stress shielding' phenomenon is not only related to the difference in material properties between the parts but also to the change in geometry at the bone-implant section. This and other matters are also demonstrated by R. Huiskes through basic mechanical considerations (Huiskes, 1979) for a simplified model of intramedullary fixation structures (The main effects for the peak stresses also apply here).

Stress Shielding:

$$\sigma_x(y) = \frac{M_b(x) * y}{I}$$

$$I_1 = \frac{\pi}{4} * (r_2^4 - r_1^4)$$

$$I_2 = \frac{bh^3}{12}$$

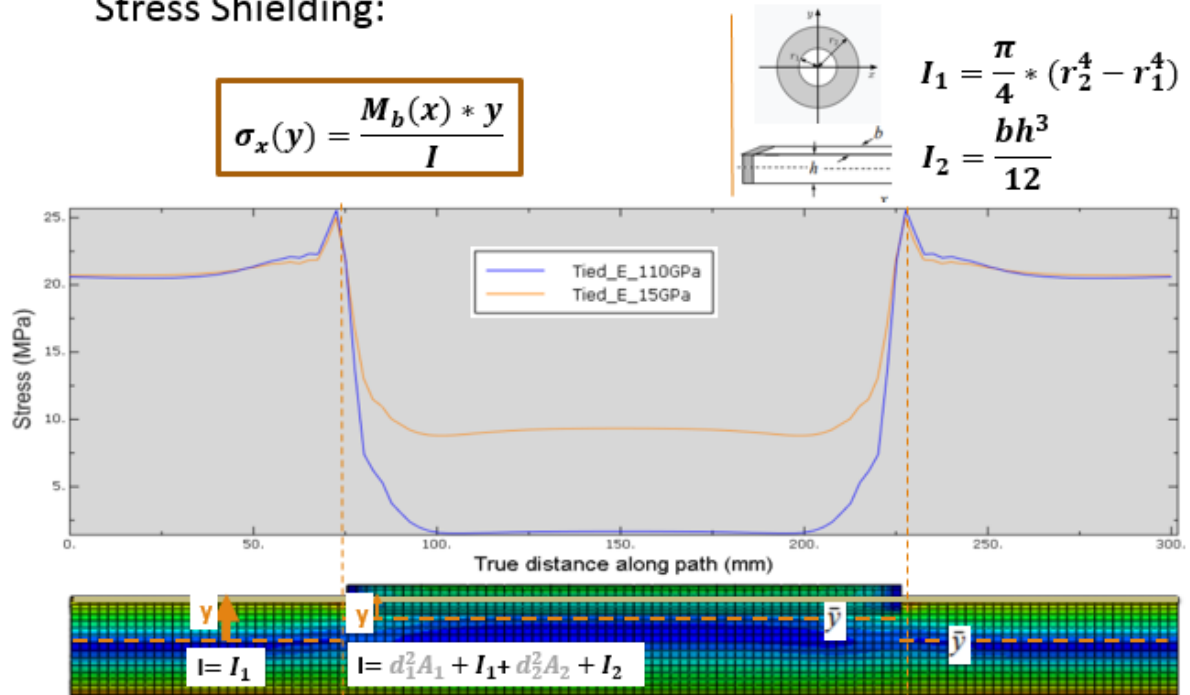$$I = I_1 \qquad I = d_1^2 A_1 + I_1 + d_2^2 A_2 + I_2$$

Figure 71: Von Mises Stress distribution along the path shown with a green thick line. The figure also shows the Inertias of the bone and plate respectively on the top right corner and the stress at any point along the length y. Moreover it shows how the Inertia of the middle section (with plate) is higher than the Inertia at the sections were there is no plate. The model is the 'Tied model'.

The parameter that most affected the interfragmentary strain (and thus the healing outcome) were the number of screws (32%) followed by the edge fillet radius (26.4%). This is quite the opposite of the results seen for the maximum Von Mises Stress effect. In an article written about the risk of fracture of long bones with locking plates (Nassiri, Macdonald and O 'byrne, 2013) the use of different number of screws was also analysed. In that study the load used was a force along the longitudinal axis of the bone rather than a moment, but otherwise the conditions were very similar to this study, using a simple tube to represent the bone, a simplified plate, as well as simple cylinders to represent the screws. They found that by omitting the two inner most screws the construct became more flexible in compression by about 39%, they found this was the most influential parameter. Thus agreeing with the results of the current study. The recommendation, validated by clinical studies, is that there are a minimum of three screws on either bone fragment.

The mentioned article (Nassiri, Macdonald and O 'byrne, 2013) also investigated the effect that other parameters have on the interfragmentary strain. They found that the plate length is of great importance too, a long plate causes a more flexible fixation. They also investigated the variation in the distance between the plate and the bone and found that by increasing this distance from 1 to 5mm the axial stiffness decreased by 27%. However, this was found to also significantly increase the risk of fracture and hence they recommend a distance of 2mm between the plate and the bone. The fracture angle was also analysed and it was observed that increasing it from 0 degrees to 5 degrees in the lateral axis, the construct stability decreased by 19%.

6.4   Optimisation:

6.4.1   Output variables selection and young's modulus distribution along plate:
Was the Von Mises Stress really the best Objective function to use?

As explained, the maximum Von Mises Stress was chosen to be the Objective function because it takes into consideration all other shear and normal stress values and hence can be considered as a good representation of the overall stress state of the bone at any location. The presented graph supports this argument. Four other fracture fixation optimisation processes through the use of the Finite Element method were reviewed. One used the axial stiffness as the objective function (Samiezadeh, Tavakkoli and Fawaz, 2015) and aimed to optimise the organization of plies in a composite plate. Another one used the signal-to-noise ratio of the factor of safety in order to optimise the combination of four parameters of the fixation plate (material, thickness, number of screws and screw angle). The third used the bending stiffness as an objective function (Chakladar, Harper and Parsons, 2016) in order to optimize the width/thickness ratio of the plate.

The last one used the strain-energy density (SED) (Huiskes and Boeklagen, 1989) as the objective function. This can be thought of as the area under a graph of stress against strain, thus for a linear relationship, it is equal to half the product of stress and strain. Although these represent local tensors describing the entire local stress and strain states as explained by R. Huiskes, H. Weinans et al. (Huiskes *et al.*, 1987). Hence, this objective function could be better for some cases where both the strain and the stress should be taken into consideration (although if one is assuming a linear relationship between them, calculating one is enough to predict the other by knowing the young's modulus E).

Was the Interfragmentary Strain (IFS) the best measure to predict the healing outcome?

As mentioned already, L. Claes et al. (Claes and Heigele, 1999) used the interfragmentary strain as well as the hydrostatic pressure to determine ranges for which intramembranous ossification, endochondral ossification or connective tissue would be stimulated. Thus, for a more thorough study, both the strain as well as the hydrostatic pressure should be taken into account. Although the hydrostatic pressure and the interfragmentary strain are related, in the article they make a distinction to argue that while compressive hydrostatic pressure is beneficial, tensile would not be. On the other hand, as can be seen on the presented figure, it is suggested that for the strain it is not important whether it is positive or negative, it stimulates the same reaction. Furthermore they specify that "in this special formulation the displacement and hydrostatic pressure, normally computed from the displacement field, are calculated by separate interpolations using ANSYS" (Claes and Heigele, 1999). Axial stiffness may also be used as a criterium as explained in the methodology.

In the study by E. Lehder (Lehder, 2018) it was shown that out of the 21 reviewed articles about the validated finite element analysis of a fracture fixation construct, 14 used the Von Mises stress as the criterion for failure and 7 used the Interfragmentary Motion (IFM) as a criterion for healing outcome.

Is it theoretically possible to control the distribution of material properties in the plate by defining the properties of each element differently?

As explained in the relevant section, if one attempts to control the properties of each element of the plate individually, the number of possible combinations would be immense (given that a moderate amount of elements is needed for a model which is accurate enough). However, when using a gradient-based optimization technique a continuous space is usually defined such that the number of possible combinations is not really relevant because only the range and the function defining the space in that range is required. Such a technique is used in the paper by R. Huiskes et al. (Huiskes and Boeklagen, 1989) and this is how one can get around the dimensionality issue of the solution space when using such a fine young's modulus distribution. In future studies it is suggested that this technique be used in order to optimize the implant.

6.4.2   Finding the optimal distribution

What conclusions can be drawn from the 2D optimisation?

Such an optimization as the one carried out here by dividing the plate along its length into three sections has not been done by any other study, to our knowledge. It is very informative as it shows us how both the Von Mises Stress as well as the IFS react to varying the material properties of the inside and outside sections of the plate. This simple optimisation proves that the main idea proposed in the hypothesis is correct: By modifying the young's modulus distribution along the length of the implant, the peak stresses can be minimised while ensuring that the IFS is acceptable for proper healing. The plot of Von Mises Stress along the length of the bone which compares the young's modulus distribution of a fully titanium plate (which yielded the highest probability of bone failure) to the distribution of the optimal plate according to this 2D optimisation, shows quite nicely again how the stress peaks at the outer-most screws are reduced with the optimal combination (very low young's modulus at the ends of 3 GPa and a relatively high inner young's modulus of 74.7 GPa).

This plot also shows that as the young's modulus at the edges is reduced, the outer peaks are also reduced, but the inner peaks are increased (not enough yet to become higher than the outer ones). The intuition that helps explain this is that reducing the young's modulus and thus density of the outer sections so much is almost like getting rid of those sections, thus reducing the length of the plate to a third. Therefore, one could argue that the peaks are always most pronounced at the edges of the plate, but the edges are gradually changing location. Moreover, it is quite clear from that same plot that there is a reduction in the 'stress shielding' experienced by the bone.

If one looks carefully at the 3D plot of the maximum stress results, it is clear that as one goes from the position where the young's modulus of the outer and inner sections is 110 GPa all the way, along the diagonal, down to the global minimum, this is effectively reducing the young's modulus of the whole plate gradually from 110 to 3GPa. Secondly, if we start again at the position where the whole plate is made of titanium (110 GPa) and go along the vertical all the way down to where the young's modulus of the inner section is 110 GPa and that of the outer edges is 3GPa we are effectively reducing only the young's modulus of the outer edges all the way to the minimum. Lastly, if we again begin at this top-right corner on the graph and follow a horizontal path leftwards to the combination where E1 is 110 GPa but E2 (inner material) is 3 GPa, we are effectively reducing the young's modulus of the inner section only, all the way to the minimum.

A plot comparing these three cases is presented further below and shows very clearly that whilst reducing the young's modulus of the outer edges reduces the peak stresses in a similar fashion to when the young's modulus of the whole plate is reduced, reducing the young's modulus of only the inner section has a much less significant effect. This allows us to conclude that modifying the outer sections of the plate is much more influential to reducing the peak stresses. The argument is further backed up by the distribution plot shown. Having the inner part of the plate be very porous can perhaps be thought of as having two very rigid plates attached by an elastic middle part. This is why, as shown both in the 3D plot and by a 2D plot comparison, reducing the young's modulus of the inner section has a higher influence in decreasing the axial rigidity of the construct and thus increasing the IFS.

What conclusions can be drawn from the 4D investigation?

This analysis was carried out in order to get further insights into how different sections of the plate affect the maximum Von Mises stress in the bone as well as the interfragmentary strain (IFS). The results quite nicely show that the most influential sections of the plate to minimise the maximum Von

Mises Stress are in fact the outer-most regions of the plate, even if these regions are a very small portion of the plate. This argument is further supported by a study done with the 'Tied model', the results for which are presented below. The plate was divided into three sections once again but now the length of the outer-most regions was reduced from 50 to 0mm, and it can be seen clearly that even with outer-most regions of 10mm (6.7% of the total length of the plate), the reduction in the peak stresses is still very significant.
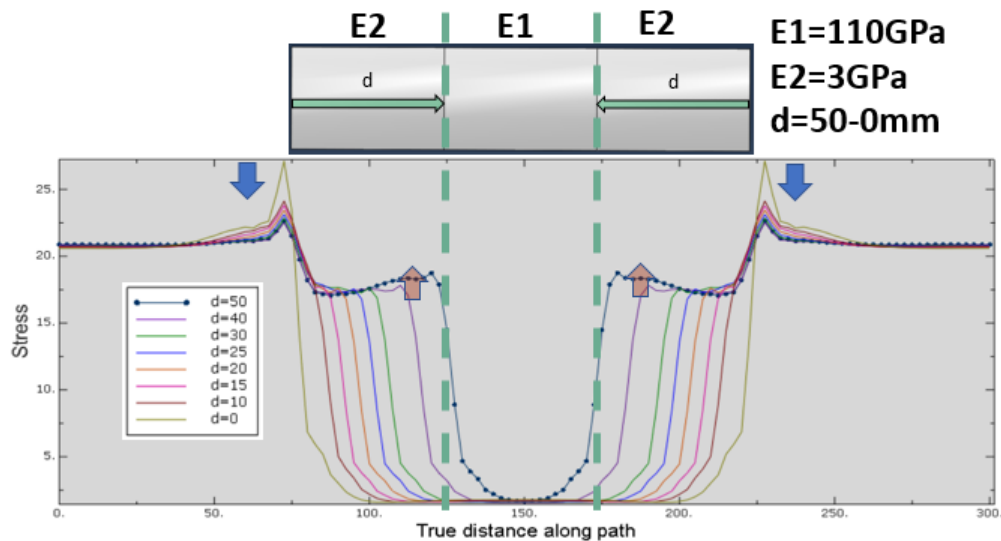

Figure 72: Figure showing how the Von Mises Stress distribution varies along a path on the top surface of the bone (the same shown in the previous figure) for different d values, where d is the distance from the end of the plate to where one of the two partitions is made. As shown, the plate is made of three parts, the inner part having a young's modulus of 110 GPa and the outer parts having a young's modulus of 3GPa.

For the interfragmentary strain, it appears that the section with the highest influence was the second from the outside to the inside. This goes somewhat against the intuition that was developed from the 2D optimization about the inner section being the most influential to increasing the IFS, but it was noted there too that the difference between the effect of the inner and outer sections on the IFS was not too significant. This is also the case here, all sections have a similar influence. Perhaps a more thorough study (more levels used for instance) is needed to draw a suitable conclusion about the effect of different sections of the plate on the IFS.

What conclusions can be drawn about the 10D optimisation?

As explained, for the 10D optimisation (called 10D because a 10-dimensional discrete space of possible combinations was initially considered, by dividing the plate into 10 mirrored segments) a constraint was used to neglect all combinations which did not have a higher young's modulus at all outer sections than their preceding inner sections. This constraint was derived from the results acquired from the previous optimizations, which show that it is the outer sections which really influence most the stress peaks. This constraint reduced the allowed number of combinations to a mere 1001 (0.01% of all the combinations). Thus, it made it possible to validate an optimisation procedure by computing the results of all these 1001 combinations and finding the optimum graphically. The genetic algorithm used did in fact find the same optimum as we did graphically.

However, it was noted that the initial optimal distribution found with the 10D optimisation did not provide as promising results as did the simple 2D optimisation. This was due to the low number of intervals used. Even though the total number of combinations for the 2D optimisation was only 100, it used 10 intervals of young's modulus from 3 to 110 GPa, whilst the initial 10D optimisation only

used 5. This is useful to understand that the number of intervals is crucial to ensure a good result. Moreover, constraining the 10D space as was done, to keeping the outer six sections of either side of the plate at 3GPa and constraining the inner sections to vary in 10 steps between 60 and 80 GPa allowed for a better young's modulus distribution to be found. This ensured a maximum Von Mises Stress which was about 2MPa lower than that found with the 2D optimization.

What conclusion can be drawn from the ABAQUS optimization?

The ABAQUS topology optimization worked very differently than the other routines discussed here, as it did not only optimize the material distribution along the length of the implant but rather in all directions because it was optimizing the density of the elements. Moreover, the routine was supplied with a different constraint, the total strain energy. The minimum found with this routine was in fact quite promising, although the fact that the distribution of the density along the implant was not symmetrical about the longitudinal centre puts in doubt the validity of the results. This routine was also the fastest, since it took only 26 iterations. It is thus suggested that in future studies, a more thorough understanding of this optimization module is developed, such that a better result can be achieved.

7   Conclusion:

Referring directly the hypothesis presented at the beginning of the report, it can firstly be concluded that there are in fact stress peaks at the edges of the plate, so this is most likely why bone fractures are seen at these regions in patients with a fracture fixation plate. Secondly it can be concluded that the material was not found to be the most influential parameter in lowering the peak stresses in the bone, but rather the second most influential (the thickness of the bone was found to be more influential). Nevertheless, as shown through a plot of maximum Von Mises stress against decreasing young's modulus of the plate, the young's modulus of the plate can very significantly reduce the peak stresses (But never make them disappear as they are also related to the change in geometry!). Thirdly, it can be concluded that as proven in various sections of the report (most clearly by the 2D optimisation), by modifying the distribution of the young's modulus of the plate along its length, the peak stresses can in fact be minimised while keeping the fracture stable enough during the healing process (subject to the validity of the relevant assumptions made).

Two questions were brought up in the introduction section. (1) To answer the first, it can be concluded that bones that have been implanted with a fracture fixation plate may be prevented from fracturing at the edges of the plate if the young's modulus is modified, as hypothesized. However, they may be more significantly affected by optimizing both the material and the thickness of the implant simultaneously. (2) It can also be concluded that in order to allow the bone to heal properly during the phase when there is a fracture, and still achieve minimal stress peaks at the edges of the plate, an optimized stiffness-graded fracture fixation plate may be used. The optimisation should be carried out using an appropriate objective function and a suitable healing constraint; such as those used here. Regarding the optimisation algorithm chosen, although the 2D and 10D optimisations carried out here did in fact optimize the plate for the given solution space (reduced the maximum stress to 47.8%), it is believed that if a gradient-based optimization algorithm is employed, such as that used by R. Huiskes and R. Boeklagen (Huiskes and Boeklagen, 1989), an even better distribution of young's modulus along the plate could be found.

8 Appendices:

8.1 Appendix A: Further parametric study

In order to more clearly represent the effect of the analysed parameters on the chosen output variables, some further results were computed by varying only one parameter at a time, and the results are presented below. Since the objective was to compare the relationship that each of the parameters has with the output variables, it was chosen to give each of them a few levels by deducting taking 50% of the initial value, then 25% and finally 12.5%. For the Fillet radius however(*), the levels were set in the reverse order as can be seen, and a case with no fillet was added since this is what was used in the optimisation.

Table 20: Table showing the values of each parameter per level. The first three parameters from left to right are decreased in halves as can be observed, but the Filler radius (*) is increased instead.

Level	Percentage*(%)	Plate Young's Modulus (Gpa)	Plate Thickness (mm)	Screws (#)	Fillet radius(mm)
4	100	110.0	4.0	8	0
3	50	55	2.0	4	1
2	25	27.5	1.0	2	2
1	12.5	13.75	0.5		4

Initially only one value plots were made using the results shown in the tables below for both the maximum Von Mises Stress and the maximum Interfragmentary Strain (IFS).

Table 21: Maximum Von Mises Stress in the bone for each of the levels of the parameters under analysis.

Max Von Mises Stress (Mpa)					
Level	Percentage*(%)	Plate Young's Modulus	Plate Thickness	Screws	Fillet
4	100	138.8	138.8	138.8	138.8
3	50	125.2	127.7	143.6	133.2
2	25	102.6	105.6	170.2	129.3
1	12.5	80.55	77.8		125.1

Table 22: Maximum Interfragmentary strain (IFS) in the fracture gap for each of the levels of the parameters under analysis.

Max IFS (%)					
Level	Percentage*(%)	Plate Young's Modulus	Plate Thickness	Screws	Fillet
4	100	0.8275	0.8275	0.8275	0.8275
3	50	0.8820	0.8731	0.8999	0.8817
2	25	0.9179	0.9213	0.9517	0.9313
1	12.5	0.9459	0.9583		0.9700

As can be observed from the graph below, reducing the number of screws causes the maximum Von Mises Stress to increase drastically, as can be expected given that now all the contact loads are concentrated in the outer screws. Varying the Fillet radius had a minimal effect on the maximum Von Mises Stress, as also predicted with the Taguchi analysis.
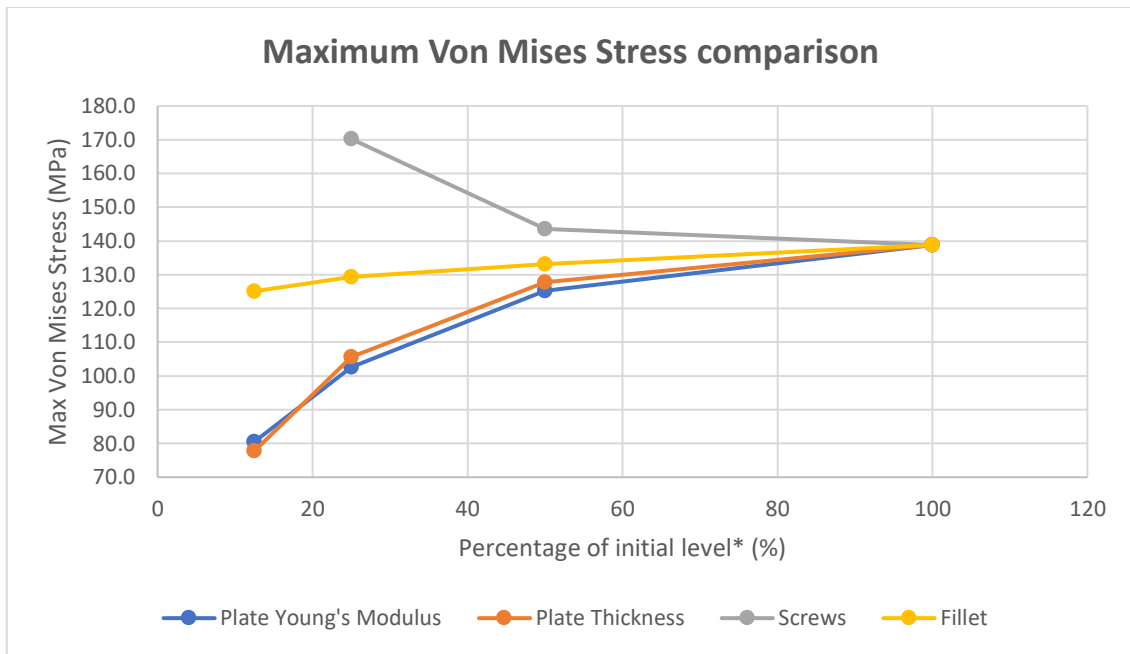
Figure 73: Plot of the results presented about the Maximum Von Mises Stress of the different parameters.

From the figure below one can see that the IFS increases most with reducing the number of screws.
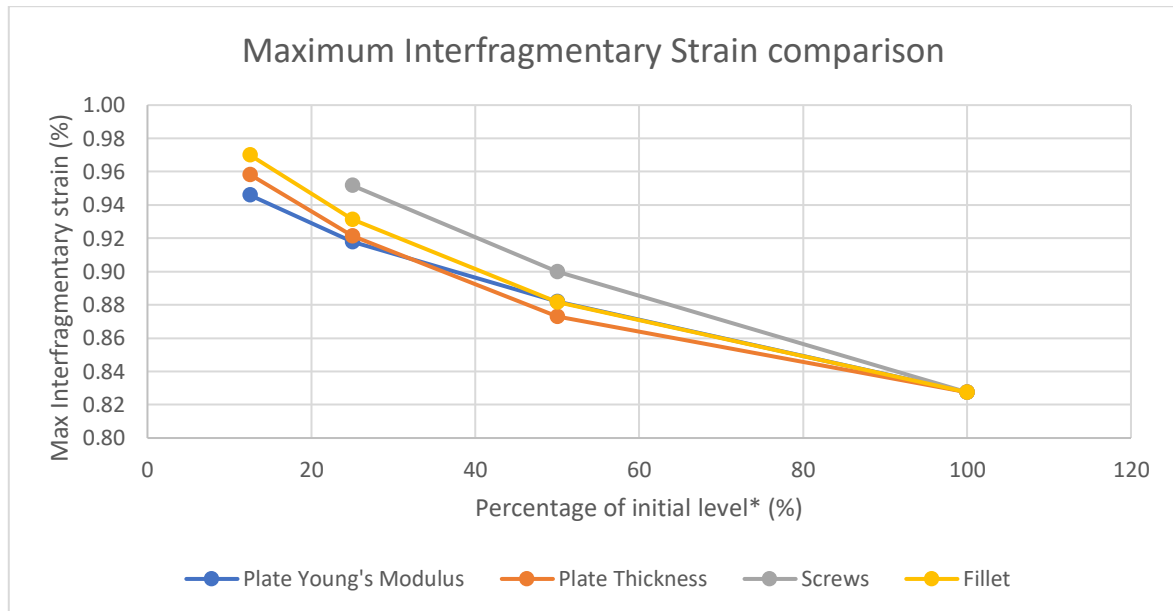

Figure 74: Maximum interfragmentary strain plot for the different parameters analysed.

Moreover, a distribution plot was made for the case of the screws, given the large impact it was shown to have in the maximum Von Mises Stress. As can be seen again in the figure below, the maximum stress is most largely affected by the change from two to one screw. Also notable is the fact that the inner peaks do not change in size between successive cases, they only disappear if the screw is no longer there. Lastly, it can be noted that as one reduces the number of screws, there is a lower amount of stress shielding.
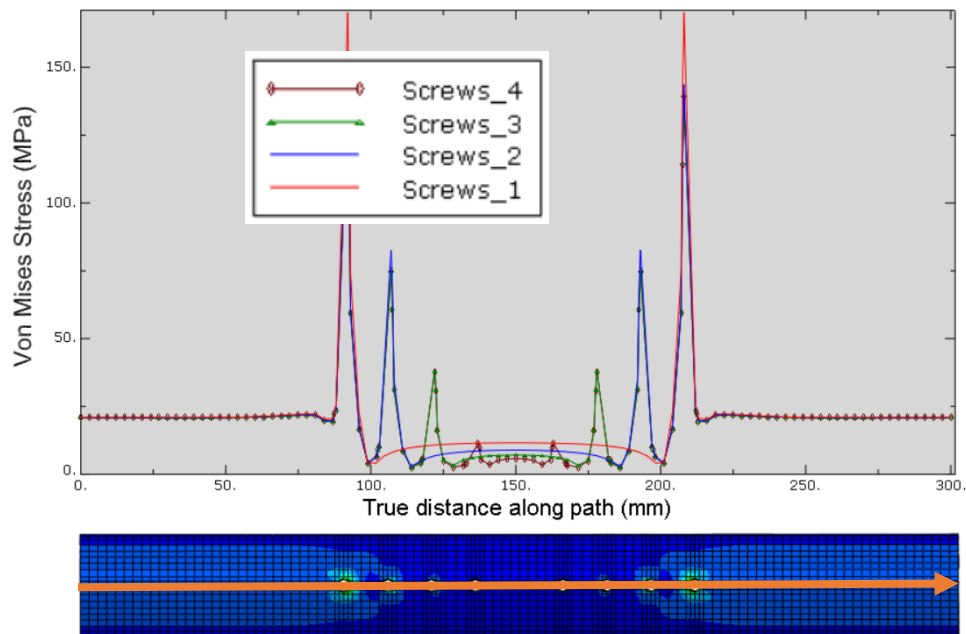
Figure 75: Von Mises Stress distribution in the bone for the given path, for cases when there are different numbers of screws.

9 References:

Albert, C. *et al.* (2017) 'Macroscopic anisotropic bone material properties in children with severe osteogenesis imperfecta', *Journal of Biomechanics*. doi: 10.1016/j.jbiomech.2017.09.003.

Arnone, J. (2013) 'Z. Computer-Aided Engineering Approach for Parametric Investigation of Locked Plating Systems Design', *Journal of Medical Devices*, 7(June 2013), p. 21001. doi: 10.1115/1.4024644.

Aro, H. T. and Chao, E. Y. (1993) 'Bone-healing patterns affected by loading, fracture fragment stability, fracture type, and fracture site compression.', *Clinical orthopaedics and related research*, pp. 8–17. doi: 10.1097/00003086-199308000-00003.

Ateshian, G. A. and Mow, V. C. (2005) 'Basic Orthopaedic Biomechanics and Mechano-Biology', *Friction, lubrication, and wear of articular cartilage and diarthrodial joints*, pp. 447–494. doi: 9780781739337.

Augat, P. *et al.* (2003) 'Shear movement at the fracture site delays healing in a diaphyseal fracture model', *Journal of Orthopaedic Research*, 21(6), pp. 1011–1017. doi: 10.1016/S0736-0266(03)00098-6.

Chakladar, N. D., Harper, L. T. and Parsons, A. J. (2016) 'ZZ. Optimisation of composite bone plates for ulnar transverse fractures'. doi: 10.1016/j.jmbbm.2016.01.029.

Chen, X. *et al.* (2017) 'A parametric approach to construct femur models and their fixation plates', *ARTICLE; MEDICAL BIOTECHNOLOGY*. doi: 10.1080/13102818.2016.1145555.

Claes, L. *et al.* (2009) 'Early dynamization by reduced fixation stiffness does not improve fracture healing in a rat femoral osteotomy model', *Journal of Orthopaedic Research*, 27(1), pp. 22–27. doi: 10.1002/jor.20712.

Claes, L. (2011) 'Biomechanical principles and mechanobiologic aspects of flexible and locked plating', *Journal of Orthopaedic Trauma*, 25(2 SUPPL.), pp. 4–7. doi: 10.1097/BOT.0b013e318207093e.

Claes, L. E. *et al.* (1995) 'Effect of dynamization on gap healing of diaphyseal fractures under external fixation', *Clinical Biomechanics*, 10(5), pp. 227–234. doi: 10.1016/0268-0033(95)99799-8.

Claes, L. E. and Heigele, C. A. (1999) 'Magnitudes of local stress and strain along bony surfaces predict the course and type of fracture healing', *Journal of Biomechanics*, 32, pp. 255–266. Available at: https://ac.els-cdn.com/S0021929098001535/1-s2.0-S0021929098001535-main.pdf?_tid=85ca999d-da62-4138-ab87-6d4222285334&acdnat=1524034109_003922b15df74f8e3cc29255306ed9e9 (Accessed: 18 April 2018).

CODE COGS (no date) *2004*. Available at: http://www.codecogs.com/library/engineering/materials/beams/strain-energy.php.

Cronier, P. *et al.* (2010) 'The concept of locking plates', *Orthopaedics and Traumatology: Surgery and Research*. Elsevier Masson SAS, 96(4 SUPPL.). doi: 10.1016/j.otsr.2010.03.008.

Dassault Systèmes Simulia, Fallis, A. . and Techniques, D. (2013) 'ABAQUS documentation', *Abaqus 6.12*, pp. 1689–1699. doi: 10.1017/CBO9781107415324.004.

DePuy Synthes (2004) 'LCP Locking Compression Plate Surgical Technique', in. Available at: http://synthes.vo.llnwd.net/o16/LLNWMB8/INT Mobile/Synthes International/Product Support Material/legacy_Synthes_PDF/DSEM-TRM-0115-0278-3_LR.pdf (Accessed: 13 February 2018).

Documentation, M. (2012) 'Matlab documentation', *Matlab*. doi: 10.1201/9781420034950.

Duda, G. N., Schneider, E. and Chaot, E. Y. S. (1997) 'INTERNAL FORCES AND MOMENTS IN THE FEMUR DURING WALKING', *J. Bmnmhonics*, 30941(933). Available at: https://ac.els-cdn.com/S0021929097000572/1-s2.0-S0021929097000572-main.pdf?_tid=32d9ff3e-dff6-11e7-ab78-00000aab0f01&acdnat=1513163597_77cd82d1470d35f236c9fe084c1d8bde (Accessed: 13 December 2017).

Ferguson, S., Wyss, U. P. and Pichora, D. R. (1996) 'Finite element stress analysis of a hybrid fracture fixation plate', 18, pp. 241–250. Available at: https://ac.els-cdn.com/1350453395000410/1-s2.0-1350453395000410-main.pdf?_tid=cd6d8770-b9c5-11e7-bea7-00000aacb35d&acdnat=1508964667_a1f9c32fa5445c85d85dc2a344e7636c (Accessed: 25 October 2017).

Frost, H. M. (1989) 'The biology of fracture healing. An overview for clinicians. Part I.', *Clinical Orthopaedics and Related Research®*. doi: 10.1016/j.injury.2011.03.031.

Ganesh, V., Ramakrishna, K. and Ghista, D. N. (2005) 'Biomechanics of bone-fracture fixation by stiffness-graded plates in comparison with stainless-steel plates'. doi: 10.1186/1475-925X-4-46.

Huiskes, R. (1979) 'Some fundamental aspects of human joint replacement : analyses of stresses and heat conduction in bone- prosthesis structures'. doi: 10.6100/IR140519.

Huiskes, R. *et al.* (1987) 'Adaptive bone-remodeling theory applied to prosthetic-design analysis', *Journal of Biomechanics*, 20(11–12), pp. 1135–1150. doi: 10.1016/0021-9290(87)90030-3.

Huiskes, R. (1988) 'Chapter 24: Stress patterns , failure modes , and bone remodeling'.

Huiskes, R. and Boeklagen, R. (1989) 'MATHEMATICAL SHAPE OPTIMIZATION OF HIP PROSTHESIS DESIGN', *I Bwmrchunrcs*, 22(8), pp. 793–804. Available at: https://ac.els-cdn.com/0021929089900638/1-s2.0-0021929089900638-main.pdf?_tid=f411280e-bb1a-11e7-8b9f-00000aab0f26&acdnat=1509111189_0048833dd74be29c2ea0f99fd3495f8a (Accessed: 27 October 2017).

Huiskes, R. and Chao, E. Y. S. (1983) 'A SURVEY OF FINITE ELEMENT ANALYSIS IN ORTHOPEDIC

BIOMECHANICS: THE FIRST DECADE', 16(6), pp. 385–409. Available at: http://www.jbiomech.com/article/0021-9290(83)90072-6/pdf (Accessed: 28 November 2017).

Kuiper, J. H. and Huiskes, R. (1996) 'Friction and stem stiffness affect dynamic interface motion in total hip replacement', *Journal of Orthopaedic Research*, 14(1), pp. 36–43. doi: 10.1002/jor.1100140108.

Kyobula, M. *et al.* (2017) '3D inkjet printing of tablets exploiting bespoke complex geometries for controlled and tuneable drug release', *Journal of Controlled Release*. Elsevier, 261(June), pp. 207–215. doi: 10.1016/j.jconrel.2017.06.025.

Lehder, E. (2018) 'Finite Element Modelling of Fracture Fixation plates : a systematic literature review'

Mason, A. (2009) 'NIH Public Access', 19(Suppl 1), pp. 389–399. doi: 10.1016/j.asieco.2008.09.006.EAST.

Nassiri, M., Macdonald, B. and O 'byrne, J. M. (2013) 'Computational modelling of long bone fractures fixed with locking plates e How can the risk of implant failure be reduced?', *Journal of Orthopaedics*, 10, pp. 29–37. doi: 10.1016/j.jor.2013.01.001.

Nelson, D. A. *et al.* (2004) 'Comparison of cross-sectional geometry of the proximal femur in white and black women from Detroit and Johannesburg', *Journal of Bone and Mineral Research*, 19(4), pp. 560–565. doi: 10.1359/JBMR.040104.

Ni, M. *et al.* (2016) 'Biomechanical comparison of locking plate and crossing metallic and absorbable screws fixations for intra-articular calcaneal fractures', *Science China Life Sciences*, 59(9), pp. 958–964. doi: 10.1007/s11427-016-0010-9.

Oh, J.-K. *et al.* (2009) 'Effect of fracture gap on stability of compression plate fixation: A finite element study', *Journal of Orthopaedic Research*, (April), p. n/a-n/a. doi: 10.1002/jor.20990.

Samiezadeh, S., Tavakkoli, P. and Fawaz, Z. (2015) 'On optimization of a composite bone plate using the selective stress shielding approach'. Elsevier, 42, pp. 138–153. doi: 10.1016/j.jmbbm.2014.11.015.

Shirurkar, A., Tamboli, A. and Jagtap, P. N. (2017) 'Mechanical Behavior of ZM21 Magnesium Alloy Locking Plates – An Experimental and Finite Element Study', *Materials Today: Proceedings*. Elsevier Ltd, 4(6), pp. 6728–6736. doi: 10.1016/j.matpr.2017.06.448.

Simon, B. R., D. T. (1977) 'EVALUATION OF ONE-. TWO-, AND THREE-DIMENSIONAL FINITE ELEMENT AND EXPERIMENTAL MODELS OF INTERNAL FIXATION PLATES*'. Available at: https://ac.els-cdn.com/0021929077900719/1-s2.0-0021929077900719-main.pdf?_tid=35aaf206-cc8a-11e7-a0fc-00000aab0f27&acdnat=1511028143_c9d9f6424e665b6c6bf0e349fa348034 (Accessed: 18 November 2017).

Sommer, C. *et al.* (2003) 'First clinical results of the Locking Compression Plate (LCP)', *Injury*, 34 Suppl 2, p. B43—54. doi: 10.1016/j.injury.2003.09.024.

Steiner, M. *et al.* (2013) 'Prediction of fracture healing under axial loading, shear loading and bending is possible using distortional and dilatational strains as determining mechanical stimuli', *Journal of the Royal Society Interface*, 10(86). doi: 10.1098/rsif.2013.0389.

Steiner, M. *et al.* (2014) 'Numerical Simulation of Callus Healing for Optimization of Fracture Fixation Stiffness', *PLoS ONE*, 9(7). doi: 10.1371/journal.pone.0101370.

Synek, A. *et al.* (2015) 'The influence of bone density and anisotropy in finite element models of distal radius fracture osteosynthesis: Evaluations and comparison to experiments', *Journal of*

Biomechanics, 48, pp. 4116–4123. doi: 10.1016/j.jbiomech.2015.10.012.

Tack, P. *et al.* (2016) '3D-printing techniques in a medical setting: a systematic literature review', *BioMedical Engineering OnLine*. BioMed Central, 15(1), p. 115. doi: 10.1186/s12938-016-0236-4.

Tiwari, M. K., Bajpai, S. and Dewangan, U. K. (2017) 'Investigation of dominant leaching factors for release of CR from Indian fly ash INVESTIGATION OF DOMINANT LEACHING FACTORS FOR RELEASE OF CR FROM INDIAN FLY ASH', (July).

Tonino, A. J. (1976) 'Protection from stress in bone and its effects'.

Udupa, G., Rao, S. S. and Gangadharan, K. V. (2014) 'Functionally Graded Composite Materials: An Overview', *Procedia Materials Science*, 5, pp. 1291–1299. doi: 10.1016/j.mspro.2014.07.442.

Uhthoff, H. K. and Dubuc, F. L. (1971) 'Bone structure changes in the dog under rigid internal fixation.', *Clinical orthopaedics and related research*. doi: 10.1097/00003086-197111000-00026.

Uhthoff, H. K., Poitras, P. and Backman, D. S. (2006) 'Internal plate fixation of fractures: short history and recent developments', *J Orthop Sci*, 11, pp. 118–126. doi: 10.1007/s00776-005-0984-7.

Varga, P. *et al.* (2018) 'Validated computational framework for efficient systematic evaluation of osteoporotic fracture fixation in the proximal humerus', *Medical Engineering and Physics*. Elsevier Ltd, 57, pp. 29–39. doi: 10.1016/j.medengphy.2018.04.011.

Wang, X.-H. *et al.* (2013) 'Mechanical properties of porous titanium with different distributions of pore size', *Trans. Nonferrous Met. Soc. China*, 23, pp. 2317–2322. doi: 10.1016/S1003-6326(13)62735-1.

Wauthle, R. *et al.* (2015) 'Revival of pure titanium for dynamically loaded porous implants using additive manufacturing', *Materials Science and Engineering C*. Elsevier B.V., 54, pp. 94–100. doi: 10.1016/j.msec.2015.05.001.

Wehner, T. *et al.* (2011) 'Improvement of the shear fixation stability of intramedullary nailing', *Clinical Biomechanics*. Elsevier Ltd, 26(2), pp. 147–151. doi: 10.1016/j.clinbiomech.2010.09.009.

Weinans, H., Huiskes, R. and Grootenboer, H. J. (1992) 'Effects of material properties of femoral hip components on bone remodeling', *Journal of Orthopaedic Research*, 10(6), pp. 845–853. doi: 10.1002/jor.1100100614.

Wysk, R. A., Niebel, B. W., Cohen, P. H., and Simpson, T. W. (2000) 'Taguchi's Robust Design Method', *Manufacturing Processes: Integrated Product and Process Design*.

Zadpoor, A. A. and Weinans, H. (2015) 'Patient-specific bone modeling and analysis: The role of integration and automation in clinical adoption', *Journal of Biomechanics*. Elsevier, 48(5), pp. 750–760. doi: 10.1016/j.jbiomech.2014.12.018.

Ziheng Wu, Timothy C. Ovaert, and G. L. N. (2013) 'Viscoelastic properties of human cortical bone tissue depend on gender and elastic modulus', 30(5), pp. 693–699. doi: 10.1002/jor.22001.Viscoelastic.